Recent advances and prospects of persistent luminescent materials as inner secondary self-luminous light source for photocatalytic applications

Kang, Fengwen; Sun, Guohuan; Boutinaud, Philippe; Wu, Haoyi; Ma, Fei Xiang; Lu, Jian; Gan, Jiulin; Bian, Haidong; Gao, Fei; Xiao, Sanshui

Published in:
Chemical Engineering Journal

Link to article, DOI:
10.1016/j.cej.2020.126099

Publication date:
2021

Document Version
Early version, also known as pre-print

Recent advances and prospects of persistent luminescent materials as inner secondary self-luminous light source for photocatalytic applications

Kang, Fengwen; Sun, Guohuan; Boutinaud, Philippe; Wu, Haoyi; Ma, Fei Xiang; Lu, Jian; Gan, Jiulin; Bian, Haidong; Gao, Fei; Xiao, Sanshui

Published in:
Chemical Engineering Journal

Link to article, DOI:
10.1016/j.cej.2020.126099

Publication date:
2021

Document Version
Peer reviewed version

Recent advances and prospects of persistent luminescent materials as inner secondary self-luminous light source for photocatalytic applications

Fengwen Kang,[a *] Guohuan Sun,[b] Philippe Boutinaud,[c] Haoyi Wu,[d] Fei-Xiang Ma,[e] Jian Lu,[e,f] Jiulin Gan,[g] Haidong Bian,[e] Fei Gao,[h] and Sanshui Xiao,[a*]

[a] *DTU Fotonik, Department of Photonics Engineering, Technical University of Denmark (DTU), Lyngby, 2800, Denmark;*

[b] *The State Key Laboratory of Experimental Hematology (SKLEH), Institute of Hematology, Chinese Academy of Medical Sciences, Tianjin 300020, P. R. China;*

[c] *Clermont Université Auvergne, SIGMA Clermont, Institut de Chimie de Clermont-Ferrand, 63000 Clermont-Ferrand, France;*

[d] *School of Physics and Optoelectronic Engineering, Guangdong University of Technology (GDUT), Guangzhou 510006, P. R. China;*

[e] *Department of Mechanical Engineering, City University of Hong Kong, 83 Tat Chee Avenue, Kowloon, Hong Kong, China;*

[f] *Center for Advanced Structural Materials, City University of Hong Kong, Shenzhen Research Institute, 8 Yuexing 1st Road, Shenzhen Hi-Tech Industrial Park, Nanshan District, Shenzhen 518057, P. R. China;*

[g] *School of Materials Science and Engineering, South China University of Technology (SCUT), Guangdong 510006, P. R. China;*

[h] *Department of Physics, Technical University of Denmark (DTU), Lyngby, 2800, Denmark.*

Corresponding authors

Email: kangfengwen0597@126.com (*Dr*. F. Kang), and saxi@fotonik.dtu.dk (*Prof*. S. Xiao),

ABSTRACT

Nowadays, materials with persistent luminescence (MPLs) have attracted growing attention in the catalytic field because they can act as an inner light source to irradiate the photocatalytic materials (PCMs) and sustain their photocatalytic activities in the absence of the external irradiation source. The motivation of the present work is to provide a review of the MPL@PCM composites that are of interest for both photocatalytic and lighting fields. In terms of the unique luminescence of MPLs and the principal optical properties of PCMs, the review is organized as follows: first, we categorize and discuss a number of rare-earth (RE)/non-RE-doped MPLs and bulk MPLs, along with their emission/persistent ranges and potentially-coupled PCM counterparts. Then, we present and discuss the intrinsic nature of the photocatalytic properties and the working principles of the MPLs that have been coupled with the PCMs. In the 4th section, we summarize the principal synthesis strategies that are reported for the MPL@PCM composites. At last, by taking advantages of some reported works, we exhibit the photocatalytic applications of the MPL@PCM composites, and give a summary, perspectives, potential challenges and future development directions to this review. With the profound impact of the persistent luminescence, we believe that this review will be not only of particular interest to the scientists in the lighting field, but can also attract those with backgrounds in the fields of the environmental science, materials and physics, chemistry, energy fuels, and their coupling subdivisions to jointly address some of the major environmental issues like degradation of organic waste, removal of gas-phased materials, *etc*.

Key words: persistent luminescence; inner light source; self-luminous; rare-earth (RE); non-RE; photocatalysis.

1. Introduction

Photocatalytic materials (PCMs) are a type of important materials that enable addressing a number of world-wide environmental problems such as organic degradation and water waste purification. Normally, these PCMs need to be exposed to an external irradiation source (*e.g.*, UV [1-2], visible [1-3], artificial solar [4-5], near infrared (NIR) light [6]), so long to sustain their photocatalytic activities continuously by absorbing the incoming photon energy from the irradiation source. In the past years, more than tens of thousands of PCMs are discovered, such as Er^{3+}-Yb^{3+}-TiO_2 [7], La^{3+}-doped TiO_2 [8], Mn^{2+}-Co^{2+} co-doped TiO_2 [9], Ag_3PO_4:Bi^{3+} [10], metal-organic frameworks (MOFs) [11], graphene quantum dots (GQDs) [12], carbon dots (CDs) [13], CdS-based molecular Ni catalyst [14], two-dimensional (2D) nanomaterials (*e.g.*, WS_2 / MoS_2 nanocluster [15], MoS_2 / graphene cocatalysts [16]), perovskite $CsPbBr_3$ QDs / graphene oxide [17], semiconductors (*e.g.*, TiO_2 [18], ZnO [19], ZnS [20], $BiVO_4$ [21-22], and BiOCl [23]), and the coupled nano- and micro-composites (*e.g.*, perovskite $CsPbBr_3$ QDs / graphene oxide [17], Ag-AgCl [24], MoS_2-TiO_2 [25], TiO_2-MOFs [26], TiO_2-Au [27], and $BiVO_4$-BiOCl [28]). However, they can continuously show the photocatalytic activity only as long as an external irradiation source is on. Once the irradiation source is off, the photocatalytic process terminates immediately. Thus, an external irradiation source that enables providing the continuous irradiation energy is the primary factor to preserve the photocatalytic process. In the context of how to alleviate the environmental pollution and energy crisis, keeping a photocatalytic reaction under an electrically-powered irradiation source is not a sustainable option due to the continuous consumption of energy. This is particularly crucial in the under-developed and poor regions that frequently face the shortage of electric power. In this concern, exploring alternative strategies that can sustain the photocatalytic reaction but do not need the external irradiation source have been focused in the past years, and they have led to great concerns to those materials with persistent luminescence and the relevant self-luminous MPL@PCM associations. In fact, the self-luminous working principle of these MPL@PCM composites is mainly based on the storage capacity of the MPLs and its correlated persistent luminescence as an inner light source for the PCMs, making it possible to generate a continuous self-induced photocatalytic activity when the external irradiation source is off. Moreover, it generally only needs to charge the MPLs in a short time (*i.e.*, usually limited to a few seconds or minutes), by use of either *x*- [29-32], α- [32], β- [32], and γ-ray [32-33], UV [34-37], visible

[38-39], NIR [36, 40], or sunlight [39, 41].

The persistent luminescence, which is also called long-lasting or afterglow luminescence [42-45], can be traced back more than one thousand years ago. In ancient China (about Tang dynasty), the legendary glow-in-the-dark pearl was the most famous natural persistent material frequently used for fabricating artworks and ornaments like the paintings and luminous wine cups [42-43, 46-47]. Nowadays, with the continuous progresses in chemical- and physical-synthesis routes and in-depth understanding on the persistent working principle (*i.e.*, the involved physics), we can easily design and manufacture numerous inorganic and organic MPLs with the persistent durations broadly ranging from several seconds up to several hours and even to several days in few special cases and the persistent spectral regions spreading from UV, visible, and to NIR light. Because of these unique persistent properties, a number of application opportunities in diverse fields have been discovered, including the photocatalysis [48-49], security and anti-counterfeiting purposes [50-51], solar energy [52], biosensing [53], information data storage [54], biological imaging [55-56] *etc*. Noteworthy is the recent design demonstration — highly efficient photocatalytic reaction for the organic pollutants degradation and hydrogen evolution from the water through the self-activated (*i.e.*, also called the external irradiation-free self-luminous) plasmonic photocatalyst composite g-C_3N_4@Ag@$SrAl_2O_4$:Eu^{2+},Dy^{3+} [57].

During the last decade (*i.e.*, 2009-2019), more than 40,000 articles (including the review and research articles), retrieved from *Web of Science* by tracing the key words “photocatalysis” or “photocatalyst”, have been published. In particular, all the mainstream publishers indexed by *Web of Science* have reported the review articles (> 2,000). To the best of our knowledge, however, among these publications, there are only 6 review papers that have involved the progress of the MPLs that are of interest for the photocatalytic fields, whose amounts are very few compared to “> 2,000” volumes of the reviews dedicated “photocatalysis” or “photocatalysts”. More Specifically, Liu *et. al.* [48] reviewed the light-conversion phosphor-based composites for photocatalysis (*i.e.*, up-conversion-, downconversion-, and afterglow-based phosphor composites), but they only listed four types of MPLs ($CaAl_2O_4$:Eu^{2+},Nd^{3+}; $SrAl_2O_4$:Eu^{2+},Nd^{3+}; $BaAl_2O_4$:Eu^{2+},Nd^{3+}; $BaZrO_3$:Mg^{2+}); Sakar *et. al.* [58] in 2018 summarized the photocatalytic materials and the relevant reaction mechanisms under light and dark conditions and used the “long-afterglow phosphor” as a key word, but they just considered a type of long-persistent phosphors as an example ($Sr_2MgSi_2O_7$:(Eu,

Dy)) to illustrate the photocatalytic reactions and did not go through the working principles of "persistent-photocatalytic" composites; Huo *et al* reviewed the design, synthesis, and applications of phosphorescent cyclometalated platinum complexes [59], but they restricted to this category of organic and briefly commented on the photocatalysis (by using less 300 words); Li *et al* [60-61] showed the persistent photocatalysis of continuously flowing gas-phase nitric oxide based upon the $CaAl_2O_4$:(Eu,Nd)@rutile $TiO_{2-x}N_y$ composites, but they only gave one type of MPLs; Qiu and his coworkers [44] reviewed the fundamentals and general applications of MPLs based on the archival literatures prior to 2016, with focusing on the synthesis methods, persistent mechanism, measurement characterization, classification of the MPLs, but only seven MPLs were introduced in correlation with the photocatalytic applications. Obviously, these reviews confine either to a specific type of photocatalytic compound or to limited MPLs, thus failing to account satisfactorily either for the latest progresses and achievements on the "persistent-photocatalytic" composites or for the prospects of other MPLs that can potentially act as an inner irradiation source to sustain the photocatalytic activity. This is one of the major motivations for us to undertake the present review whose synoptic organization is illustrated in **Figure 1**.

We start by reviewing in **Section 2**, with disclosing the most attractive MPLs for fabricating the MPL@PCM composites and their photocatalytic application. These MPLs are classified based on the nature of their dopants, irradiation wavelength, emission spectral regions and peak positions, as well as persistent duration. As we can see, most of MPLs have not yet been tested for photocatalytic purposes, opening a wide field of study in the matter. Then, we dedicate to review the mainstream PCMs and reported MPL@PCM composites, with paying special attention to the working principles and mechanistic models involved in the self-luminous MPL@PCM composites (**Section 3**), and to some selected synthesis methodologies of relevant MPL@PCM counterparts (**Section 4**). Meanwhile, in **Section 4**, we also select 29 SEM / FESEM / TEM / HRTEM images of the MPLs, PCMs, or MPL@PCM system to illustrate the design consideration. In **Section 5**, some typical examples of the MPL@PCM composites, which are applied for, *e.g.*, degradation of organic molecules, removal of poisonous gas-phased materials, and water splitting into H_2 and O_2, and so forth, are reviewed. Then, in **Section 6**, we summarize this review and, from the side of our logical thinking, disclose some perspectives, insights, potential challenges and future directions of the use of the MPL@PCM composites for other emerging applications, including but not limited

to the lighting and photocatalytic fields.

2. Principal MLs and relevant optical properties

According to the database from the *Web of Science* database, more than 20,000 articles associated with the key wordw of "long persistent luminescence", "afterglow luminescence", and/or long-lasting luminescence" have been reported. In this case, it is impossible for us to list all in this review; instead, we have chosen to review the MPLs that have been reported to work with the PCMs or feature potentially attractive contributions for the "persistent-photocatalytic" purpose. Along with those materials featuring the up-converted persistent luminescence, the MPLs are classified based on the category of their emitting species, including the rare-earth (RE)-doped MPLs, transition metal (TM) ions doped MPLs, ns^2-type cation-doped MPLs, self-activated bulk MPLs and NIR-converted MPLs.

2.1 RE-doped MPLs

In RE-doped MPLs, the persistent luminescence mainly originates either from *d-f* transition RE ions (*i.e.*, Eu^{2+}, and Ce^{3+}) [31, 33-34, 42, 44, 49, 57, 60-106], well-shielded 4*f* (*e.g.*, Eu^{3+}, Pr^{3+}, Tb^{3+}, Sm^{3+}, Tm^{3+}, Gd^{3+}, and Dy^{3+}) [35-37, 51-52, 107-142], or from the coupling arrangements of these RE ions [33-34, 38, 42, 44, 52, 57, 64, 67-69, 72-77, 79-82, 85-89, 92-94, 96-99, 101, 103, 105-107, 118, 120, 125, 127, 134]. Besides, with the purposes of creating the defects, modifying the trap depths, or constructing the energy transfer paths, the non-RE (*e.g.*, Bi^{3+} [91, 130, 141], Mn^{2+} [90, 92], Cr^{3+} [40, 56, 84, 87]), or some of other RE (*e.g.*, Nd^{3+} [49, 61, 70-71, 142], Pr^{3+} [38, 56, 98, 101, 107], Ho^{3+} [95, 125] *etc*) are also often used as the co-dopants for RE-doped MPLs.

The *d-f* RE (*i.e.*, Eu^{2+}, and Ce^{3+}) doped MPLs (**Table 1**, and **Figure 2**) can exhibit a broad range of fluorescent and persistent luminescence, and the spectral edge can start either from the visible or from the UV, and end to the NIR region, depending on the nearby chemical microenvironment that the *d-f* RE ions have experienced. Although the *d-f* RE-doped MPLs usually feature broad emission bands (**Figure 2a**), they could also show multiple bands (*i.e.*, including the emission and persistent bands) if the related crystal contains multiple crystal sites (**Figure 2a**(**iii**)) or in case of inefficient energy transfer from the host or the co-doping ion to the *d-f* transition RE ion [77-78, 82-85, 87, 96-98]. In addition, accessing the *d-f* RE MPLs needs a reductive atmosphere such as the N_2 + H_2, and N_2 + CO atmosphere, so as to reduce the europium and cerium ion with the high valence, *i.e.*, from Eu^{3+} and Ce^{4+} to Eu^{2+} and Ce^{3+}, respectively. Considering different persistent

spectral ranges and their potentially-matched PCMs, in **Table 1**, we summarize not only the *d-f* RE emission or persistent positions but also relevant persistent durations, although many of them use the same *d-f* RE ion as the emission or persistent activator.

Unlike the *d-f* RE MPLs, the well-shielded 4*f* RE-doped MPLs are characterized by the persistent lines analogous to their respective fluorescent lines and colors (**Table 2**, and **Figure 3**). Different 4*f* RE ions show their own spectral properties (*i.e.*, the fixed spectral shape and peak positions, sharp lines and narrow band width), independent of the crystal lattice. The persistent luminescence is then confined to the given spectral regions, which limits the spectral overlap with the absorption of PCMs. This is one of the major reasons why the *d-f* RE ions are often used to design the "persistent-photocatalytic" MPL@PCM composites rather than the *f-f* RE ions (next section). In the cases of some 4*f* RE ions like Dy^{3+} [129, 144-146], Tb^{3+} [144-145, 147-148], and Eu^{3+} [145, 148-149] ions, the dominant persistent lines usually appear beyond 450 nm (**Figure 3a**, **Figure 3b**(**iii**)) and overlap only very weakly the optical absorption of a few PCMs. However, we still can find the 4*f* RE like Tb^{3+} or Tm^{3+} have a wide range of emissions individually distributed in the visible region, and some of their emission lines fall in the UV region. Thus, their energy can be easily re-absorbed by the PCMs, such as the $Sr_4Al_{14}O_{25}$:Tb^{3+} [114], $Ca_3Ga_2Ge_3O_{12}$:Tb^{3+},Tm^{3+} [118], $CdSiO_3$:Tb^{3+} [115, 150], and Ca_2SnO_4:Tm^{3+} [132]. As a result, narrow emission lines of the 4*f* RE ions can allow unique coupling with a given specific absorption band of PCMs with which the *d-f* RE ions cannot have. That is to say, in principle, they could be used for coupling some specific PCMs if the MPL@PCM designer wants the dominant emission lines of the *f-f* RE ions to couple with the strongest absorption of the PCMs. For example, the Eu^{3+}-dominant line of 616 nm matches with one of the surface plasmon resonance (SPR) absorption peaks (~615 nm) of Ag nanoparticles (NPs) in the ZnO:Co/Ag PCMs [68]. Although this is based on the spectra-selective characteristics and still has not been proved by previous works, such MPLs also show the potential desirable for the photocatalytic reactions in the absence of external irradiation source.

2.2 Transition metal (TM)-doped MPLs

Previous research works dedicated to TM-doped MPLs mostly concern 3*d* ions like Mn^{4+} [142, 151-157], Cr^{3+} [39, 55-56, 158-197], and Mn^{2+} (**Table 3**) [53, 90, 92, 194, 198-235]. Among them, Mn^{4+}-doped MPLs are still undeveloped, the number and type of which are limited. Generally, in an oxidic environment, exciting with the UV and visible light, the Mn^{4+} MPLs exhibit an

excitation range broadly covering the whole UV and part of the visible light (usually ≤ 550), but a relatively fixed and narrow persistent spectral band in the range of 600-800 nm (**Figure 4**). In many reports [142, 150-155, 157], the red Mn^{4+} luminescence is also referred to the NIR or deep red, because its emission range (or part of the emission wavelength) falls precisely in the NIR optical window (*i.e.*, 650-1350 nm). Because of the site occupancy preferential issue or the crystal field strength change, however, the Mn^{4+} enables showing different dominant emission positions (**Figure 4a**(**iii**-**iv**)), but basically sustains in the range of 600-800 nm, allowing the persistent range of Mn^{4+}-doped MPLs to match those PCMs with the absorption wavelength larger than 600 nm. Similar to the Mn^{4+}-doped case, the spectra of Cr^{3+} ion also feature a relatively narrow and fixed deep red or NIR persistent range whose edge usually starts from ~600 nm but, relying on the crystal hosts, ends to different positions (**Figure 5**). The excitation range of Cr^{3+} ion can cover the whole UV and visible region (**Figure 5a**(**iii**-**iv**)), showing much broader when compared to that of Mn^{4+} ion. In several cases (*e.g.*, $Zn_{2-x}Al_{2x}Sn_{1-x}O_4:Cr^{3+}$ [164], $Sr_4Al_{14}O_{25}:Cr^{3+},Eu^{2+},Dy^{3+}$ [174], $SrAl_2O_4:Cr^{3+},Eu^{2+},Dy^{3+}$ [179], and $CaGa_2O_4:Cr^{3+},Yb^{3+}$ [183]), the persistent luminescence of Cr^{3+} can be generated. Normally, the Cr^{3+} ion shows not only broad spectral range (**Figure 5**) but also ultralong persistent luminescence (**Figure 5b**). Thus, the Cr^{3+} MPLs can be used for coupling with the PCMs with the absorption in the range of 600-900 nm. Moreover, the Cr^{3+} ion can also feature the tunable red/NIR positions like in $Zn_{2-x}Al_{2x}Sn_{1-x}O_4:Cr^{3+}$ (**Figure 5a**(**i**-**ii**)) [164], thus providing multiple choices for the practical need of photocatalytic purposes to achieve the desirable persistent wavelength and intensity maxima. For Mn^{2+}-doped MPLs, they often exhibit bandlike persistent band whose intensity maxima, band width, persistent duration and color largely depend on the chemical environment the Mn^{2+} ion experienced (**Table 3**, and **Figures 6**-**7**). Moreover, co-doping with other RE/non-RE ions usually broadens the persistent range owning to the integrated contributions of all involved emitting species. For example, the spectral range of co-$ZnGa_2O_4:Mn^{2+},Eu^{2+}$ MPLs is composed of the Mn^{2+} and Eu^{2+} bands, showing a persistent range broader than that of single Mn^{2+}-doped cases. In other situations, the Mn^{2+} ion can also act as a sensitizer for RE (*e.g.*, Ce^{3+} [232], Eu^{3+} [236], Tb^{3+} [237], Pr^{3+} [238], Sm^{3+} [233, 239], Dy^{3+} [90, 220, 240], Tm^{3+} [241], Eu^{2+} [90, 92, 241, 242]), multiple RE/non-RE [92, 240-241, 243-248], and non-RE co-dopants (*e.g.*, Bi^{3+} [234-235, 249-253], Cr^{3+} [194, 254], Mn^{4+} [255] *etc*), which is a relevant strategy for broadening and harvesting the emission spectral range as well as enhancing

the spectral intensity and realizing the tunable fluorescence for the solid-state lighting technology such as phosphor-converted white LEDs. With these spectral properties, the Mn^{2+} MPLs, similarly to one previous work that uses the fluorescent Zn_2GeO_4:Mn^{2+} (noted that it is not MPL) as photocatalyst [256], can couple with the PCMs to form the MPL@PCM composites.

2.3 ns^2-type cation-doped MPLs

Bandlike persistent luminescence can also be achieved in MPLs doped with ns^2 cations like Bi^{3+} [141, 149, 234, 257-269] or Pb^{2+} ion [270-273] (**Table 4**). Unlike the Mn^{4+} and Cr^{3+} ions yet similar to the Eu^{2+}, Ce^{3+}, and Mn^{2+} ions, single Bi^{3+} ion, depending on different crystal hosts, can exhibit the fluorescence broadly spanning from UV, blue, yellow and to reddish/red [45, 274-285]. In many cases, the Bi^{3+} ion also can be used as an efficient sensitizer for the RE or non-RE co-dopants (*e. g.*, Mn^{2+} [234-235, 249-250, 253], Eu^{3+} [91, 130, 149, 286-288], Tb^{3+} [150, 287], Dy^{3+} [288-289], Pr^{3+} [290], Sm^{3+} [291-292], 3*d* Mn^{4+} [293-296], and Cr^{3+} ions [189, 297]), and multiple RE/non-RE co-dopants [288, 298-301] to improve or influence the fluorescent properties of these co-dopants. Sometimes, the Bi^{3+} can spread the persistent potentialities toward the short wavelength region, allowing the persistent range being broader than that with single RE and TM dopant. This, as we will discuss further, is of particular interest and importance for the MPL@PCM composites design. In addition, the up-converting optical properties of the RE ions like the Yb^{3+} [183, 302], Er^{3+}/Yb^{3+} [303], and Er^{3+}/Tm^{3+}/Yb^{3+} [304] can sometimes be modified by Bi^{3+} ion. Although the number and type of Bi^{3+} MPLs are also not plentiful as compared to those RE-based MPLs, they are desirable for the photocatalytic purposes due to the broad and host-dependent persistent range (**Figure 8**). Besides, the Pb^{2+} ion is also found to have the persistent phenomenon, but its number is much more limited as regard to its severe toxicity. As some works have indicated, however, the intensity maxima of Pb^{2+} ion strongly depends on crystal host, excitation wavelength, doping concentration and external temperature [269-273, 305-309], but its emission and persistent regions are usually located in the UV region (**Figure 8c**). Thus, this UV persistent feature allows the Pb^{2+} ion to have the potential to couple with the absorption region of many PCMs. In fact, all the ns^2-type MPLs feature broad spectral range, with a full width at half maxima (fwhm) value larger than 50 nm (in some cases, the fwhm value like in $CaGa_2O_4$:Bi^{3+} [269] can nearly reach 200 nm). As for ns^2-type cations, they have a significant contribution in the UV region (**Table 4**, and **Figure 8**), which may couple with the PCMs in the MPL@PCM

composites. These UV features are unique for ns^2-type ions that other ions like the *f-f* and *d-f* RE and 3*d* ions do not have.

2.4 Self-activated bulk MPLs

Unlike the above RE and non-RE MPLs that require at least an external RE or non-RE ion as the luminescent center, interesting to mention here is that the bandlike persistent luminescence are also observed frequently in some self-activated compounds, where the luminescence is assigned to the complex groups and/or defects [168, 170, 177, 199, 215, 225, 310-342]. In general, the emitted spectra are ultra-broad and excitation / temperature-dependent (**Table 5**, and **Figure 9**). However, the self-activated MPLs usually sustain a relatively short persistent duration and low intensity when compared to the RE and non-RE MPLs, although a few MPLs (*e.g.*, $Zn_3Al_2Ge_2O_{10}$ [177], $Mg(Mg,Sn)O_4$ [323]) are able to sustain their duration for several hours (**Table 5**). Although the emission and persistent bands of the self-activated MPLs can match with the absorption region of a variety of photocatalysts (even at some conditions at a given temperature) and some of them like $ZnGa_2O_4$ [310, 325], and $Zn_xGa_2O_{3+x}$ [342]) have been tested as photocatalysts to decompose the Rhodamine B (PhB), most of them have not yet been explored for the photocatalytic purpose.

2.5 NIR-converted MPLs

The last category of MPLs involves the conversion of NIR radiation (typically 800 - 1000 nm) to the visible / UV persistent luminescence. These compounds are referred to the up-converted MPLs (UC-MPLs), and they are mostly activated with the 808 nm and 980 nm NIR light. In this case, to realize the UC process in UC-MPLs, it generally needs an Yb^{3+} ion that efficiently absorbs the 980 nm NIR photons or an Nd^{3+} ion that can absorb the 808 nm NIR photons [40, 135, 143, 193, 302-304, 343-359].

To access the UC NIR, UC visible or UCPL light, except for Nd^{3+} and/or Yb^{3+} ions, it also needs other RE and/or non-RE ions like Cr^{3+} [40, 178, 183, 193, 343-344, 346-347, 349-350], Pr^{3+} [125], Ce^{3+} [347, 351], Mn^{2+} [352-353, 355, 359], Tb^{3+} [301], Eu^{2+} [359-361], Eu^{3+} [183, 301], Tm^{3+} [144, 249, 301, 304, 350, 358, 359], and Er^{3+} [40, 144, 178, 303-304, 346, 349, 354, 359] (**Table 6**, **Figures 10-11**), or to construct the hybrid composite consisting of the NIR-to-visible UC nanocrystals aggregated onto the MPLs so as to activate the persistent luminescence through re-absorbing the UV or visible photons that are emitted from the UC nanomaterials (*e.g.*, the core / shell β-$NaYF_4$:Yb,Er/$NaYF_4$@CaS:Eu^{2+},Tm,Ce [343], $NaYF_4$:Yb,Tm@$CaAl_2O_4$:Eu^{2+},Nd [360],

$NaYF_4$:Yb,Tm@(CaSr)S:Eu^{2+} [360], and β-$NaYbF_4$:Tm/$NaYF_4$@$Zn_{1.1}Ga_{1.8}Ge_{0.1}O_4$:Cr [361]). As a result, exciting with the 980 nm or 808 nm NIR light not only leads to the Er^{3+} (**Figure 10b**) and the Tm^{3+} fluorescence (**Figure 11a**) but also sometimes brings about the persistent luminescence from the co-dopants like the yellow, red or NIR light from the Cr^{3+} (**Figure 10a**,**d**, and **Figure 11c**), Mn^{2+} (**Figure 10c**, and **Figure 11a**), and Ce^{3+} ions (**Figure 11b**)). Note that the UC-MPLs based on the phonon-assisted UC charging are also reported in some Cr^{3+}-doped crystal systems (*e.g.*, $Zn_3Ga_2GeO_8$:Cr^{3+}, **Figure 10d**) [362], and $ZnGa_2O_4$:Cr^{3+} [363]), although the cases are rare.

At last, it is worth noting that the MPLs could sometimes act as the photocatalysts by themselves if their persistent spectra have overlapped with the absorption range of the photocatalytic-toward materials (PTM). Attempts based on the MPLs have made for the H_2 production or RhB degradation, such as $Sr_2MgSi_2O_7$:Eu^{2+},Dy^{3+} [66], $Sr_4Al_{14}O_{25}$:Eu,Dy,Bi [66], $ZnGa_2O_4$:Cr^{3+} [197], $ZnGa_2O_4$ [310, 325], $Zn_xGa_2O_{3+x}$ [342], Ga_2O_3:Cr^{3+},In^{2+} [364], Ga_2O_3:Cr^{3+},Zn^{2+} [365]. However, the photocatalytic efficiency of such MPLs taken alone is always lower than that under the corresponding MPL@PCM composites when there is no external light source to continuously provide the photon energy. All in all, from the above summarization, the MPLs exhibit a bright future in the photocatalytic field.

3. PCMs, MPLs, and MPL@PCM composites: working principles and design consideration

3.1 Consideration of PCMs

In a semiconductor photocatalyst, the photocatalysis is based on the photon-induced electrons and holes separation, followed by their migration to the surface of PCMs. Thus, the carriers provide a chemical potential by means of a redox process to molecules adsorbed onto the materials [366-367]. Except for the photon-induced charge separation which is a beginning of photocatalytic reaction, the two major aspects, *i.e.*, the band gap of semiconductor and charge migration, play an important role in the photocatalytic efficiency in its following processes.

Band gap of the semiconductor

Whether the photons can or not induce the electron-hole pairs strongly depends on the comparison of how the photon energy scales respective to the optical bandgap of a semiconductor. Only the photons with the energy larger than the optical bandgap can induce the electron-hole pairs, *i.e.*, the smaller the optical bandgap the longer the wavelength of the incoming absorbed photons. As a result, the optical window available for photocatalysis should be broader than the photon energy

of an external irradiation source. However, a smaller optical bandgap is equivalent to a smaller redox potential, showing that it is not advantageous to decompose the stable chemical bonds of the associated organic matter. In **Figure 12**, we can see, for instance, that the anatase form of TiO_2 (α-TiO_2) has an optical bandgap of 3.2 eV that corresponds to ~387 nm photons [367-368]. Its oxidation energy level (*i.e.*, the bottom of the conduction band) is lower than the O_2/H_2O level, while the reduction energy level (*i.e.*, the top of the conduction band) is higher than H_2/H^+ (SHE) [369]. This makes the α-TiO_2 particularly relevant to produce the radicals for small organic dyes molecules decomposition [370], water splitting [371], CO_2 reduction [372] *etc*. Although the small optical bandgap could extend the optical window for the photon-induced photocatalysis process, it does not favor the degradation of chemical bonds with high reduction or low oxidation energy levels. For example, Bi_2O_3 has an optical bandgap smaller than TiO_2, but its reduction energy is insufficient to the H_2 - H^+ photocatalytic reaction.

Charge migration

Charge migration of photon-induced electrons and holes to the surface of PCMs is the second critical issue. In fact, this step is usually affected by recombination of the charge carriers or by defects that both contribute to lower the number of reactive charge carriers from PCMs [366, 369, 371]. Thus, the number of reactive carriers contributing to the photocatalysis is determined by: (**i**) the distance separating, where the charge carriers generated to the PCM surface must be as small as possible while the mean free path of charge carriers in the host fundamental bands must be as large as possible, and (**ii**) the distance that the charge carriers can transport in the conduction band. Thus, to achieve (**i**), small particle diameter is often required so as to confine the carriers in a small region [373]; but for (**ii**), the transportation distance of the carriers is directly determined by the lifetime of the carriers in the conduction band that usually inverses proportional to the recombination rate, thus the inhibition of electron-hole recombination is advantageous to the charge migration and improve the photocatalytic efficiency [374]. However, controlling the electron-hole recombination rate is still now a difficult issue because it seems to be only determined by the band structure of materials rather than the external condition, although the change of band structure can be controlled in atomic scale by using the doping method, such as doping of TiO_2 with Fe^{3+} or Nb^{5+} ions [375]. Furthermore, the stacking of particles is usually not advantageous to the light penetration, thus the desirable photocatalytic particles should distribute

homogeneously and the thickness should be controllable, with the aim of optimizing the photon absorption and enhancing the photocatalytic efficiency. In this case, we have summarized in **Table 7** several mainstream PCMs and corresponding synthesis treatment route, along with their average particle size and optical characteristics.

3.2 Consideration of MPLs

The consideration of MPLs is mainly based on the ability of their photon management. That is the quantum efficiency (QE) of the photon emission, which includes the photoluminescence (PL) and persistent luminescence simultaneously [105]. On one hand, in an MPL@PCM system consisting of PCMs deposited onto the surface of MPLs, we expect first that the MPL can absorb the excess photons that pass through the PCM layer and then generates a secondary luminescence to excite the PCMs again. On the other hand, the MPL is also expected to store the incoming photon energy by trapping carriers for a desirable time. With the aid of the thermal release, these trapped carriers gradually return to the luminescent centers and generate the persistent luminescence, continuously acting as the photon resource for the PCMs after switching off the external excitation source. In this frame, both the PL and persistent luminescence contribute to the photocatalytic process and, thus, can optimize the incoming of photon energy and the resulting photocatalytic efficiency [61, 106]. With these considerations, a MPL with stronger PL and persistent intensity as well as longer persistent duration is more desirable for providing the photons to the PCM when there is no external excitation source. In addition, the persistent spectral region should lie in a spectral region where the PCMs also lie in, for instance, those MPLs (**Tables 1-6**) with the spectral regions that can match with the absorption range of the PCMs (*e.g.*, Ag-AgCl [63], g-C_3N_4 [65], $BiVO_4$ [72], and Ag_3PO_4 PCMs [64, 376], whose optical bandgap fall in the range of 2.5~3.0 eV). So far, the PCMs that meet the above conditions include, such as, aluminates like $MAl_2O_4:Eu^{2+},Dy^{3+}/Nd^{3+}$ (M: alkaline) [60-62, 64, 67, 70-71], and silicates like $M_2MgSi_2O_7:Eu^{2+},Dy^{3+}$ [66, 72, 376-379].

Moreover, another working principle of the MPLs we need to consider is the physicochemical stability, typically in presence of moisture. For this aspect, aluminate-based MPLs are not stable in water or moisture environment for a long time [75], because they can decompose easily and cause loose luminescence. As a matter of comparison, silicate-based MPLs are, in this context, largely preferred because they can sustain the persistent luminescence in water for a relatively long term, with persistent intensity degradation in an acceptable range. In fact, the MPLs we listed in **Table 8**

confirm the conclusion, in which almost all of the MPLs@ PCMs composites that are proved for the photocatalytic degradation of aqueous phase pollutant are now those silicate-based MPLs.

3.3 Consideration of MPL@PCM composites

The first basic requirement for the design of "persistent-photocatalytic" MPL@PCM composites is that the persistent spectrum of the MPLs overlaps the absorption region of the PCMs (**Figure 13**) so that the reabsorbed photons can generate the electron-hole pairs continuously when the external irradiation source is off. Looking back **Section 2**, however, the MPLs do not have equivalent attributes, because those showing a persistent duration shorter than a few tens of minutes and/or having a persistent band lying out of the absorption range of PCMs or narrow un-tunable spectra are, in practice, no use for the current purpose, except for some specific situations where a specific persistent line of the MPLs for the PCMs is wanted. Conversely, the MPLs featuring broad band and long persistent duration, especially for those showing a spectral contribution extending to the UV spectral range, are privileged. For example, the melilite-type Ce^{3+}-doped $Ca_2MgSi_2O_7$ whose persistent band peaks at 380 nm is suitable for a TiO_2 PCM that presents an absorption cut-off at 387 nm, whereas other types of PMLs like $CaAl_2O_4:Eu^{2+},Nd^{3+}$ with emission peaking at ~440 nm [49, 60-61, 71], $SrAl_2O_4:Eu^{2+},Dy^{3+}$ with ~520 nm emission [64, 379], and $Sr_2MgSi_2O_7:Eu^{2+},Dy^{3+}$ with ~465 nm emission [66, 72] are unsuitable. With this logical thinking, the TiO_2 is usefully associated with MPLs, as proved by the $Sr_4Al_{14}O_{25}:Eu^{2+},Dy^{3+},Bi^{3+}@TiO_2$ for the MB degradation [69], $BaAl_2O_4:Eu^{2+},Nd^{3+}@TiO_2$ for the benzene decomposition, $Ca_2MgSi_2O_7:Ce@TiO_2$ [366] and $Mg_3Y_2Ge_3O_{12}:Bi@TiO_2$ [380] for the MO degradation, *etc*. Noteworthy, the absorption efficiency of PCMs can be boosted by widening or adapting their absorption range to the persistent range of MPLs by using some appropriate strategies. For example, the absorption efficiency of TiO_2 can be improved by doping with nitrogen [60, 106, 378], building the hybrid photocatalysts [16, 25-27], or attaching onto its surface a certain type of noble metal nanoparticles with suitable fermi-level from which the hot electrons can be extracted and transferred, like TiO_2-Ag [367] and Ag-BiOBr [381] (**Figure 12**). In particular, there is no band gap in metal, but in theory an electron at low energy level could be excited to high level when the photon is adsorbed by nano-metal particles. Then a hole is induced in a low level. An instantaneous charge separation is induced at that time. Hence, this process involves the excitation of an electron located in low energy levels to high energy levels of the noble metal nanoparticles, leaving a hole in low energy levels. An

instantaneous charge separation follows at this time. The electron at high level (*i.e.*, hot electron) then travels through in noble metal and thus has some probability to migrate to the surface of the nano-particle. Here, the hot electron can be transferred to the conduction band of another material that has close contact to the metal, subject that the Fermi-level of the two associated materials have the suitable energy. With this process, the hot electron can contribute to the photocatalytic activity if it is located at the surface of the relevant materials. For example, introducing the Ag nanocrystals in the ZnO:Co-Ag composite leads to three additional absorption bands in the range of 500-700 nm in superimposition with the UV-vis absorption of the ZnO:Co catalyst [68]. Thus, in general, enlarging the absorption range can improve the corresponding photocatalytic ability.

The MPL@PCM composite structure typically consists of fine particles of the PCMs attached onto the MPL with a coating process that depends strongly on the specific type of the PCMs, the synthesis strategies, and the post- or after-treatment routes. For instance, $BiVO_4$ and g-C_3N_4 can be *in-situ* grown onto the surface of the $Sr_2MgSi_2O_7:Eu^{2+},Dy^{3+}$ by using hydrothermal [72] and sintering methods [379], respectively; while nano-TiO_2 particles are preferably deposited onto the surface of $CaAl_2O_4:Eu^{2+},Nd^{3+}$ [61, 71] or $Ca_2MgSi_2O_7:Ce^{2+}$ [366] particles rather than grown. Thus, constructing a suitable type of "persistent-photocatalytic" MPL@PCM composite actually is a process of constructing PCMs coating or loading MPLs structure.

3.4 Mechanistic models

An ideal mechanistic model established for illustrating the "persistent-photocatalytic" process needs to meet at least the two requirements, *i.e.*, efficient photon utilization and effective charge separation. Upon irradiation with a suitable light, both the MPLs and PCMs in the MPL@PCM composites can be excited if this irradiation light is located either in the excitation range of MPLs and the absorption range of PCMs, or only in the the excitation range of MPLs but the emission range from MPLs overlaps with the absorption range of PCMs. In the PCMs, the absorbed energy can be converted to charge carriers; while in the MPLs, it is partly stored in traps and partly converted to photoluminescence (PL). Upon a continuous light irradiation, the PCMs can be sensitized from both sides, namely, the photons directly emitted from the external irradiation source, and the photons emitted from the MPLs. When the external light is cut off, the thermal release of the traps allows MPLs to generate the persistent luminescence [105] that can act as the inner light resource for the PCMs until the MPL@PCM composite is recharged again. Once the

PCMs are irradiated, separation and transport of charge carriers to the surface of PCMs must be achieved with minimum losses. Besides, if PCMs and MPLs have a very close contact (*i.e.*, a clean interface, and a suitable band structure) [366], the charge separation, which is confirmed by recording a photocurrent, can be achieved *via* a charge transfer process. In this concern, the formation of a hybridized hetero-junction within the MPL@PCM composite is highly desired, because it can have efficient charge separation (**Figure 14**). In such a hybridized hetero-junction, the electrons would tend to migrate to MPLs with a low energy (more oxidative) location, while the holes tend to migrate to PCMs with a high energy (more reductive) location. If the MPLs and PCMs have band alignment, the above migrations happen simultaneously, leading to the accumulation of holes and alignment in the two respective materials and the formation of the reduction and oxidation centers accordingly. As a result, the charge recombination is inhibited. However, since it requires a clean interface (*i.e.*, without other impurity materials such as the excessive chemical reagents) and suitable structures of both components, we find, for instance, in $Sr_2MgSi_2O_7:Eu^{2+},Dy^{3+}@Ag_3PO_4$ [377] (**Figure 15)**, that the band-to-band transition in the PCMs is often followed by the transfer of an electron to the conduction band of the MPLs. The better photon utilization by the inner light photons from $Sr_2MgSi_2O_7:Eu^{2+},Dy^{3+}$, along with a charge separation between the Ag_3PO_4 and the MPL, improve the catalytic efficiency of this hybridized hetero-junction composite substantially.

4. Synthesis strategies of "persistent-photocatalytic" MPL@PCM composites

The photocatalytic performance of "persistent-photocatalytic" MPL@PCM composites can be influenced by various factors such as the particle size and morphology, microstructure, persistent intensity and duration of MPLs and PCMs, and the photocatalytic efficiency of PCMs. All these factors are initially determined by the synthesis methods. Once a given synthesis route is selected to fabricate the MPL@PCM composite, the corresponding photocatalytic behavior is usually determined unless other factors like the oxygen and moisture in the air, the variation of external temperature and post-synthesis route appear. Based upon the previous works [60-73, 107, 310-312, 342, 364-366, 376-385], we show the synthesis methods of the reported MPL@PCM composites (**Table 8**). The synthesis consideration of the MPL@PCM composites is more complicated than that of singly achieving the MPLs and PCMs, because it needs to take into a joint consideration all the possible properties of both materials. Except for the MPLs that are directly used as

photocatalyst (*e.g.*,$Sr_2MgSi_2O_7:Eu^{2+},Dy^{3+}$ [66], $Sr_4Al_{14}O_{25}:(Eu^{2+},Dy^{3+},Bi^{3+})$ [69], $ZnGa_2O_4:Cr^{3+}$ [197], $ZnGa_2O_4$ [310], $Zn_xGa_2O_{3+x}$ ($0.8 \leq x \leq 1.0$) [342], $Ga_2O_3:Cr^{3+},In^{3+}$ [364], $Ga_2O_3:Cr^{3+},Zn^{2+}$ [365], and $ZnGa_2O_4$:Ti [382]), the synthesis method generally contains three step processes, and it usually uses the powder reagents as the starting materials, *i.e.*, first the MPLs are synthesized basing upon a nominal stoichiometric chemical ratio of MPLs, then the PCMs are bought (if commercially available, such as TiO_2), or specifically processed (*e.g.*, the hydrothermal, chemical, or sol-gel methods) for the optimization of the photocatalytic properties (*e.g.*, TiO_2:N and $BiVO_4$), and at last the two components are assembled to form the MPL@PCM composite. Because of the powder-typed mixtures, different synthesis strategies can be applied for achieving the MPCs, depending on the desired processing cost, production scale, and targeted particle size. Normally, the solid-state reaction method is used for micro-sized MPLs, while the sol-gel and hydrothermal routes are used for nanoscale MPLs. We summarize in **Tables 7-8** the principal routes that are used for the synthesis of MPLs, PCMs, and MPL@PCM composites, and show in **Figures 16-17** representative SEM, FESEM, TEM, and HRTEM images revealing the structural organization of the MPLs, PCMs, and MPL@PCM composites. We focus below on reviewing the solid-state reaction, sol-gel, hydrothermal, combustion, mechano-chemical, and chemical vapor deposition (CVD) synthesis routes for MPL@PCM composites.

4.1 Solid-state reaction & combustion routes

The solid-state & combustion reaction routes are the most frequently used. The synthesis process is relatively simple, low-cost, and quite suitable for large-scale production. However, they easily lead to distortions and imperfections of MPLs crystals, including various kinds of “bad, and ugly” defects (*e.g.*, surface and interstitial cation and anion vacancies, point defects [44]), which affect the persistent luminescent properties. The two routes are especially desirable for producing the MPL@PCM composites with micro-size particles, such as the $ZnGa_2O_4:Cr^{3+}$ [197], $BaZrO_3:Mg^{2+}@TiO_2$ [311], $Ca_2MgSi_2O_7:Ce^{3+}@TiO_2$ [366], $Sr_2MgSi_2O_7:Eu^{2+},Ce^{3+}@g\text{-}C_3N_4$ [379], $(3ZnO:Ga_2O_3:2GeO_2):Cr^{3+}@TiO_2$ [383], as depicted in **Figures 12a-f**. To better make the PCMs being individually deposited onto the surface of the MPLs, the PCMs should feature nano-sized particles, such as Ag_3PO_4 [377], $g\text{-}C_3N_4$ [379], and TiO_2 [311, 383] (**Figures 16f-h**). Taking the $Ca_2MgSi_2O_7:Ce^{3+}@TiO_2$ composite for example, Wu *et al* [366] synthesized the $Ca_2MgSi_2O_7:Ce^{3+}$ MPL at 1300 ^oC and then compressed into a pellet. Followed by sintering at a temperature of 900

^{o}C, the pellet was transformed into a ceramic substrate that immobilizes the nano-sized TiO_2 (P25, Macklin) particles onto its surface. After dropping the TiO_2 powder onto the surface of the MPL ceramic substrate and sintering again at 400 ^{o}C, the $Ca_2MgSi_2O_7:Ce^{3+}@TiO_2$ composite features the persistent luminescence and the photocatalytic properties simultaneously. Such strategies are also applied for the MO degradation using the $Mg_3Y_2Ge_3O_{12}:Bi^{3+}@TiO_2$ composite [380].

4.2 Sol-gel and hydrothermal approaches

Unlike the solid-state & combustion reaction routes, the hydrothermal and sol-gel methods are popular for the synthesis of MPL@PCM nanocomposites with regular particle size and smooth particle surface, as proved by the $Sr_2MgSi_2O_7:Eu^{2+},Dy^{3+}$ [66], $CaAl_2O_4$:(Eu,Nd)@Fe_2O_3-$SrTiO_3$ [70], and $Sr_2MgSi_2O_7:Eu^{2+},Dy^{3+}@BiVO_4$ [72]. Although they sometimes can make the composites featuring irregular micro-size particles and rough surfaces (*e.g.*, $Ca_2Al_2SiO_7:Ce^{3+}$@Ag-AgCl [63], $Sr_4Al_{14}O_{25}$:(Eu,Dy)@g-C_3N_4 [65], $MgAl_2O_4:(Pr^{3+},Dy^{3+})$@Cr-$TiO_2$ [107], and GP@Fe-N-TiO_2 [384], **Figures 17a-d**), the particle size and surface morphology of the MPLs after being loaded or coated with the PCMs do not change significantly. If the whole synthesis processes were based on the sol-gel or hydrothermal route, the chance of achieving irregular micro particle size and rough surface becomes less, such as the GP@Fe-N-TiO_2 achieved by a hydrothermal approach [382].

4.3 Chemical vapor deposition (CVD) route

Compared to the above approaches, the CVD route is infrequently used. So far, to the best of our knowledge, only Kim *et al* in 2015 [71] and 2016 [73] have used the CVD method to prepare the $CaAl_2O_4$:Eu,Nd@TiO_2 and $Sr_4Al_{14}O_{25}$:Eu,Dy@TiO_2 composites by deposition of the TiO_2 onto the surface of the solid-state processed $CaAl_2O_4:Eu^{2+},Nd^{3+}$ and $Sr_4Al_{14}O_{25}:Eu^{2+},Dy^{3+}$ particles, respectively. In the synthesis process, the $Ti[OC(CH_3)_2]_4$ was used as the TiO_2 precursor and the oxygen gas was used as reaction gases under a very low-pressure condition (*i.e.*, at 1 Torr).

4.4 Others

As for any composite system, the quality of the interfacial contact between the MPLs and PCMs is essential to yield a synergistic coupling between the two constituents of "persistent-photocatalytic" MPL@PCM composites. In this purpose, *in-situ* growth of the PCMs onto the surface of the MPLs, such as directly coating the photocatalytic precursors onto the surface of the MPLs [379], is preferred. The PCMs can be also synthesized firstly, and then load on the surface of MPLs directly [60, 73], but this process usually needs a hydrophilic surface to attract the MPLs and PCMs *via*

chemical bonding. Thus, it often needs to modify the surface of PCMs or MPLs using some type of materials such as kaolin [366, 380, 386-387] to favor the grafting. However, the surface chemical functional groups of the PCMs or MPLs are often instable and even can be eliminated easily when the synthesis process is at high temperature, leading to a clean surface of PCMs or MPLs. That is, there is no PCMs and/or MPLs components in the targeted MPL@PCM composites. Obviously, although the "a clean interface" mentioned here is different from the case of "a clean interface" mentioned in "**3.4 Mechanistic models**" section, both lead to a bad photocatalytic acitivity.

Furthermore, a single synthesis route can also be used for directly obtaining the MPL@PCM composites, but some hybridized MPL@PCM composites generally need a coupling arrangement of multiple approaches to achieve an optimized photocatalytic property. Hence, such MPL@PCM composites needs to explore and develop other approaches. Typically, an in-depth study on the energy transfer from the MPLs to the PCMs is necessary. For example, Li *et al* [62] in 2010 used the sol-gel method to prepare the $BaAl_2O_4$:Eu,Dy@TiO_2 composite by deposition of the TiO_2 onto the surface of $BaAl_2O_4$:Eu,Dy and adjustment of the TiO_2 loading content, but the photocatalytic efficiency is not desirable because of a low utility of persistent energy by the PCMs, owning to the interface gap between MPLs and PCMs.

5. Photocatalytic application of self-luminous MPL@PCM composites

Until now, a number of materials, composites, and hybrids, such as the Ag-TiO_2 [1, 71], TiO_2 [16, 49, 71, 388], Ag-AgCl [24, 63], MoS_2-TiO_2 [25], TiO_2-MOF [26], Au-TiO_2 [27], BiOCl-$BiVO_4$ [28], Ag_3PO_4 [64, 374-375, 390], ZnO:Co-Ag [68], g-C_3N_4 [379], COF [389], AgBr-Ag_3PO_4 [391], $YFeO_3$ [392], g-C_3N_4-Cs_xWO_3 [393], g-C_3N_4-Bi_2WO_6 [394], Co_3O_4-g-C_3N_4 [395], ZnO-SnO_2 [396], BiOCl [23, 397], BiOCl-rGO [398], $M_2Sb_2O_7$ (M = Ca, Sr) [399], CNTs/P-TiO_2 [400], $BiFeO_3$ [401], and AgBr-WO_3 [402], are reported to have the photocatalytic properties, and they have been suggested for use in, *e.g.*, photocatalytic elimination of bacterial pathogens [9], degradation of methyl orange (MO) [63, 68, 391, 396, 403-405], methylene blue (MB) and RhB [141, 311, 342, 376, 381, 406-407], removal of gas-phased materials [61, 67, 70, 385, 408-413], production of hydrogen (H_2) and oxygen (O_2) and splitting of water [57, 66, 414-423], degradation of pesticide atrazine and antibiotic oxytetracycline [384], reduction and oxidation of gas such as CO_2 [424], cleavage and amination of chemical bonds such as the C-C bond [425], *etc*. However,

only a tiny of these PCMs have been reported to couple with the MPLs to fabricate the hybrid MPL@PCM composites (**Table 8**). Attempts made for other PCMs still have not been tried in previous works, leaving a big room of investigation for this research subject in the future. Until now, the photocatalytic applications of the hybrid MPL@PCM composites are mainly focused on the degradation of MO, MB, and RhB dyes, removal of poisonous gas such as nitric oxide (NO) and benzene, and photocatalytic production of hydrogen (H_2) and oxygen (O_2).

5.1 Methyl orange (MO) degradation

The MO is a relevant and widely used model organic dye to qualify the photocatalytic degradation performances of a PCM and it, under different conditions (*e.g.*, at different pH values, temperature, external irradiation intensity and duration), can be conveniently monitored by using UV-visible spectroscopy. Normally, in distilled water, the MO shows two absorption bands with the intensity maxima peaking at 270 nm and 465 nm [403-404], as shown in **Figure 18a**. The intensity and position of the latter band are in general used to monitor the degradation rate upon continuous irradiation with an external sources such as sunlight [388], UV [389], arc lamp [391], and NIR light [304, 358]. When the MO is placed in presence of the $Sr_2MgSi_2O_7:Eu^{2+},Dy^{3+}@Ag_3PO_4$ [377] (**Figure 18b**), and $Mg_3Y_2Ge_3O_{12}:Bi^{3+}@TiO_2$ [380], its photocatalytic degradation persists for a relatively long time after removal of the UV light source. In the cases of $Ca_2Al_2SiO_7:Ce^{3+}$ MPL (**curve 1**), Ag-AgCl PCM (**curve 2**), and $Ca_2Al_2SiO_7:Ce^{3+}$@Ag-AgCl composite (**curve 3**) [63] (**Figure 18c**), it is found that after putting in dark for 30 min (*i.e.*, with light off), the MO concentration, corresponding to the $Ca_2Al_2SiO_7:Ce^{3+}$, Ag-AgCl, and $Ca_2Al_2SiO_7:Ce^{3+}$@Ag-AgCl composite, respectively, is reduced from 1.0 to ~0.93, ~0.98, and ~0.99 (**Figure 18c**). This indicates that the MO can be decomposed even though there is no external UV light source. Such experimental observations can also be found in other PCMs like Ag-AgCl [63], and TiO_2 [369, 371, 375, 426], which are attributed to the self- or/and photocatalyst-sensitized MO degradation [426]. Hence, the self-sensitized degradation issue should attract significant attention in the future research. Under a simulated solar light irradiation for 5 min, the residual MO in the Ag-AgCl PCM and $Ca_2Al_2SiO_7:Ce^{3+}$@Ag-AgCl composite is decreased dramatically; the photocatalytic activity of the Ag-AgCl PCM being above that of the $Ca_2Al_2SiO_7:Ce^{3+}$@Ag-AgCl composite. Moreover, the MO concentration in $Ca_2Al_2SiO_7:Ce^{3+}$, along with its next process with the light off (35-55 min), does not change, indicating that $Ca_2Al_2SiO_7:Ce^{3+}$ does no longer decompose the MO

when the MPL-sensitized MO degradation is finished. This $Ca_2Al_2SiO_7:Ce^{3+}$-sensitized MO degradation, as this work reveals, is independent of whether the light source is off or on. Besides, despite the $Ca_2Al_2SiO_7:Ce^{3+}$@Ag-AgCl composite can continue the MO degradation with the light off (**curve 3**, 35-55min), its final MO concentration is lower than that of the Ag-AgCl PCM alone (**curve 2**, 35-55min). This may be because the MPL can partially block the light reaching the PCM and thus induce the decrease of the overall MO degradation content. As a result, the light filtering effect of the MPL and/or the decrease of the active surface of the PCM (which is due to its binding to the MPL) is more significant than the possible decrease in the electron-hole recombination due to the migration of the generated conduction band electron to MPL. As for the continuous MO degradation within 35-55min, it can be assigned to the gradual release of the stored photon energy from the $Ca_2Al_2SiO_7:Ce^{3+}$ followed by transferring to the Ag-AgCl. As a result, when compared to the photocatalytic effect of the Ag-AgCl alone, ~15% of the retained MO content is decomposed further in the $Ca_2Al_2SiO_7:Ce^{3+}$@Ag-AgCl composite after removal of the light for 20 min (**Figure 18d**). Hence, the above findings reveal that the persistent luminescence of the $Ca_2Al_2SiO_7:Ce^{3+}$ (its duration can last several days after instantly pre-exciting and removal of a 254 nm UV source [63, 406]) plays an essential role in sustaining the photocatalytic activity of the Ag-AgCl for MO degradation. Such results are confirmed by other MPL@PCM composites like $Sr_4Al_{14}O_{25}$:Eu,Dy@ZnO:Co-Ag [68], $Sr_2MgSi_2O_7$:Eu,Ce@Ag_3PO_4 [377] (**Figure 18b**), and $Mg_3Y_2Ge_3O_{12}:Bi^{3+}$@$TiO_2$ [380].

5.2 Methylene blue (MB) and Rhodamine B (RhB) degradation

Similar to the MO, the MB and RhB are also two frequently-used aqueous-phase organic dyes for modeling the photocatalytic activity of a PCM, but the absorption position and shape are different from the MO. The MB organic dye features a broad absorption band in the red spectral region (*i.e.*, 550-720 nm) with the maxima intensity at 663 nm and ~608 nm (shoulder), and it can be degraded using the PCMs like Ag–In–Ni–S nanocomposites upon irradiation with the sunlight and 100 W tungsten lamp [406], or by the β-$NaYF_4:Yb^{3+},Er^3$@BiOCl-rGO composites under UV irradiation [398]. The RhB dye features a substantially absorption range similar to that of the MO, but its absorption band is shifted to the range of 450-600 nm with two intensity maxima at 554 nm and ~520 nm (shoulder). The RhB dye can be degraded well using the ZnO-Au nanocomposites [427]. Both the MB and RhB dyes as the irradiation time goes on experience a gradual increase of

degradation. Typically, when the irradiation light source is off, they can be also decomposed (see **Figure 19a** (in dark condition, -1–0 min), **Figure 20a** (in dark condition, -0.5–0 min), and **Figure 20d** (in dark condition, -60–0 min)), independent of whether or not they are placed in the presence of PCMs, MPLs, and MPL@PCM composites. These observations are analogous to the case of the MO decomposition [369], and they are also assigned to the self- and/or photcatalysts-sensitized RhB degradation. Although the MPLs, such as the oxygen vacancy-rich $Zn_xGa_2O_{3+x}$ whose persistent spectral band matches the absorption region of RhB dyes [342], sometimes can be directly used as the PMC for the RhB decomposition and its decomposition effect is higher than the RhB self-sensitized degradation (**Figure 19c**), it needs a continuous UV light source to sustain this photocatalytic activity. This is because the persistent luminescent intensity and duration (about 10 min) of the $Zn_xGa_2O_{3+x}$ is not enough to efficiently degrade the RhB dye. Conversely, the degradation efficiency of the MB and RhB dyes can be continued for a relatively long time in the MPL@PCM composites where the MPLs can show the persistent duration for several hours, *e.g.*, $SrAl_2O_4$:Eu,Dy@g-C_3N_4@Au [57], $SrAl_2O_4$:Eu,Dy@Ag_3PO_4 [64], $Sr_2MgSi_2O_7$:Eu,Dy@Ag_3PO_4 [376], $Sr_2MgSi_2O_7$:Eu,Dy@g-C_3N_4 [379], and NL-PA@BiOBr [381]. Besides, for instance, the BiOBr@NL-PA under a 300 W Xe lamp shows the improved photocatalytic RhB decomposition compared to the BiOBr PCM alone [381] (**Figure 19d**), which directly proves that the use of MPL@PCM composite is beneficial to the photocatalysis. Although the NL-PA may partially block the light reaching the BiOBr, the effect seems not to make the final RhB concentration being lower than that of the BiOBr alone, which is different from some of the MO degradation [369].

Although it is well known that in the heterogeneous photocatalysis the dependence of pollutants degradation rate (r) on the photon flow (p) features a linear relationship when the irradiation photon flow is low (*i.e.*, $r = k^*p$, where k is the constant) and show an independent form at high photon flow [428], but all the reported works involving the use of MPL@PCM composites for photocatalysis still have not studied this relationship. Li *et al* [376] studied the influence of the persistent duration on RhB degradation by using the Ag_3PO_4@$Sr_2MgSi_2O_7$:Eu,Dy and Ag_3PO_4@ $Sr_4Al_{14}O_{25}$:Eu,Dy,Er composites in dark condition, and found that the photocatalytic activity keeps excellent stability after ten cyclic experiments (**Figure 19b**). Furthermore, previous works also reveal that other external environmental factors, such as the added content of MPLs and PCMs, and the persistent spectral position and duration of MPLs, have significant impact on the

photocatalytic MB degradation when the light source is off (**Figure 19c**, **Figures 20a-d**)). Along with "**5.1 Methyl orange (MO) degradation**" section and the following sections, we can notice that different works sometimes use different irradiation or pre-irradiation light as the main photon source for the photocatalysis. As revealed by several previous works that only involve the PCMs, we can realize further that the light source is also a very important factor affecting the final photocatalytic results. A given PCM under different light sources can sometimes show different photocatalytic activities, but so far it still lacks a systematic study on how different light sources influence on the photocatalytic activities of the MPL@PCM composites, leaving an open room for future research.

5.3 Removal of gas-phased nitric oxide (NO) and benzene

In addition to the soluble organic molecules or dyes degradation, the PCMs are also widely used for removing poisonous gas-phased materials such as TiO_2 for photocatalytic oxidation of NO_x gas [61, 67, 70, 408-410], TiO_2-polyacrylonitrile nanofibers for photocatalytic desulfurization and denitrification of flue gas [411], TiO_2-Y-zeolite for photocatalytic removal of toluene and benzene gas [412], and TiO_2-aluminum silicate fiber for removal of SO_2, NO and mercury gases [413]. However, all the removal process analogous to traditional photocatalytic process is performed under a continuous external irradiation. These PCMs terminate their photocatalytic activity after cutting-off irradiation source unless they are coupled with a type of suitable MPLs or directly using the MPLs as the PCMs. For example, Li *et al* [385] used the Ti-contained materials (*i.e.*, $SrTiO_3$ and Cr^{3+}-doped $SrTiO_3$) featuring the visible light-responsive activity as the PCMs to model the removal of NO gas under various LED lamps irradiation. They found that both the $SrTiO_3$ and Cr^{3+}-doped $SrTiO_3$ under red, green, blue, and UV LEDs have good photocatalytic activities in the shorter wavelength light regions, but only the Cr^{3+}-doped $SrTiO_3$ exhibits the photocatalytic performance in the longer wavelength regions (*i.e.*, 627 nm, and 530 nm) (**Figure 21a**). Further analysis reveals futher that the former is due to the presence of the oxygen vacancies in nonstoichiometric $SrTiO_3$ (Sr/Ti = 1.67), while the latter is attributed to formation of new donor levels by doping $SrTiO_3$ with Cr ion. Moreover, in this work, the authors revealed that doping with the external Cr^{3+} ion is a good strategy to extend the photocatalytic wavelength range. The drawback is, however, that once the irradiation UV light in the range of >290 nm is off, the Ti-contained materials stop their photocatalytic process. Even though they are coupled with the

$CaAl_2O_4$:(Eu^{2+},Nd^{3+}) MPL, this situation cannot be changed (*i.e.*, in the range of 0-5 min, **Figure 21b**). Although the $SrTiO_3$ under the UV irradiation (λ > 290 nm) removes the NO gas more effective than that with the Cr-doped $SrTiO_3$ (*i.e.*, in the range of 5-45 min, **Figure 21b**), it can sustain the superiority of NO removal in the $CaAl_2O_4$:(Eu,Nd)@Cr-doped $SrTiO_3$ composite after removal of the irradiation light (*i.e.*, the range of 45-200 min, **Figure 21b**). Specifically, the $CaAl_2O_4$:(Eu^{2+},Nd^{3+})@Cr-doped $SrTiO_3$ composite retains 8.2% of NO removal at 180 min, higher than 3.4% of that in the $CaAl_2O_4$:(Eu^{2+},Nd^{3+})/$SrTiO_3$ composite. Moreover, Li *et al* found that the light irradiation intensity also influences the photocatalytic removal of NO gas in the above composite systems significantly. To verify whether other MPL@PCM composites could be used for removing the NO gas, Li *et al* also tried the $CaAl_2O_4$:(Eu,Nd)@$TiO_{2-x}N_y$ (**curves 1-2**) and $CaAl_2O_4$:(Eu,Nd)@TiO_2 (**curve 3**) (**Figures 21c-d**) [61], $CaAl_2O_4$:(Eu,Nd)@TiO_2/Fe_2O_3:(Ta,N) [67], and $CaAl_2O_4$:(Eu,Nd)@$SrTiO_3$-Fe_2O_3 [70]. They also found that all of the composites under UV irradiation can remove the NO gas efficiently. The removal process is basically the same, but differs from that involved in the $CaAl_2O_4$:(Eu,Nd)@$SrTiO_3$ composite in the time range 5-45 min (**Figure 21b**). After turning off the UV irradiation, these MPL@PCM composites also keep highly efficient removal of NO gas in the time range 45-200 min. However, the final photocatalytic effects in the absence of the external light source are different from each other due to the coupled PCMs, although all of them use the persistent luminescence of the $CaAl_2O_4$:Eu^{2+},Nd^{3+} as the same inner irradiation source. In addition to the NO gas, a few years ago, Kim *et al* found that the $CaAl_2O_4$:Eu^{2+},Nd^{3+} [71] and $Sr_4Al_{14}O_{25}$:Eu^{2+},Dy^{3+} [73] can relevantly combine with TiO_2 and TiO_2-Ag PCMs to remove the benzene gas for more than 20 h after cutting off the light source. In particular, the TiO_2 or TiO_2-Ag PCMs under UV and visible light efficiently remove the benzene gas, but fail to remove the benzene gas without the light irradiation. Meanwhile, they found that the photocatalytic efficiency is reinforced by co-coupling the TiO_2 with Ag NPs, which is because the Ag NPs retard the electron-hole pairs recombination.

Although the previous works, based on the use of MPLs and PCMs to fabricate the MPL@PCM composites, are still not widely reported for removing or filtering poisonous gas-phased materials, the above-mentioned works prove that this design idea can broaden the application range of the MPL@PCM composites, providing some insights into removing other poisonous gas in the absence of available external irradiation source.

5.4 Hydrogen (H_2) and oxygen (O_2) production

Recently, Liu *et al* [57] used the $SrAl_2O_4:Eu^{2+},Dy^{3+}$ MPL in association with pristine g-C_3N_4-xAu PCM composites to design a novel self-luminous visible-light plasmonic photocatalyst composite (*i.e.*, g-C_3N_4-Au@$SrAl_2O_4:Eu^{2+},Dy^{3+}$) for photocatalytic hydrogen (H_2) evolution (**Figure 22**). In this multiscale composite, the gold nanocrystals were introduced to expand the absorption range of g-C_3N_4 to the visible region in order to better overlap the emission band of the $SrAl_2O_4:Eu^{2+},Dy^{3+}$ (**Figure 22a**). Despite the introduction of g-C_3N_4@Au, the persistent spectral position and shape of the $SrAl_2O_4:Eu^{2+},Dy^{3+}$ do not vary. By using a 300 W Xe lamp as continuous irradiatiation source, the optimal g-C_3N_4@0.6%Au composite produces 4.5 times more H_2 compared to the pristine g-C_3N_4 (**Figure 22b**), indicating the positive role of a suitable Au NPs amount on the H_2 production. For those systems without the pristine g-C_3N_4, however, there is no photocatalytic H_2 generation in the $SrAl_2O_4:Eu^{2+},Dy^{3+}$ and $SrAl_2O_4:Eu^{2+},Dy^{3+}$@Au under the same visible light (**Figure 22b**, red line), indicating the role of the pristine g-C_3N_4 in the photocatalytic H_2 generation. When the light is off, those systems without the $SrAl_2O_4:Eu^{2+},Dy^{3+}$ cannot show the photocatalytic H_2 generation. This is different from the MO, MB and RhB degradation cases where the three aqueous phase dyes can be decomposed slightly in the absence of the external irradiation source owning to the self- and/or photocatalyst-sensitized degradation. Thus, Liu *et al* proved the synergistic effect of the Au SPR in the g-C_3N_4-Au composite and the persistent luminescence in the $SrAl_2O_4:Eu^{2+},Dy^{3+}$, where only the g-$C_3N_4$@Au@$SrAl_2O_4:Eu^{2+},Dy^{3+}$ can sustain the photocatalytic H_2 evolution from water in a sunless environment (*i.e.*, in the absence of external irradiation light).

Unlike the above work reported by Liu *et al*, Cui *et al* [66] demonstrated that the brick-like and micrometer-sized $Sr_2MgSi_2O_7:Eu^{2+},Dy^{3+}$ MPLs could be directly used as a PCM for producing H_2 by the photocatalytic methanol reforming method under UV, visible light and dark conditions. The results reveal that the solar-to-hydrogen (STH) conversion efficiency under UV irradiation can be up to ~5.2%, which is slightly more than the highest STH conversion efficiency of 5 % for a particulate photocatalyst system [429-431]. In particular, the STH value can still be up to ~0.2 % in dark after removal of the UV light for 8 h. Moreover, the research conducted by Liu [57] and Cui *et al* [66] demonstrated that there are other factors that influence the photocatalytic efficiency of H_2 and O_2 production, among which the chemical nature and amounts of MPLs, PCMs, and

MPL@PCM composite, the assistance of surface plasmonic effect for spectral adaptation, the photocatalytic cycles, chemical and thermal stability of MPLs, PCMs and MPL@PCM composite, the external photocatalytic working conditions such as the PH value, temperature, and irradiation conditions (**Figure 23**). These factors provide insights into directing the future photocatalytic works by use of MPLs as an inner excitation light source to keep the photocatalytic activity. Since the persistent intensity of MPLs, such as $SrAl_2O_4:Eu^{2+},Dy^{3+}$ [57] and NL-PA [381], can be gradually decreased in the absence of the external irradiation light, intermediately recharging the storage energy by re-exciting the MPL is a feasible approach to keep the persistent intensity at a certain intensity, leading to a new concept, *i.e.*, "around-the-clock" photocatalytic activity.

6. Conclusions, challenges, and perspectives

Looking back on this review, we discloses the recent advances and prospets of the MPLs as inner secondary excitation light for photocatalytic application. We first compile the MPLs attractive for coupling with the PCMs to form the self-luminous MPL@PCM composites, including the MPLs doped with RE ions such as the *d-f* transition ions (*i.e.*, Eu^{2+}, and Ce^{3+}) and the well-shielded 4*f* ions (*e.g.*, Eu^{3+}, Pr^{3+}, Tb^{3+}, Sm^{3+}, Er^{3+}, Tm^{3+}, Gd^{3+}, Dy^{3+}), non-RE ions (*i.e.*, Bi^{3+}, Pb^{2+}, Mn^{2+}, Cr^{3+}, Mn^{4+}), and the coupling arrangements of these RE and non-RE ions, as well as bulk MPLs. In the meanwhile, other RE and non-RE(*e.g.*, Nd^{3+}, Ho^{3+}, Li^{3+} *etc*) ions that do not act as the luminescent centers but can be used to create the defects or modify the trap depth are also listed in this work. The persistent spectral region of these MPLs broadly covers the visible light, and/or parts of UV and NIR region. We hope that this summarization can promote the discovery of more novel MPLs, PCMs and self-luminous MPL@PCM composites for addressing some of the major photocatalytic challenges, *i.e.*, the continuously supplied energy problem required in the photocatalytic activity. Then, we review the already-reported MPL@PCM composites. Along with the persistent spectral positions, excitation and photoemission spectra of MPLs and the absorption regions of PCMs, we discuss how to select a MPL to couple with a PCM to design the "persistent-photocatalytic" MPL@PCM composites. The major working principles and relevant mechanistic models are also discussed. In addition, we disclose the principal methods used for achieving the MPL@PCM composites, including the solid-state reaction, combustion route, CVD approach, hydrothermal and sol-gel methods. These methods are expected to promote the discovery of new synthesis routes, typically those needing to couple with different methods. At last, we take some examples

to illustrate the photocatalytic application of the MPL@PCM composites, including degradation from MO, MB and RhB dyes, removal of poisonous gas-phased materials, splitting of water, H_2 and O_2 production, decontamination of waste water, drugs and industrial waste *etc*.

As we have discussed and highlighted in the main text, the design and use of the self-luminous MPL@PCM composites for photocatalysis is still an open field, but will be of great significance for forthcoming future investigations. When compared to those photocatalytic activities that only involve the use of the PCMs or heterogeneous photocatalyts, the MPL@PCM composites have many in-depth issues needing to be resolved and explored, in terms of the fundamental research and technical-economic spin offs. At the current stage, all of the studies are still in academic study and thus waiting for the full-scale (or even bench-scale) practical applications in the future, but the potential challenges we shown below would be a great help for any researcher working in the photocatalytic field. On the whole, through the review, we realize: (**i**) how important number of possible combinations of MPLs and PCMs that have still to be tested to produce the self-luminous MPL@PCM composites; (**ii**) the strategic importance of chemistry in this concern, in terms of micro-, nano- and multiscale organization of materials, MPL-PCM interface engineering for an optimized synergy, adjustment of the persistent spectral range of MPLs through appropriate doping and/or co-doping, control of the persistent luminescent duration of the MPLs through careful management of the defects, adaptation of the absorption spectra of PCMs for an optimized overlap at the MPL@PCM composite interface, light extraction by surface texturation; (**iii**) the importance of how to widen the research logical thinking, not just limited to the current state, for example, the dependence of pollutants degradation rate (r) on the photon flow (p) is a very important influence factor in the heterogeneous photocatalysis [428], which, together with some theoretical calculations (*e.g.*, DFT modeling), can be used to qualitatively analyze and discuss the in-depth photocatalytic principles behind the MPL@PCM and then confirm whether or not the use of a MPL@PCM composite could be beneficial to the overall rate of photocatalytic degradation, and to establish some reliable models to explain the photocatalytic activity. Moreover, although the MPL@PCM composites can sustain the photocatalytic activities in the absence of an external irradiation source, they still need an external pre-irradiation step. When the pre-irradiation step is finished, the persistent intensity and duration as the delay time goes on are decreased gradually, resulting in the weakening of photocatalytic reaction. Fortunately, with the assistance of the

regular decrease of the persistent intensity, the delay process of a given MPL can be easily parametrized. As a result, it is possible for us to design an automatic "round-the-clock" procedure that can allow for recharging the MPL@PCM composites repeatedly once the persistent intensity is low to a certain value or dose. Hence, the persistent duration and intensity problems of the MPLs, which are a first order lock in the context of the self-luminous MPL@PCM composites, can be intermittently and continuously renewed and complemented by using the same irradiation light source once the persistent intensity of MPLs is decreased to a given level. Unfortunately, however, except for the observation of the improved photocatalytic performance that is due to the improved photon utilization, it still lacks relevant study on how to monitor the photon efficiency of the persistent irradiation (*i.e.*, how many photons at a given excitation wavelength are required to obtain the afterglow photons). For this concern, since the emission of a MPL can be quenched by means of photon absorption and scattering or somehow internal filtering effect and the quenching process can be presented by the decrement of luminescent intensity which is also estimated by the quantum efficiency [375], the energy transfer efficiency from a MPL to a PCM can be deduced to depend strongly on the contact or the distance between the MPL and PCM, and their matching (*i.e.*, overlapping) spectral area between the emission spectra of MPL and the absorption spectra of PCM. Besides, as we have mentioned in the "**5. Photocatalytic application of self-luminous MPL@PCM composites**" section, in different works, the light sources used for the photocatalytic application of MPL@PCM composites are not the same. Some works use the sunlight as main photon source, while others would like to use the artificial light. Since the emission wavelength and the photon flux of the artificial light source, together with the PCMs and the reactor geometry, can be optimized while the emission wavelength and intensity of sunlight are relatively fixed, the use of different light source may lead to different photocatalytic results. Thus, a systematic study on how different light sources influence on the photocatalytic activities of the MPL@PCM composites should also attract more attention. As shown in **Table 6**, most of the MPLs successfully used nowadays for coupling with the PCMs for the photocatalytic application are aluminates- and silicate-based MPLs that address well the continuous persistent duration and intensity issues and meet different practical applications. Nevetheless, this situation encourages us to continue to explore new compositions of MPLs with longer persistent duration, stronger intensity and higher structural, thermal, chemical and moisture-resisted stability, as well

as more desirable persistent spectral region that can match the absorption range or the optical bandgap of the PCMs. In this case, engineering a suitable optical band gap in a given PCM is a very important thing if there are no so suitable MPLs. Because of this consideration, we present in **Figure 24** a graph that summarizes the persistent positions (*i.e.*, the dominant positions from RE and non-RE ions doped MPLs and bulk MPLs we exhibited in this review), from which we can identify easily the most desirable positons of MPLs for the PCMs. Furthermore, we should also notice that when the light source is used for irradiating to the PCMs, only one side of the MPLs continuously emits the photons if the thicknesses of the MPL@PCM composites were too thick. Last but not the least, we point out the interesting perspectives that may also follow the use of the NIR light as a pre-irradiation light source to promote the MO degradation, H_2 evolution and RhB/phenol degradation, as done recently by Huang *et al* [304], Shi *et al* [393], Kang *et al* [405] who used the oxide nanocrystal-coupled PCMs (*i.e.*, $NaY(WO_4)_2$-TiO_2-YF_3:Er^{3+},Tm^{3+},Yb^{3+},Bi^{3+}, g-C_3N_4@Cs_xWO_3, g-C_3N_4@F-doped $(NH_4)_{0.33}WO_3$) as the NIR-converting PCMs, although the photocatalytic activities were still under the continuous NIR irradiation. In fact, these perspectives are also the motivations of this review.

Looking forwards to the future, with the profound impact of the persistent luminescence in the photocatalytic field, allowing the MPLs to act as an inner excitation source for sustaining the photocatalytic process will be very attractive. Although more new self-NIR-luminous MPL@PCM systems are still waiting to be invented, we should treat the MPL@PCM composites like baby or like something new just appeared, bringing more of the scientists' attention to them and let them grow up. In the end, we believe that this topic will promote the significant development of the MPL@PCM composite for addressing some of the major environmental challenges we are facing, and attract more and more attention of the scientists from different disciplines and fields, typically those with the backgrounds in chemistry, energy fuels, materials, physics environmental science, and optoelectronics, as well as the relevant subdivisions and multidisciplinary. In future, a number of new experimental observations, along with corresponding new physicochemical mechanisms and other previously-unnoticed applications, may appear. On the whole, this review contains many core points and implications, including but not limited to those we mentioned above. Disclosing this review can allow to understanding better the use of MPL@PCM composite for photocatalysis.

Acknowledgements

This work was financially supported by the European Union's Horizon 2020 research and innovation program under the Marie Sklodowska-Curie grant agreement no. 713683. Meanwhile, we also thank Dr. Fei Gao (Department of Physics, Technical University of Denmark) for her contribution to the 3D TOC picture.

References

[1] Sung-Suh H. M.; Choi J. R.; Hah H. J.; Koo S. M.; Bae Y. C. Comparison of Ag deposition effects on the photocatalytic activity of nanoparticulate TiO_2 under visible and UV light irradiation. *J. Photoch. Photobio. A*, **2004**, 163, 37-44.

[2] Zhu H. Y.; Chen X.; Zheng Z. F.; Ke X. B.; Jaatinen E.; Zhao J. C.; Guo C.; Xie T. F.; Wang D. J. Mechanism of supported gold nanoparticles as photocatalysts under ultraviolet and visible light irradiation. *Chem. Comm.*, **2009**, 7524-7526.

[3] Schultz D. M.; Yoon T. P. Solar Synthesis: Prospects in Visible Light Photocatalysis. *Science*, **2014**, 343, 1239176.

[4] Mohapatra L.; Parida K.; Satpathy M. Molybdate/Tungstate Intercalated Oxo-Bridged Zn/Y LDH for Solar Light Induced Photodegradation of Organic Pollutants. *J. Phys. Chem. C*, **2012**, 116, 13063-13070.

[5] Devi L. G.; Kavitha R. A review on non-metal ion doped titania for the photocatalytic degradation of organic pollutants under UV/solar light: Role of photogenerated charge carrier dynamics in enhancing the activity. *Appl. Catal. B - Environ.*, **2013**, 140-141, 559-587.

[6] Tian Q. Y.; Yao, W. J.; Wu, W.; Jiang, C. Z. NIR light-activated upconversion semiconductor photocatalysts. *Nanoscale Horiz.*, **2019**, 4, 10-25.

[7] Reszczyńska J.; Grzyb T.; Sobczak J. W.; Lisowski W.; Gazda M.; Ohtani B.; Zaleska A. Visible light activity of rare earth metal doped (Er^{3+}, Yb^{3+} or Er^{3+}/Yb^{3+}) titania photocatalysts. *Appl. Catal. B - Environ.*, **2015**, 163, 40-49.

[8] Dai K.; Peng T. Y.; Chen H.; Liu J.; Zan L. Photocatalytic Degradation of Commercial Phoxim over La-Doped TiO_2 Nanoparticles in Aqueous Suspension. *Environ. Sci. Technol.*, **2009**, 43, 1540-1545.

[9] Danae V.; Antonia F.; Maria K.; Efthalia C.; Vassilios B.; Apostolos Z.; George K.; Dionissios M. Solar light and metal-doped TiO_2 to eliminate water-transmitted bacterial pathogens: Photocatalyst characterization and disinfection performance. *Appl. Catal. B - Environ.*, **2014**, 154-155, 93-101.

[10] Zhang S. N.; Zhang S. J.; Song L. M. Super-high activity of Bi^{3+} doped Ag_3PO_4 and enhanced photocatalytic mechanism. *Appl. Catal. B - Environ.*, **2014**, 152-153, 129-139.

[11] Zhang T.; Lin W. B. Metal-organic frameworks for artificial photosynthesis and photocatalysis. *Chem. Soc. Rev.*, **2014**, 43, 5982-5993.

[12] Zhuo S. J.; Shao M. W.; Lee S. T. Upconversion and Downconversion Fluorescent Graphene Quantum Dots: Ultrasonic Preparation and Photocatalysis. *ACS Nano*, **2012**, 6, 1059-1064.

[13] Yu H. J.; Shi R.; Zhao Y. F.; Waterhouse G. I. N.; Wu L. Z.; Tung C. H.; Zhang T. R. Smart Utilization of Carbon Dots in Semiconductor Photocatalysis. *Adv. Mater.*, **2016**, 28, 9454-9477.

[14] Kuehnel M. F.; Orchard K. L.; Dalle K. E.; Reisner E. Selective Photocatalytic CO_2 Reduction in Water through Anchoring of a Molecular Ni Catalyst on CdS Nanocrystals. *J. Am. Chem. Soc.*, **2017**, 139, 7217-7223.

[15] Ho W. K.; Yu J. C.; Lin J.; Yu J. G.; Li P. S. Preparation and Photocatalytic Behavior of MoS_2 and WS_2 Nanocluster Sensitized TiO_2. *Langmuir*, **2004**, 20, 5865-5869.

[16] Xiang Q. J.; Yu J. G.; Jaroniec M. Synergetic Effect of MoS_2 and Graphene as Cocatalysts for Enhanced Photocatalytic H_2 Production Activity of TiO_2 Nanoparticles. *J. Am. Chem. Soc.*, **2012**, 134, 6575-6578.

[17] Xu Y. F.; Yang M. Z.; Chen B. X.; Wang X. D.; Chen H. Y.; Kuang D. B.; Su C. Y. A $CsPbBr_3$ Perovskite Quantum Dot/Graphene Oxide Composite for Photocatalytic CO_2 Reduction. *J. Am. Chem. Soc.*, **2017**, 139, 5660-5663.

[18] Chen X. B.; Liu L.; Yu P. Y.; Mao S. S. Increasing Solar Absorption for Photocatalysis with Black Hydrogenated Titanium Dioxide Nanocrystals. *Science*, **2011**, 331, 746-750.

[19] Mclaren A.; Valdes-Solis T.; Li G. Q.; Tsang S. C. Shape and Size Effects of ZnO Nanocrystals on Photocatalytic Activity. *J. Am. Chem. Soc.*, **2009**, 131, 12540-12541.

[20] Zhang Y. H.; Zhang N.; Tang Z. T.; Xu Y. J. Graphene Transforms Wide Band Gap ZnS to a Visible Light Photocatalyst. The New Role of Graphene as a Macromolecular Photosensitizer. *ACS Nano*, **2012**, 6, 9777-9789.

[21] Tokunaga S.; Kato H.; Kudo A. Selective Preparation of Monoclinic and Tetragonal $BiVO_4$ with Scheelite Structure and Their Photocatalytic Properties. *Chem. Mater.*, **2001**, 13, 4624-4628.

[22] Kudo A.; Omori K.; Kato H. A Novel Aqueous Process for Preparation of Crystal Form-Controlled and Highly Crystalline $BiVO_4$ Powder from Layered Vanadates at Room Temperature and Its Photocatalytic and Photophysical Properties. *J. Am. Chem. Soc.*, **1999**, 121, 11459-11467.

[23] Li H.; Li J.; Ai Z. H.; Jia F. L.; Zhang L. Z. Oxygen Vacancy-Mediated Photocatalysis of BiOCl: Reactivity, Selectivity, and Perspectives. *Angew. Chem. Int. Ed.*, **2018**, 57, 122-138.

[24] Wang P.; Huang B. B.; Qin X. Y.; Zhang X. Y.; Dai Y.; Wei J. Y.; Whangbo M. -H. Ag@AgCl: A Highly Efficient and Stable Photocatalyst Active under Visible Light. *Angew. Chem. Int. Ed.*, **2008**, 47, 7931-7933.

[25] He H. Y.; Lin J. H.; Fu W.; Wang X. L.; Wang H.; Zeng Q. S.; Gu Q.; Li Y. M.; Yan C.; Tay B. K.; Xue C.; Hu X.; Pantelides S. T.; Zhou W.; Liu Z. MoS_2/TiO_2 Edge-On Heterostructure for Efficient Photocatalytic Hydrogen Evolution. *Adv. Energy Mater.*, **2016**, 6, 1600464.

[26] Crake A.; Christoforidis K. C.; Kafizas A.; Zafeiratos S.; Petit C. CO_2 capture and photocatalytic reduction using bifunctional TiO_2/MOF nanocomposites under UV-vis irradiation. *Appl. Catal. B - Environ.*, **2017**, 210, 131-140.

[27] Li H. X.; Bian Z. F.; Zhu J.; Huo Y. N.; Li H.; Lu Y. F. Mesoporous Au/TiO_2 Nanocomposites with Enhanced Photocatalytic Activity. *J. Am. Chem. Soc.*, **2007**, 129, 4538-4539.

[28] He Z. Q.; Shi Y. Q.; Gao C.; Wen L. N.; Chen J. M.; Song S. $BiOCl/BiVO_4$ p-n Heterojunction with Enhanced Photocatalytic Activity under Visible-Light Irradiation. *J. Phys. Chem. C*, **2014**, 118, 389-398.

[29] Costa E.; Frontera F.; Heise J.; Feroci M.; in't Zand J.; Fiore F.; Cinti M. N.; Dal Fiume D.; Nicastro L.; Orlandini M.; Palazzi E.; Rapisarda M.; Zavattini G.; Jager R.; Parmar A.; Owens A.; Molendi S.; Cusumano G.; Maccarone M. C.; Giarrusso S.; Coletta A.; Antonelli L. A.; Giommi P.; Muller J. M.; Piro L.; Butler R. C. Discovery of an X-ray afterglow associated with the γ-ray burst of 28 February 1997. *Nature*, **1997**, 387, 783-785.

[30] Ma L.; Zou X. J.; Bui B.; Chen W.; Song K. H.; Solberg T. X-ray excited ZnS:Cu,Co afterglow nanoparticles for photodynamic activation. *Appl. Phys. Lett.*, **2014**, 105, 013702.

[31] Yan J.; Liu C.; Vlieland J.; Zhou J.; Dorenbos P.; Huang Y.; Tao Y.; Liang H. Intense emission of $Ba_2MgSi_2O_7:Eu^{2+}$ under X-ray excitation for potential detecting applications. *J. Lumin.*, **2017**, 183, 97-101.

[32] Kowatari M.; Koyama D.; Satoh Y.; Iinuma K.; Uchida S. The temperature dependence of luminescence from a long-lasting phosphor exposed to ionizing radiation. *Nucl. Instrum. Meth. A*, **2002**, 480, 431-439.

[33] Bedyal A. K.; Kumar V.; Singh V. K.; Lochab S. P.; Singh F.; Ntwaeaborwa O. M.; Swart H. C. Thermo-luminescence kinetic parameters of γ-irradiated $Sr_4Al_{14}O_{25}:Eu^{2+},Dy^{3+}$ phosphors. *Radiat. Eff. Defect. S.*, **2013**, 168, 1022-1029.

[34] Luo, D.; Bos, J.; Dobrowolska, A.; Dorenbos, P. Low-temperature VUV photoluminescence and thermoluminescence of UV excited afterglow phosphor $Sr_3Al_xSi_{1-x}O_5:Ce^{3+},Ln^{3+}$ (Ln = Er, Nd, Sm, Dy and Tm). *Phys. Chem. Chem. Phys.*, **2015**, 17, 15419-15427.

[35] Liu Y. L.; Lei B. F.; Shi C. S. Luminescent Properties of a White Afterglow Phosphor $CdSiO_3:Dy^{3+}$. *Chem. Mater.*, **2005**, 17, 2108-2113.

[36] Zhang J.; Wang Y. H.; Guo L. N.; Huang Y. Vacuum Ultraviolet-Ultraviolet, X-Ray, and Near-Infrared Excited Luminescence Properties of $SrR_2O_4:RE^{3+}$ (R = Y and Gd; RE = Tb, Eu, Yb, Tm, Er, and Ho). *J. Am. Ceram. Soc.*, **2012**, 95, 243-249.

[37] Jin Y. H.; Hu Y. H.; Chen L.; Wang X. J.; Ju G. F.; Mou Z. F. Luminescence Properties of Dual-Emission (UV/Visible) Long Afterglow Phosphor $SrZrO_3:Pr^{3+}$. *J. Am. Ceram. Soc.*, **2013**, 96, 3821-3827.

[38] Kojima Y.; Aoyagi K.; Yasue T. Afterglow mechanism and thermoluminescence of red-emitting $CaS:Eu^{2+},Pr^{3+}$ phosphor with incorporated Li^+ ion upon visible light irradiation. *J. Lumin.*, **2007**, 126, 319-322.

[39] Pan Z. W.; Lu Y. Y.; Liu F. Sunlight-activated long-persistent luminescence in the near-infrared from Cr^{3+}-doped zinc gallogermanates. *Nat. Mater.*, **2011**, 11, 58-63.

[40] Liu F.; Liang Y. J.; Pan Z. W. Detection of Up-converted Persistent Luminescence in the Near Infrared Emitted by the $Zn_3Ga_2GeO_8:Cr^{3+},Yb^{3+},Er^{3+}$ Phosphor. *Phys. Rev. Lett.*, **2014**, 113, 177401.

[41] Xu S.; Chen R. F.; Zheng C.; Huang W. Excited State Modulation for Organic Afterglow: Materials and Applications. *Adv. Mater.*, **2016**, 28, 9920-9940.

[42] Van den Eeckhout K.; Smet P. F.; Poelman D. Persistent Luminescence in Eu^{2+}-Doped Compounds: A Review. *Materials*, **2010**, 3, 2536-2566.

[43] Wu S. L.; Pan Z. F.; Chen R. F.; Liu X. G. Applications of Inorganic Afterglow Phosphors. In: *Long Afterglow Phosphorescent Materials*. Springerbriefs in materials. Springer, Cham, **2017**, 101-116.

[44] Li Y.; Gecevicius M.; Qiu J. R. Long persistent phosphors — from fundamentals to applications. *Chem. Soc. Rev.*, **2016**, 45, 2090-2136.

[45] Xiong, P. X.; Peng, M. Y. Recent advances in ultraviolet persistent phosphors. *Opt. Mater. X*, **2019**, 2, 100022.

[46] Li Z. J.; Zhang Y. W.; Wu X.; Huang L.; Li D. S.; Fan W.; Han G. Direct Aqueous-Phase Synthesis of Sub-10 nm "Luminous Pearls" with Enhanced in Vivo Renewable Near-Infrared Persistent Luminescence. *J. Am. Chem. Soc.*, **2015**, 137, 5304-5307.

[47] Zhuang Y. X.; Katayama Y.; Ueda J.; Tanabe S. A brief review on red to near-infrared persistent luminescence in transition-metal-activated phosphors. *Opt. Mater.*, **2014**, 36, 1907-1912.

[48] Liu X. J.; Chu H. P.; Li J. L.; Niu L. Y.; Li C.; Li H. L.; Pan K.; Sun C. Q. Light converting phosphor-based photocatalytic composites. *Catal. Sci. Technol.*, **2015**, 5, 4727-4740.

[49] Li H. H.; Wang Y. H., Photocatalytic Properties of TiO_2-Coatings Mounted on $CaAl_2O_4$:Eu^{2+}, Nd^{3+} without Light Source. *Mater. Sci. Forum*, **2009**, 620-622, 671-674.

[50] Liu L.; Zhang Z. L.; Zhang L. M.; Zhai Y. C. The effectiveness of strong afterglow phosphor powder in the detection of fingermarks. *Forensic Sci. Int.*, **2009**, 183, 45-49.

[51] Dhanalakshmi M.; Basavaraj R. B.; Darshan G. P.; Sharma S. C.; Nagabhushana H. Pivotal role of fluxes in $BaTiO_3$:Eu^{3+} nano probes for visualization of latent fingerprints on multifaceted substrates and anti-counterfeiting applications. *Microchem. J.*, **2019**, 145, 226-234.

[52] Lian S. X.; Qi Y.; Rong C. Y.; Yu L. P.; Zhu A. L.; Yin D. L.; Liu B. Effectively Leveraging Solar Energy through Persistent Dual Red Phosphorescence: Preparation, Characterization, and Density Functional Theory Study of $Ca_2Zn_4Ti_{16}O_{38}$:Pr^{3+}. *J. Phys. Chem. C*, **2010**, 114, 7196-7204.

[53] Wang J.; Ma Q. Q.; Zheng W.; Liu H. Y.; Yin C. Q.; Wang F. B.; Chen X. Y.; Yuan Q.; Tan W. H. One-Dimensional Luminous Nanorods Featuring Tunable Persistent Luminescence for Autofluorescence-Free Biosensing. *ACS Nano*, **2017**, 11, 8185-8191.

[54] Zhuang Y. X.; Wang L.; Lv Y.; Zhou T. L.; Xie R. J. Optical Data Storage and Multicolor Emission Readout on Flexible Films Using Deep-Trap Persistent Luminescence Materials. *Adv. Funct. Mater.*, **2018**, 28, 1705769.

[55] Thomas M.; Aurélie BB.; Johanne S.; Eliott T.; Suchinder K. S.; Bruno V.; Adrie J. J. B.; Pieter D.; Michel B.; Didier G.; Daniel S.; Cyrille R. The *in vivo* activation of persistent nanophosphors for optical imaging of vascularization, tumours and grafted cells. *Nat. Mater.*, **2014**, 13, 418-426.

[56] Abdukayum A.; Chen J. T.; Zhao Q.; Yan X. P. Functional Near Infrared-Emitting Cr^{3+}/Pr^{3+} Co-Doped Zinc Gallogermanate Persistent Luminescent Nanoparticles with Superlong Afterglow for in Vivo Targeted Bioimaging. *J. Am. Chem. Soc.*, **2013**, 135, 14125-14133.

[57] Liu, X. M.; Chen, X. Y.; Li, Y. Z.; Wu, B. Q.; Luo, X. B.; Ouyang, S.; Luo, S. L.; Al Kheraif, A. A.; Lin, J. A g-C_3N_4@Au@$SrAl_2O_4$:Eu^{2+},Dy^{3+} composite as an efficient plasmonic photocatalyst for round-the-clock environmental purification and hydrogen evolution. *J. Mater. Chem. A*, **2019**, 7, 19173-19186.

[58] Sakar M.; Nguyen C. C.; Vu M. H.; Do T. O. Materials and Mechanisms of Photo-Assisted Chemical Reactions under Light and Dark Conditions: Can Day Night Photocatalysis be Achieved? *ChemSusChem.*, **2018**, 11, 809-820.

[59] Huo S. Q.; Carroll J.; Vezzu D. A. K. Design, Synthesis, and Applications of Highly Phosphorescent Cyclometalated Platinum Complexes. *Asian J. Org. Chem.*, **2015**, 4, 1210-1245.

[60] Li H. H.; Yin S.; Sato T. Persistent photocatalysis of continuously flowing gas-phase nitric oxide using $CaAl_2O_4$:(Eu,Nd)/rutile phase $TiO_{2-x}N_y$ composites. *Res. Chem. Intermediat.*, **2013**, 39, 1501-1507.

[61] Li H. H.; Yin S.; Sato T. Persistent $deNO_x$ Ability of $CaAl_2O_4$:(Eu,Nd)/$TiO_{2-x}N_y$ Luminescent Photocatalyst. *Nanoscale Res Lett.*, **2010**, 6, 5.

[62] Li S.; Wang W. C.; Chen Y. Q.; Zhang L. J.; Guo J. X.; Gong M. C. Fabrication and characterization of TiO_2/$BaAl_2O_4$:Eu^{2+},Dy^{3+} and its photocatalytic performance towards oxidation of gaseous benzene. *Catal. Commun.*, **2009**, 10, 1048-1051.

[63] Wu H. Y.; Peng W. Q; Wang Z. M.; Koike K. Cerium-doped gehlenite supporting silver/silver chloride for continuous photocatalysis. *RSC Adv.*, **2016**, 6, 37995-38003.

[64] Li H. H.; Xu Q. J.; Ge H. H. Persistent Degradation of RhB Dyes on Ag_3PO_4 with the Assistance of $SrAl_2O_4$:(Eu,Dy). *Adv, Mater. Res.*, **2014**, 864-867.

[65] Li H. H.; Yin S.; Sato T.; Wang Y. H. Enhanced Photocatalytic Performance of Luminescent g-C_3N_4 Photocatalyst in Darkroom. *Nanoscale Res. Lett.*, **2016**, 11, 91.

[66] Cui G. W.; Yang X. L.; Zhang Y. J.; Fan Y. Q.; Chen P.; Cui H. Y.; Liu Y.; Shi X. F.; Shang Q. Y.; Tang B. Round-the-Clock Photocatalytic Hydrogen Production with High Efficiency by a Long-Afterglow Material. *Angew. Chem. Int. Ed.*, **2019**, 58, 1354-1358.

[67] Li H. H.; Yin S.; Wang Y. H.; Sato T. Efficient persistent photocatalytic decomposition of nitrogen monoxide over a fluorescence-assisted $CaAl_2O_4$:(Eu,Nd)/(Ta,N)-codoped TiO_2/Fe_2O_3. *Appl. Catal. B - Environ.*, **2013**, 132-133, 487-492.

[68] Havasi V.; Vodredi B.; Kukovecz A. Photocatalytic performance of $Sr_4Al_{14}O_{25}$:Eu,Dy phosphor assisted ZnO:Co + Ag nanocomposite under continuous and pulsed illumination. *Catal. Today*, **2017**, 284, 107-113.

[69] Casillas C. Á.; Garcia C. R.; Guzman M.; Diaz-Torres L. A. Optical and Photocatalytic studies of long persistent Bi co-doped $Sr_4Al_{14}O_{25}$:Eu,Dy. *Latin America Optics and Photonics Conference*, Optical Society of America: Cancun, 2014, LTh4A.55.

[70] Li H. H.; Yin S.; Wang Y. H; Sato T. Microwave-Assisted Hydrothermal Synthesis of Fe_2O_3-Sensitized $SrTiO_3$ and its Luminescent Photocatalytic $deNO_x$ Activity with $CaAl_2O_4$:(Eu, Nd) Assistance. *J. Am. Ceram. Soc.*, **2013**, 96, 1258-1262.

[71] Kim J. S.; Sung H. J.; Kim B. J. Photocatalytic characteristics for the nanocrystalline TiO_2 on the Ag-doped $CaAl_2O_4$:(Eu,Nd) phosphor. *Appl. Surf. Sci.*, **2015**, 334, 151-156.

[72] Meng Y. Z.; Shen Y.; Hou L. Y.; Zuo G. F.; Wei X. L.; Wang X. M.; Li F. F. Study on photocatalysis and dynamics properties of self-catalysis $BiVO_4$ assembled in porous $Sr_2MgSi_2O_7$:Eu^{2+},Dy^{3+}. *J. Alloy Compd.*, **2016**, 655, 1-5.

[73] Kim J. S.; Sung H. J.; Jung S. C. Synthesis of the TiO_2-Long Lasting Phosphor ($Sr_4Al_{14}O_{25}$:Eu^{2+},Dy^{3+}) Composite and its Photocatalytic Reaction Properties. *Ceram. Environ. Syst.*, **2016**, 257, 23-33.

[74] Li G.; Tian Y.; Zhao Y.; Lin J. Recent progress in luminescence tuning of Ce^{3+} and Eu^{2+}-activated phosphors for pc-WLEDs. *Chem. Soc. Rev.*, **2015**, 44, 8688-8713.

[75] Guo C. F.; Luan L.; Huang D. X.; Su Q.; Lv Y. H. Study on the stability of phosphor $SrAl_2O_4:Eu^{2+},Dy^{3+}$ in water and method to improve its moisture resistance. *Mater. Chem. Phys.*, **2007**, 106, 268-272.

[76] Lin Y. H.; Zhang Z. T.; Tang Z. L.; Wang X. X.; Zhang J. Y.; Zheng Z. S. Luminescent properties of a new long afterglow Eu^{2+} and Dy^{3+} activated $Ca_3MgSi_2O_8$ phosphor. *J. Eur. Ceram. Soc.*, **2001**, 21, 683-685.

[77] Lakshminarasimhan N.; Varadaraju U. V. Luminescence and afterglow in $Sr_2SiO_4:Eu^{2+}$, RE^{3+} [RE = Ce, Nd, Sm and Dy] phosphors-Role of co-dopants in search for afterglow. *Mater. Res. Bull.*, **2008**, 43, 2946-2953.

[78] Luo Y.; Xia Z. G. Effect of Al/Ga Substitution on Photoluminescence and Phosphorescence Properties of Garnet-Type $Y_3Sc_2Ga_{3-x}Al_xO_{12}:Ce^{3+}$ Phosphor. *J. Phys. Chem. C*, **2014**, 118, 23297-23305.

[79] Ju G. F.; Hu Y. H.; Chen L.; Wang X. J.; Mu Z. F. The influence of auxiliary codopants on persistent phosphor $Sr_2P_2O_7:Eu^{2+},R^{3+}$ (R=Y, La, Ce, Gd, Tb and Lu). *Mater. Res. Bull.*, **2013**, 48, 4743-4748.

[80] Li J. F.; Lei B. F.; Qin J. L.; Liu Y. L.; Liu X. T. Temperature-Dependent Emission Spectra of $Ca_2Si_5N_8:Eu^{2+},Tm^{3+}$ Phosphor and its Afterglow Properties. *J. Am. Ceram. Soc.*, **2013**, 96, 873-878.

[81] Zeng W.; Wang Y. H.; Han S. C.; Chen W. B.; Li G.; Wang Y. Z.; Wen Y. Design, synthesis and characterization of a novel yellow long-persistent phosphor: $Ca_2BO_3Cl:Eu^{2+},Dy^{3+}$. *J. Mater. Chem. C*, **2013**, 1, 3004-3011.

[82] Van den Eeckhout K.; Smet P. F.; Poelman D. Luminescent Afterglow Behavior in the $M_2Si_5N_8$:Eu Family (M = Ca, Sr, Ba). *Materials*, **2011**, 4.

[83] Sharma S. K.; Pitale S. S.; Manzar Malik M.; Dubey R. N.; Qureshi M. S. Luminescence studies on the blue-green emitting $Sr_4Al_{14}O_{25}:Ce^{3+}$ phosphor synthesized through solution combustion route. *J. Lumin.*, **2009**, 129, 140-147.

[84] Ueda J.; Kuroishi K.; Tanabe S. Bright persistent ceramic phosphors of Ce^{3+}-Cr^{3+}-codoped garnet able to store by blue light. *Appl. Phys. Lett.*, **2014**, 104, 101904.

[85] Jia D.; Meltzer R. S.; Yen W. M.; Jia W.; Wang X. Green phosphorescence of $CaAl_2O_4:Tb^{3+}$,Ce = through persistence energy transfer. *Appl. Phys. Lett.*, **2002**, 80, 1535-1537.

[86] Guo H. J.; Wang Y. H.; Chen W. B.; Zeng W.; Han S. C.; Li G.; Li Y. Y. Controlling and revealing the trap distributions of $Ca_6BaP_4O_{17}:Eu^{2+},R^{3+}$ (R = Dy, Tb, Ce, Gd, Nd) by codoping different trivalent lanthanides. *J. Mater. Chem. C*, **2015**, 3, 11212-11218.

[87] Zhong R. X.; Zhang J. H.; Zhang X.; Lu S. Z.; Wang X. J. Energy transfer and red phosphorescence in strontium aluminates co-doped with Cr^{3+}, Eu^{2+} and Dy^{3+}. *J. Lumin.*, **2006**, 119-120, 327-331.

[88] Gong Y.; Wang Y. H.; Li Y. Q.; Xu X. H.; Zeng W. Fluorescence and phosphorescence properties of new long-lasting phosphor $Ba_4(Si_3O_8)_2:Eu^{2+},Dy^{3+}$. *Opt. Express*, **2011**, 19, 4310-4315.

[89] Gong Y.; Wang Y. H.; Li Y. Q.; Xu X. H. Ce^{3+},Dy^{3+} Co-Doped White-Light Long-Lasting Phosphor: $Sr_2Al_2SiO_7$ Through Energy Transfer. *J. Electrochem. Soc.*, **2010**, 157, J208-J211.

[90] Li L. K.; Zeng R. J.; Wang H. H. $Ba_{1.3}Ca_{0.7}SiO_4:Eu^{2+},Mn^{2+}$: A white-lighting-emitting phosphor with extra afterglow properties via YF_3 addition. *J. Alloy Compd.*, **2018**, 765, 249-252.

[91] Xie W.; Zou C. W.; Li S. Q.; Sun J. H.; Kang F. W.; Sun G. H. Simultaneous enhancement of photoluminescence and afterglow luminescence through Bi^{3+} co-doping in the $Sr_3Al_2O_5Cl_2:Eu^{2+}$ phosphor. *Phys. Chem. Chem. Phys.*, **2018**, 20, 13983-13993.

[92] Zhang J. S.; Chen B. J.; Sun J. S.; Li X. P.; Cheng L. H.; Zhong H. Y. White long-lasting phosphorescence generation in a $CaAl_2Si_2O_8:Eu^{2+},Mn^{2+},Dy^{3+}$ system through persistent energy transfer. *J. Phys. D: Appl. Phys.*, **2012**, 45, 325105.

[93] Chen W. B.; Wang Y. H.; Zeng W.; Li G.; Guo H. J. Design, synthesis and characterization of near-infrared long persistent phosphors $Ca_4(PO_4)_2O:Eu^{2+},R^{3+}$ (R = Lu, La, Gd, Ce, Tm, Y). *RSC Adv.*, **2016**, 6, 331-337.

[94] Pal S.; Tadge, P.; Rawat N. S.; Koul D. K.; Mehare C. M.; Dhoble S. J.; Ray S. $RbBaScSi_3O_9$: A suitable host of generating blue emitting phosphor doped with Ce^{3+} and cyan-green emitting persistent phosphor co-doped with Eu^{2+} and Dy^{3+}. *J. Lumin.*, **2020**, 117335, accepted, // DOI: 10.1016/j.jlumin.2020.117335.

[95] Wang M. W.; Lin W.; Liu N.; Ye Y. P. Luminescence properties of a novel bluish green long-lasting phosphor $LiBaPO_4:Eu^{2+},Ho^{3+}$. *J. Lumin.*, **2018**, 194, 682-685.

[96] Lei B. F.; Machida K. I.; Horikawa T.; Hanzawa H.; Kijima N.; Shimomura Y.; Yamamoto H. Reddish-Orange Long-Lasting Phosphorescence of $Ca_2Si_5N_8:Eu^{2+},Tm^{3+}$ Phosphor. *J. Electrochem. Soc.*, **2010**, 157, A196-J201.

[97] Wang P. J.; Xu X. H.; Qiu J. B.; Yu X.; Wang Q. Effects of Er^{3+} doping on the long-persistent luminescence properties of $Ba_4(Si_3O_8)_2:Eu^{2+}$ phosphor. *Opt. Mater.*, **2014**, 36, 1826-1829.

[98] Guo H. J.; Wang Y. H.; Li G.; Liu J.; Feng P.; Liu D. W. Cyan emissive super-persistent luminescence and thermoluminescence in $BaZrSi_3O_9:Eu^{2+},Pr^{3+}$ phosphors. *J. Mater. Chem. C*, **2017**, 5, 2844-2851.

[99] Zhao R.; Pang R.; Li H. F.; Jia Y. L.; Jiang L. H.; Sun W. Z.; Li C. Y. Luminescent properties of blue long-lasting phosphorescence phosphors $Sr_6Al_{18}Si_2O_{37}:Eu^{2+},RE^{3+}$. *J. Rare Earth.*, **2014**, 32, 797-801.

[100] Li G.; Wang Y. H.; Zeng W.; Chen W. B.; Han S. C.; Guo H. J.; Wang X. C. Luminescence properties of a new green afterglow phosphor $NaBaScSi_2O_7:Eu^{2+}$. *Dalton Trans.*, **2015**, 44, 17572-17578.

[101] Wang B.; Lin H.; Yu Y. L.; Chen D. Q.; Zhang R.; Xu J.; Wang Y. S. Ce^{3+}/Pr^{3+}: YAGG: A Long Persistent Phosphor Activated by Blue-Light. *J. Am. Ceram. Soc.*, **2014**, 97, 2539-2545.

[102] Saito M.; Adachi N.; Kondo H. Full-color illumination that needs no electric power. *Opt. Express*, **2007**, 15, 1621-1626.

[103] Luitel H. N.; Watari T.; Chand R.; Torikai T.; Yada M.; Mizukami H. Tuning the luminescence color and enhancement of afterglow properties of $Sr_{(4-x-y)}Ca_xBa_yAl_{14}O_{25}:Eu^{2+},Dy^{3+}$ phosphor by adjusting the composition. *Mater. Sci. Eng. B*, **2013**, 178, 834-842.

[104] Ueda J.; Aishima K.; Nishiura S.; Tanabe S. Afterglow Luminescence in Ce^{3+}-Doped $Y_3Sc_2Ga_3O_{12}$ Ceramics. *Appl. Phys. Express*, **2011**, 4, 042602.

[105] Aitasalo T.; Holsa J.; Jungner H.; Lastusaari M.; Niittykoski J. Thermoluminescence Study of Persistent Luminescence Materials: Eu^{2+}- and R^{3+}-Doped Calcium Aluminates, $CaAl_2O_4:Eu^{2+},R^{3+}$. *J. Phys. Chem. B*, **2006**, 110, 4589-4598.

[106] Li H. H.; Yin S.; Sato T. Novel luminescent photocatalytic deNO_x activity of $CaAl_2O_4$:(Eu,Nd)/$TiO_{2-x}N_y$ composite. *Appl. Catal. B - Environ.*, **2011**, 106, 586-591.

[107] Fan J. M.; Zhao Z. H.; Gong C.; Xue Y. Q.; Yin S. Y. Persistent Methyl Orange Degradation Ability of $MgAl_2O_4:(Pr^{3+},Dy^{3+})$/M-$TiO_2$ Luminescent Photocatalyst. *J. Nanosci. Nanotechnol.*, **2018**, 18, 1675-1681.

[108] Zhang J. C.; Qin Q. S.; Yu M. H.; Zhou M. J.; Wang Y. H., The photoluminescence, afterglow and upconversion photostimulated luminescence of Eu^{3+} doped Mg_2SnO_4 phosphors. *J. Lumin.*, **2012**, 132, 23-26.

[109] Kang F. W.; Hu Y. H.; Chen L.; Wang X. J.; Mu Z. F.; Wu H. Y.; Ju G. F. Eu^{3+} Doped $CaWO_4$ - A Potential Red Long Afterglow Phosphor. *Appl. Phys. B*, **2012**, 107, 833-837.

[110] Liu D.; Cui C.; Huang P.; Wang L.; Jiang G. W. Luminescent properties of red long-lasting phosphor $Y_2O_2S:Eu^{3+},M^{2+}$ (M=Mg, Ca, Sr, Ba),Ti^{4+} nanotubes via hydrothermal method. *J. Alloy Compd.*, **2014**, 583, 530-534.

[111] Jin Y. H.; Hu Y. H.; Chen L.; Wang X. J.; Ju G. F. Luminescent properties of a red afterglow phosphor $Ca_2SnO_4:Pr^{3+}$. *Opt. Mater.*, **2013**, 35, 1378-1384.

[112] Wu H. Y.; Hu Y. H.; Kang F. W.; Chen L.; Wang X. J.; Ju G. F.; Mu Z. F. Observation on long afterglow of Tb^{3+} in $CaWO_4$. *Mater. Res. Bull.*, **2011**, 46, 2489-2493.

[113] Liu C. B.; Che G. B.; Xu Z. L.; Wang Q. W. Luminescence properties of a Tb^{3+} activated long-afterglow phosphor. *J. Alloy Compd.*, **2009**, 474, 250-253.

[114] Zhang S.; Pang R.; Li C. Y.; Su Q. Green photoluminescence, but blue afterglow of Tb^{3+} activated $Sr_4Al_{14}O_{25}$. *J. Lumin.*, **2010**, 130, 2223-2225.

[115] Rodrigues L. C. V.; Brito H. F.; Hölsä J.; Stefani R.; Felinto M. C. F. C.; Lastusaari M.; Laamanen T.; Nunes L. A. O. Discovery of the Persistent Luminescence Mechanism of $CdSiO_3:Tb^{3+}$. *J. Phys. Chem. C*, **2012**, 116, 11232-11240.

[116] Marques A. P. de A.; Künzel R.; Umidedo N. K.; Latini R. M.; Mateus E.; Okuno E. Tm^{3+} doped barium molybdate: A potential long-lasting blue phosphor. *J. Alloy Compd.*, **2018**, 735, 707-717.

[117] Chen W. B.; Wang Y. H.; Zeng W.; Han S. C.; Li G. Filling of trap and green long persistent luminescence in $Sr_3Al_2O_5Cl_2:Tb^{3+}$. *Opt. Mater.*, **2014**, 36, 1850-1854.

[118] Fan X. T.; Xu X. H.; Yu X.; Chen W. B.; Zhou D. C.; Qiu J. B. Wide band long persistent luminescence of $Ca_3Ga_2Ge_3O_{12}:Tb^{3+},Tm^{3+}$ phosphor with synergistic effect of different traps. *Mater. Res. Bull.*, **2018**, 99, 398-402.

[119] Trojan-Piegza J.; Zych E.; Hölsä J.; Niittykoski J. Spectroscopic Properties of Persistent Luminescence Phosphors: $Lu_2O_3:Tb^{3+},M^{2+}$ (M = Ca, Sr, Ba). *J. Phys. Chem. C*, **2009**, 113, 20493-20498.

[120] Tang W.; Wang M. W.; Meng X. X.; Lin W. Luminescence properties of tunable white-light long-lasting phosphor $YPO_4:Eu^{3+},Tb^{3+},Sr^{2+},Zr^{4+}$. *Opt. Mater.*, **2016**, 54, 120-125.

[121] Pedroso C. C. S.; Carvalho J. M.; Rodrigues L. C. V.; Hölsä J.; Brito H. F. Rapid and Energy-Saving Microwave-Assisted Solid-State Synthesis of Pr^{3+}-, Eu^{3+}-, or Tb^{3+}-Doped Lu_2O_3 Persistent Luminescence Materials. *ACS Appl. Mater. Interfaces*, **2016**, 8, 19593-19604.

[122] Zhang L.; Zhou X. M.; Zeng H. H.; Chen H. Q.; Dong X. P. White-light long-lasting phosphor $Sr_2SiO_4:Pr^{3+}$. *Mater. Lett.*, **2008**, 2539-2541.

[123] Liu B.; Kong L. J.; Shi C. S. White-light long-lasting phosphor $Sr_2MgSi_2O_7:Dy^{3+}$. *J. Lumin.*, **2007**, 122-123, 121-124.

[124] Kuang J. Y.; Liu Y. L. White-emitting Long-lasting Phosphor $Sr_2SiO_4:Dy^{3+}$. *Chem. Lett.*, **2005**, 34, 598-599.

[125] Lecointre A.; Bessière A.; Bos A. J. J.; Dorenbos P.; Viana B.; Jacquart S. Designing a Red Persistent Luminescence Phosphor: The Example of $YPO_4:Pr^{3+},Ln^{3+}$ (Ln = Nd, Er, Ho, Dy). *J. Phys. Chem. C*, **2011**, 115, 4217-4227.

[126] Maurya A.; Bahadur A.; Rai S. B. Enhanced red emission from Eu^{3+}, A^+ (Li^+, Na^+, K^+) co-doped $CaZrO_3$ phosphor. *J. Lumin.*, **2018**, 203, 714-722.

[127] Kang F. W.; Hu Y. H.; Wu H. Y.; Mu Z. F.; Ju G. F.; Fu C. J.; Li N. N. Luminescence and red long afterglow investigation of Eu^{3+}-Sm^{3+} Co-doped $CaWO_4$ phosphor. *J. Lumin.*, **2012**, 132, 887-894.

[128] Swati G.; Bishnoi S.; Singh P.; Rajesh B.; Kumar G.; Seth P.; Haranath D. Novel flux-assisted synthesis for enhanced afterglow properties of $(Ca,Zn)TiO_3:Pr^{3+}$ phosphor. *J. Alloy Compd.*, **2017**, 698, 930-937.

[129] Wei R. P.; Ju Z. H.; Ma J. X.; Zhang D.; Zang Z. P.; Liu W. S. A novel white afterglow phosphorescent phosphor $Ca_3SnSi_2O_9:Dy^{3+}$. *J. Alloy Compd.*, **2009**, 486, L17-L20.

[130] Wang W. X.; Sun Z. Y.; He X. Y.; Wei Y. D.; Zou Z. H.; Zhang J. C.; Wang Z. F.; Zhang Z. Y.; Wang Y. H. How to design ultraviolet emitting persistent materials for potential multifunctional applications: a living example of a $NaLuGeO_4:Bi^{3+},Eu^{3+}$ phosphor. *J. Mater. Chem. C*, **2017**, 5, 4310-4318.

[131] Lei B. F.; Yue S.; Zhang Y. Z.; Liu Y. L. Luminescence Properties of $Sr_2SnO_4:Sm^{3+}$ Afterglow Phosphor. *Chin. Phys. Lett.*, **2010**, 27, 037201.

[132] Li H. F.; Sun W. Z.; Jia Y. L.; Ma T. F.; Fu J. P.; Li D.; Zhang S.; Jiang L. H.; Pang R.; Li C. Y. Investigation on Luminescence Properties of a Long Afterglow Phosphor $Ca_2SnO_4:Tm^{3+}$. *Chem. Asian J.*, **2015**, 10, 2361-2367.

[133] Rodrigues V.; Hölsä, J.; Lastusaari M.; Felinto M. C.; Brito H. F. Defect to R^{3+} energy transfer: colour tuning of persistent luminescence in $CdSiO_3$. *J. Mater. Chem. C*, **2014**, 2, 1612-1618.

[134] Guo X. P.; Zhang Z. Y.; Wang C.; Xu J.; Ju Z. H.; An Y. Q.; Liu W. S. The Persistent Energy Transfer and Effect of Oxygen Vacancies on Red Long-Persistent Phosphorescence Phosphors $Ca_2SnO_4:Gd^{3+},Eu^{3+}$. *J. Electrochem. Soc.*, **2011**, 158, J405-J408.

[135] Ning L.; Tanner P. A.; Harutunyan V. V.; Aleksanyan E.; Makhov V. N.; Kirm M. Luminescence and excitation spectra of $YAG:Nd^{3+}$ excited by synchrotron radiation. *J.* Lumin., **2007**, 127, 397-403.

[136] Wu H.; Hu Y.; Kang F.; Li N.; Ju G.; Mu Z.; Yang Z. Luminescent Properties of Praseodymium in $CaWO_4$ Matrix. *J. Am. Ceram. Soc.*, **2012**, 95, 3214-3219.

[137] Aamili A.; Mahiou R.; Linares C.; Zambon D.; Avignant D.; Cousseins J. C. Luminescence of Gd^{3+} activated $LiNaY_2F_8$. *J Solid State Chem.*, **1991**, 95, 307-312.

[138] Pang R.; Li C.Y.; Jiang L. H.; Su Q. Blue long lasting phosphorescence of Tm^{3+} in zinc pyrophosphate phosphor. *J. Alloy Compd.*, **2009**, 471, 364-367.

[139] Garbout A.; Turki T.; Férid M. Structural and photoluminescence characteristics of Sm^{3+} activated $RE_2Ti_2O_7$ (RE = Gd, La) as orange-red emitting phosphors. *J. Lumin.*, **2018**, 196, 326-336.

[140] Du F. P.; Nakai Y.; Tsuboi T.; Huang Y. L.; Seo H. J. Luminescence properties and site occupations of Eu^{3+} ions doped in double phosphates $Ca_9R(PO_4)_7$ (R = Al, Lu). *J. Mater. Chem.*, **2011**, 21, 4669-4678.

[141] Feng P. F.; Wei Y. D.; Wang Y. N.; Zhang J. C.; Li H. H.; Ci Z. P. Long Persistent Phosphor $CdSiO_3$:Gd^{3+},Bi^{3+} and Potential Photocatalytic Application of $CdSiO_3$:Gd^{3+},Bi^{3+}@TiO_2 in Dark. *J. Am. Ceram. Soc.*, **2016**, 99, 2368-2375.

[142] Uzun E.; Öztürk E.; Ozpozan K.; Karacaoglu E. Thermoluminescence and photoluminescence properties of Mn^{4+}, $Pr^{3+,4+}$, Nd^{3+} and Eu^{3+} in $MgAl_2Si_2O_8$. *J. Lumin.*, **2016**, 173, 73-81.

[143] Zhao H. W.; Shi M. M.; Zou J.; Yang B. B.; Li Y.; Wang Z. M.; Chang C. K. Synthesis and luminescent properties of a new cyan afterglow phosphor $CaSnO_3$:Gd^{3+}. *Ceram. Int.*, **2017**, 43, 2750-2755.

[144] Gai S. L.; Yang P. P.; Wang D.; Li C. X.; Niu N.; He F.; Li X. B. Monodisperse Gd_2O_3:Ln (Ln = Eu^{3+}, Tb^{3+}, Dy^{3+}, Sm^{3+}, Yb^{3+}/Er^{3+}, Yb^{3+}/Tm^{3+}, and Yb^{3+}/Ho^{3+}) nanocrystals with tunable size and multicolor luminescent properties. *CrystEngComm*., **2011**, 13, 5480-5487.

[145] Que M. D.; Ci Z. P.; Wang Y. H.; Zhu G.; Shi Y. R.; Xin S. Y. Synthesis and luminescent properties of $Ca_2La_8(GeO_4)_6O_2$:RE^{3+} (RE^{3+} = Eu^{3+}, Tb^{3+}, Dy^{3+}, Sm^{3+}, Tm^{3+}) phosphors. *J. Lumin.*, **2013**, 144, 64-68.

[146] Marciniak L.; Hreniak D.; Strek W. Controlling luminescence colour through concentration of Dy^{3+} ions in $LiLa_{1-x}Dy_xP_4O_{12}$ nanocrystals. *J. Mater. Chem. C*, **2014**, 2, 5704-5708.

[147] Geng D. L.; Shang M. M.; Zhang Y.; Lian H. Z.; Lin J. Color-Tunable and White Luminescence Properties via Energy Transfer in Single-Phase $KNaCa_2(PO_4)_2$:A (A = Ce^{3+}, Eu^{2+}, Tb^{3+}, Mn^{2+}, Sm^{3+}) Phosphors. *Inorg. Chem.*, **2013**, 52, 13708-13718.

[148] Kang F. W.; Sun G. H.; Wang A. W.; Xiao X. F.; Li Y. Y.; Lu J.; Huang B. L. Multicolor Tuning and Temperature-Triggered Anomalous Eu^{3+}-Related Photoemission Enhancement via Interplay of Accelerated Energy Transfer and Release of Defect-Trapped Electrons in the Tb^{3+},Eu^{3+}-Doped Strontium-Aluminum Chlorites. *ACS Appl. Mater. Interfaces*, **2018**, 10, 36157.

[149] Kang F. W.; Zhang Y.; Peng M. Y. Controlling the Energy Transfer via Multi Luminescent Centers to Achieve White Light/Tunable Emissions in a Single-Phased X2-Type Y_2SiO_5:Eu^{3+},Bi^{3+} Phosphor For Ultraviolet Converted LEDs. *Inorg. Chem.*, **2015**, *54*, 1462-1473.

[150] Xu Y.; Yang Z. W.; Qiu J. B.; Song Z. G. Investigation of ultraviolet and visible persistence luminescence property of $CdSiO_3$:Bi^{3+},Tb^{3+} phosphors. *Mater. Express*, **2018**, 8, 99-104.

[151] Li Y.; Li Y. Y.; Sharafudeen K.; Dong G. P.; Zhou S. F.; Ma Z. J.; Peng M. Y.; Qiu J. R. A strategy for developing near infrared long-persistent phosphors: taking $MAlO_3:Mn^{4+},Ge^{4+}$ (M = La, Gd) as an example. *J. Mater. Chem. C*, **2014**, 2, 2019-2027.

[152] Yan W. Z.; Lin L.; Chen Y. H.; Yin M. New Red Long Afterglow Aluminate Materials Doped with Mn^{4+}. *Chin. J. Lumin.*, **2008**, 29, 114-118.

[153] Zhang X. W.; Nie J. M.; Liu S. S,; Li Y.; Qiu J. R. Deep-red photoluminescence and long persistent luminescence in double perovstkite-type $La_2MgGeO_6:Mn^{4+}$. *J. Am. Ceram. Soc.*, **2018**, 101, 1576-1584.

[154] Liu J. M.; Liu Y.; Zhang D. D.; Fang G. Z.; Wang S. Synthesis of $GdAlO_3:Mn^{4+},Ge^{4+}$@Au Core-shell Nanoprobes with Plasmon-Enhanced Near-Infrared Persistent Luminescence for in Vivo Trimodality Bioimaging. *ACS Appl. Mater. Inter.*, **2016**, 8, 29939-29949.

[155] Xue F. H.; Hu Y. H.; Chen L.; Wu H. Y.; Ju G. F.; Wang T.; Yang L. A novel rare-earth free red long-persistent phosphor: $Mg_2GeO_4:Mn^{4+}$. *Ceram. Int.*, **2017**, 43, 15141-15145.

[156] Du J. R.; Poelman D. Near-infrared persistent luminescence in Mn^{4+} doped perovskite type solid solutions. *Ceram. Int.*, **2019**, 45, 8345-8353.

[157] Li S. Y.; Zhu Q.; Li X. D.; Sun X. D.; Li J. G. $LaAlO_3:Mn^{4+}$: Defects engineering *via* Ge^{4+} doping for greatly enhanced luminescence and improved afterglow. *J. Alloy Compd.*, **2020**, 827, 154365.

[158] Li Z. J.; Zhang Y. W,; Wu X.; Wu X. Q.; Maudgal R.; Zhang H. W.; Han G. In Vivo Repeatedly Charging Near-Infrared-Emitting Mesoporous $SiO_2/ZnGa_2O_4:Cr^{3+}$ Persistent Luminescence Nanocomposites. *Adv. Sci.*, **2015**, 2, 1500001.

[159] Castaig V.; Sontakke A. D.; Fernández-Carrión A. J.; Touati N.; Binet L.; Allix M.; Gourier D.; Viana B. Persistent Luminescence of $ZnGa_2O_4:Cr^{3+}$ Transparent Glass Ceramics: Effects of Excitation Wavelength and Excitation Power. *Eur. J. Inorg. Chem.*, **2017**, 5114-5120.

[160] Li Y.; Zhou S. F.; Li Y Y.; Sharafudeen K.; Ma Z. J.; Dong G. P.; Peng M. Y.; Qiu J. R. Long persistent and photo-stimulated luminescence in Cr^{3+}-doped Zn-Ga-Sn-O phosphors for deep and reproducible tissue imaging. *J. Mater. Chem. C*, **2014**, 2, 2657-2663.

[161] Li J. L.; Shi J. P.; Wang C. C.; Li P. H.; Yu Z. F.; Zhang H. W. Five-nanometer $ZnSn_2O_4$:Cr,Eu ultra-small nanoparticles as new near infrared-emitting persistent luminescent nanoprobes for cellular and deep tissue imaging at 800 nm. *Nanoscale*, **2017**, 9, 8631-8638.

[162] Shen F. J.; Deng C. Y.; Wang X.; Zhang C. Effect of Cr on long-persistent luminescence of near-infrared phosphor $Zn_3Ga_2Ge_2O_{10}:Cr^{3+}$. *Mater. Lett.*, **2016**, 178, 185-189.

[163] Basavaraju N.; Priolkar K. R.; Gourier D.; Sharma S. K.; Bessière A.; Viana B. The importance of inversion disorder in the visible light induced persistent luminescence in Cr^{3+} doped AB_2O_4 (A = Zn or Mg and B = Ga or Al). *Phys. Chem. Chem. Phys.*, **2015**, 17, 1790-1799.

[164] Li Y.; Li Y. Y.; Chen R. C.; Sharafudeen K.; Zhou S. F.; Gecevicius M.; Wang H. H.; Dong G. P.; Wu Y. L.; Qin X. X.; Qiu J. R. Tailoring of the trap distribution and crystal field in Cr^{3+}-doped non-gallate phosphors with near-infrared long-persistence phosphorescence. *NPG Asia Mater.*, **2015**, 7, e180.

[165] Zhang Y.; Huang R.; Li H. L.; Hou D. J.; Lin Z. X.; Song J.; Guo Y. Z.; Lin H. H.; Song C.; Lin Z. W.; Robertson J. Germanium substitution endowing Cr^{3+}-doped zinc aluminate phosphors

with bright and super-long near-infrared persistent luminescence. *Acta Mater.*, **2018**, 155, 214-221.

[166] Xu D. D.; Qiu Z. C.; Zhang Q.; Huang L. J.; Ye Y. Y.; Cao L. W.; Meng J. X. $Sr_2MgWO_6:Cr^{3+}$ phosphors with effective near-infrared fluorescence and long-lasting phosphorescence. *J. Alloy Compd.*, **2019**, 781, 473-478.

[167] Qiu K. L.; Li P. L.; Meng X. Y.; Liu J. J.; Bao Q.; Li Y. B.; Li X.; Wang Z. P.; Yang Z. P.; Wang Z. J. Trap distribution and mechanism for near infrared long-afterglow material $AlMgGaO_4:Cr^{3+}$. *Dalton T.*, **2019**, 48, 618-627.

[168] Xue F. H.; Hu Y. H.; Fan L. M.; Ju G. F.; Lv Y.; Li Y. Cr^{3+}-activated $Li_5Zn_8Al_5Ge_9O_{36}$: A near-infrared long-afterglow phosphor. *J. Am. Ceram. Soc.*, **2017**, 100, 3070-3079.

[169] Zhou X. Q.; Ju G. F.; Dai T. S.; Li Y.; Wu H. Y.; Jin Y. H.; Hu Y. H. $Li_5Zn_8Ga_5Ge_9O_{36}$: Cr^{3+}, Ti^{4+}: A Long Persistent Phosphor Excited in a Wide Spectral Region from UV to Red Light for Reproducible Imaging through Biological Tissue. *Chem. Asian J.*, **2019**, 14, 1506-1514.

[170] Jin Y. H.; Hu Y. H.; Yuan L. F.; Chen L.; Wu H. Y.; Ju G. F.; Duan H.; Mu Z. F. Multifunctional near-infrared emitting Cr^{3+}-doped $Mg_4Ga_8Ge_2O_{20}$ particles with long persistent and photostimulated persistent luminescence, and photochromic properties. *J. Mater. Chem. C*, **2016**, 4, 6614-6625.

[171] Wang Q. W.; Zhang S. Y.; Li Z. W.; Zhu Q. Near Infrared-Emitting Cr^{3+}/Eu^{3+} Co-doped Zinc Gallogermanate Persistence Luminescent Nanoparticles for Cell Imaging. *Nanoscale Res. Lett.*, **2018**, 13, 64.

[172] Lu Y. Y.; Liu F.; Gu Z. J.; Pan Z. W. Long-lasting near-infrared persistent luminescence from β-$Ga_2O_3:Cr^{3+}$ nanowire assemblies. *J. Lumin.*, **2011**, 131, 2784-2787.

[173] De Clercq O. Q.; Martin L. I. D. J.; Korthout K.; Kusakovskij J.; Vrielinck H.; Poelman D. Probing the local structure of the near-infrared emitting persistent phosphor $LiGa_5O_8:Cr^{3+}$. *J. Mater. Chem. C*, **2017**, 5, 10861-10868.

[174] Zhong R. X.; Zhang J. H.; Zhang X.; Lu S.; Wang X. J. Red phosphorescence in $Sr_4Al_{14}O_{25}:Cr^{3+},Eu^{2+},Dy^{3+}$ through persistent energy transfer. *Appl. Phys. Lett.*, **2006**, 88, 201916.

[175] Xu D. D.; Wu X. M.; Zhang Q.; Li W. W.; Wang T.; Cao L. W.; Meng J. X. Fluorescence property of novel near-infrared phosphor $Ca_2MgWO_6:Cr^{3+}$. *J. Alloy Compd.*, **2018**, 731, 156-161.

[176] Sun F. Q.; Xie R. R.; Guan L.; Zhang C. Y. The near-infrared long-persistent phosphorescence of Cr^{3+}-activated non-gallate phosphor. *Mater. Lett.*, **2016**, 164, 39-43.

[177] Bai Q. Y.; Li P. L.; Wang Z. J.; Li T.; Xu S. C.; Yang Z. P. Using Ca^{2+} ions to induce the long afterglow and bluish white emission of red emitting phosphor $Zn_3Al_2Ge_2O_{10}:Cr^{3+}$. *Mater. Design*, **2016**, 91, 28-36.

[178] Cheng Y.; Sun K. N.; Ge P. H. Yb^{3+} and Er^{3+} co-doped $ZnGa_2O_4:Cr^{3+}$ powder phosphors: Combining green up-conversion emission and red persistent luminescence. *Opt. Mater.*, **2018**, 83, 13-18.

[179] Teng Y.; Zhou J. J.; Khisro S. N.; Zhou S. F.; Qiu J. R. Persistent luminescence of $SrAl_2O_4$: Eu^{2+},Dy^{3+},Cr^{3+} phosphors in the tissue transparency window. *Mater. Chem. Phys.*, **2014**, 147, 772-776.

[180] Zhang Y.; Huang R.; Lin Z. X.; Song J.; Wang X.; Guo Y. Q.; Song C.; Yu Y. Co-dopant influence on near-infrared luminescence properties of Zn_2SnO_4:Cr^{3+},Eu^{3+} ceramic discs. *J. Alloy Compd.*, **2016**, 686, 407-412.

[181] Li J. L.; Wang C. C.; Shi J. P.; Li P. H.; Yu Z. F.; Zhang H. W. Porous $GdAlO_3$:Cr^{3+},Sm^{3+} drug carrier for real-time long afterglow and magnetic resonance dual-mode imaging. *J. Lumin.*, **2018**, 199, 363-371.

[182] Lin X. H.; Zhang R. L.; Tian X. M.; Li, Y.; Du B. S.; Nie J. M.; Li Z. Z.; Chen L.; Ren J. J.; Qiu J. R.; Hu Y. H. Coordination Geometry-Dependent Multi-Band Emission and Atypically Deep-Trap-Dominated NIR Persistent Luminescence from Chromium-Doped Aluminates. *Adv. Opt. Mater.*, **2018**, 6, 1701161.

[183] Rai M.; Mishra K.; Rai S. B.; Morthekai P. Tailoring UV-blue sensitization effect in enhancing near infrared emission in X, Yb^{3+}: $CaGa_2O_4$ (X = Eu^{3+}, Bi^{3+}, Cr^{3+}) phosphor for solar energy conversion. *Mater. Res. Bull.*, **2018**, 105, 192-201.

[184] Kang R.; Nie J. M.; Dou X. J.; Zhang S. A.; Ju G. F.; Chen L.; Hu Y. H.; Li Y. Tunable NIR long persistent luminescence and discovery of trap-distribution-dependent excitation enhancement in transition metal doped weak-crystal-field $CaZnGe_2O_6$. *J. Alloy Compd.*, **2018**, 735, 692-699.

[185] Zhuang Y. X.; Ueda J.; Tanabe S. Tunable trap depth in $Zn(Ga_{1-x}Al_x)_2O_4$:Cr,Bi red persistent phosphors: considerations of high-temperature persistent luminescence and photostimulated persistent luminescence. *J. Mater. Chem. C*, **2013**, 1, 7849-7855.

[186] Sun F. Q.; Xie R. J.; Guan L.; Zhang C. Y. Cr^{3+} doped $Ca_{14}Zn_6Ga_{10}O_{35}$: A near-infrared long persistent luminescence phosphor. *J. Lumin.*, **2016**, 180, 251-257.

[187] Wang Q.; Mu Z. F.; Zhang S. A.; Zhang Q. T.; Zhu D. Y.; Feng J. Q.; Du Q. P.; Wu F. G. A novel near infrared long-persistent phosphor La_2MgGeO_6:Cr^{3+}, RE^{3+} (RE = Dy, Sm). *J. Lumin.*, **2019**, 206, 618-623.

[188] Chen D. Q. Near-infrared long-lasting phosphorescence in transparent glass ceramics embedding Cr^{3+}-doped $LiGa_5O_8$ nanocrystals. *J. Eur. Ceram. Soc.*, **2014**, 34, 4069-4075.

[189] Zou Z. H.; Tang X.; Wu C.; Wang D. Y.; Zhang J. C.; Ci Z. P.; Du S. S.; Wang Y. H. How to tune trap properties of persistent phosphor: Photostimulated persistent luminescence of $NaLuGeO_4$:Bi^{3+},Cr^{3+} tailored by trap engineering. *Mater. Res. Bull.*, **2018**, 97, 251-259.

[190] Basavaraju N.; Sharma S.; Bessiere A.; Viana B.; Gourier D.; Priolkar K. R. Red persistent luminescence in $MgGa_2O_4$:Cr^{3+}: a new phosphor for in vivo imaging. *J. Phys. D: Appl. Phys.*, **2013**, 46, 375401.

[191] Lin H. H.; Bai G. X.; Yu T.; Tsang M. K.; Zhang Q. Y.; Hao J. H. Site Occupancy and Near-Infrared Luminescence in $Ca_3Ga_2Ge_3O_{12}$:Cr^{3+} Persistent Phosphor. *Adv. Opt. Mater.*, **2017**, 5, 1700227.

[192] Wang X. S.; Li W. S.; Situ J. Q.; Ying X. Y.; Chen H.; Jin Y.; Du Y. Z. Multi-functional mesoporous β-Ga_2O_3:Cr^{3+} nanorod with long lasting near infrared luminescence for in vivo imaging and drug delivery. *RSC Adv.*, **2015**, 5, 12886-12889.

[193] Lin H. H.; Yu T.; Bai G. X.; Tsang M.-K.; Zhang Q. Y.; Hao J. H. Enhanced energy transfer in Nd^{3+}/Cr^{3+} co-doped $Ca_3Ga_2Ge_3O_{12}$ phosphors with near-infrared and long-lasting luminescence properties. *J. Mater. Chem. C*, **2016**, 4, 3396-3402.

[194] Cong Y.; He Y. Y.; Dong B.; Xiao Y.; Wang L. M. Long afterglow properties of $Zn_2GeO_4:Mn^{2+},Cr^{3+}$ phosphor. *Opt. Mater.*, **2015**, 42, 506-510.

[195] Asami K.; Ueda J.; Tanabe S. Trap depth and color variation of Ce^{3+}-Cr^{3+} co-doped $Gd_3(Al,Ga)_5O_{12}$ garnet persistent phosphors. *Opt. Mater.*, **2016**, 62, 171-175.

[196] Zhuang Y. X.; Ueda J.; Tanabe S. Enhancement of Red Persistent Luminescence in Cr^{3+}-Doped $ZnGa_2O_4$ Phosphors by Bi_2O_3 Codoping. *Appl. Phys. Exp.*, **2013**, 6, 052602.

[197] Li L.; Wang Y. H.; Li H.; Huang H. J.; Zhao H. Suppression of photocatalysis and long-lasting luminescence in $ZnGa_2O_4$ by Cr^{3+} doping. *RSC Adv.*, **2015**, 5, 57193-57200.

[198] Mu Z. F.; Hu Y. H.; Wang Y. H.; Wu H. Y.; Fu C. J.; Kang F. W. The structure and luminescence properties of long afterglow phosphor $Y_{3-x}Mn_xAl_{5-x}Si_xO_{12}$. *J. Lumin.*, **2011**, 131, 676-681.

[199] Che G. B.; Liu C. B.; Li X. Y.; Xu Z. L.; Liu Y.; Wang H. Luminescence properties of a new Mn^{2+}-activated red long-afterglow phosphor. *J. Phys. Chem. Solids*, **2008**, 69, 2091-2095.

[200] Lei B. F.; Liu Y. L.; Ye Z. R.; Shi C. S. Luminescence properties of $CdSiO_3:Mn^{2+}$ phosphor. *J. Lumin.*, **2004**, 109, 215-219.

[201] Lei B. F.; Li B.; Wang X. J.; Li W. L. Green emitting long lasting phosphorescence (LLP) properties of $Mg_2SnO_4:Mn^{2+}$ phosphor. *J. Lumin.*, **2006**, 118, 173-178.

[202] Ye S.; Zhang J. H.; Zhang X.; Wang X. J. Mn^{2+} activated red long persistent phosphors in $BaMg_2Si_2O_7$. *J. Lumin.*, **2007**, 122-123, 914-916.

[203] Liu Z. R.; Zhong R. X. Green and red long lasting phosphorescence (LLP) in γ-$Zn_3(PO_4)_2:Mn^{2+}/Ga^{3+}$. *J. Alloy Compd.*, **2013**, 556, 6-11.

[204] Patra A.; Baker G. A.; Baker S. N. Effects of dopant concentration and annealing temperature on the phosphorescence from $Zn_2SiO_4:Mn^{2+}$ nanocrystals. *J. Lumin.*, **2005**, 111, 105-111.

[205] Uheda K.; Maruyama T.; Takizawa H.; Endo T. Synthesis and long-period phosphorescence of $ZnGa_2O_4:Mn^{2+}$ spinel. *J. Alloy Compd.*, **1997**, 262-263, 60-64.

[206] Li X. D.; Tang X.; Wang Z. B.; Zou Z. H.; Zhang J. C.; Ci Z. P.; Wang Y. H. Structural, persistent luminescence properties and trap characteristics of an orthosilicate phosphor: $LiGaSiO_4:Mn^{2+}$. *J. Alloy Compd.*, **2017**, 721, 512-519.

[207] Xie T.; Guo H. X.; Zhang J. Y.; He Y. N.; Lin H.; Chen G. L.; Zheng Z. S. Effects of oxygen vacancies on luminescent properties of green long-lasting phosphorescent (LLP) material α-$Zn_3(PO_4)_2:Mn^{2+},K^+$. *J. Lumin.*, **2016**, 170, 150-154.

[208] Luo H. Y.; Cao J. K.; Li X. Y.; Wang X.; Peng M. Y. Topological tailoring of structure and defects to enhance red to near-infrared afterglow from Mn^{2+}-doped germanate photonic glasses. *J. Mater. Chem. C*, **2018**, 6, 11525-11535.

[209] Sun D Y.; Sung W. P.; Chen R. Preparation of a Novel Red Long Lasting Phosphorescent Material $CaAl_2Si_2O_8:Mn^{2+}$ and Investigation of its Luminescent Properties. *Appl. Mech. Mater.*, **2011**, 71-78, 3151-3155.

[210] Takemoto M.; Iseki T. Fluorescence and afterglow of $Ca_2Sn_2Al_2O_9:Mn^{2+}$. *J. Phys. Chem. Solids*, **2018**, 114, 88-93.

[211] Jin Y. H.; Hu Y. H.; Chen L.; Ju G. F.; Wu Y.; Mu F.; He M.; Xue H. Luminescent properties of a green long persistent phosphor $Li_2MgGeO_4:Mn^{2+}$. *Opt. Mater. Express*, **2016**, 6, 929-937.

[212] Xu J.; Cherepy N. J.; Ueda J.; Tanabe S. Red persistent luminescence in rare earth-free $AlN:Mn^{2+}$ phosphor. *Mater. Lett.*, **2017**, 206, 175-177.

[213] Liu Z. R.; Zhong R. X.; Zhao H.; Zhang X. Y. Influence on Afterglow Spectra due to Different Phases of $Zn_3(PO_4)_2:Mn^{2+}$. *Appl. Mech. Mater.*, **2013**, 423-426, 415-418.

[214] Li D. L.; Zheng D. W.; Shi J. Long Lasting Phosphorescence in Mn^{2+}-Activeted $ZnO-B_2O_3$ Glass. *Mater. Res. Appl.*, **2014**, 875-877, 54-58.

[215] Jin Y. H.; Hu Y. H.; Duan H.; Chen L.; Wang X. J. The long persistent luminescence properties of phosphors: Li_2ZnGeO_4 and $Li_2ZnGeO_4:Mn^{2+}$. *RSC Adv.*, **2014**, 4, 11360-11366.

[216] Xue F. H.; Hu Y. H.; Fan L. M.; Wang X. J.; Ju G. F.; He M.; Lv Y. Photoluminescence and afterglow of Mn^{2+} doped lithium zinc silicate. *J. Lumin.*, **2017**, 183, 68-72.

[217] Chen B. S.; Chen L. F.; Lin H.; Chen G. L.; Zheng Z. S.; Lin H.; Guo H. X.; Chen Z. H.; Huang L. F.; Zhou W. H. Zr^{4+} Co-Dopant Enhancing Afterglow Green Phosphor of $Zn_2SiO_4:Mn^{2+}$. *Adv, Mater. Res.*, **2012**, 393-395, 503-506.

[218] Jiang B.; Chi F. F.; Zhao L.; Wei X. T.; Chen Y. H.; Yin M. Luminescence properties of a new green emitting long afterglow phosphor $Ca_{14}Zn_6Ga_{10}O_{35}:Mn^{2+},Ge^{4+}$. *J. Lumin.*, **2019**, 206, 234-239.

[219] Wu M. H.; Chen W.; Zhang Y. H.; Zhang J. Y.; Chen G. L.; Zheng Z. S. Defects enhanced photoluminescence of Mn^{2+}-doped ZrP_2O_7 blue LLP materials. *J. Alloy Compd.*, **2019**, 789, 375-380.

[220] Lin L.; Yin M.; Shi C. S.; Zhang W. P. Luminescence properties of a new red long-lasting phosphor: $Mg_2SiO_4:Dy^{3+},Mn^{2+}$. *J. Alloy Compd.*, **2008**, 455, 327-330.

[221] Wang X. J.; Jia D.; Yen W. M. Mn^{2+} activated green, yellow, and red long persistent phosphors. *J. Lumin.*, **2003**, 102-103, 34-37.

[222] Li P. F.; Peng M. Y.; Wondraczek L.; Zhao Y. Q.; Viana B. Red to near infrared ultralong lasting luminescence from Mn^{2+}-doped sodium gallium aluminum germanate glasses and (Al,Ga)-albite glass-ceramics. *J. Mater. Chem. C*, **2015**, 3, 3406-3415.

[223] Wang J.; Su Q.; Wang S. B. Blue and red long lasting phosphorescence (LLP) in β-$Zn_3(PO_4)_2:Mn^{2+},Zr^{4+}$. *J. Phys. Chem. Solids*, **2005**, 66, 1171-1176.

[224] Wang J.; Wang S. B.; Su Q. Synthesis, photoluminescence and thermostimulated-luminescence properties of novel red long-lasting phosphorescent materials β-$Zn_3(PO_4)_2:Mn^{2+},M^{3+}$ (M = Al and Ga). *J. Mater. Chem.*, **2004**, 14, 2569-2574.

[225] Jin Y. H.; Hu Y. H.; Fu Y. R.; Ju G. F.; Mu Z. F.; Chen R.; Lin J. L.; Wang Z. H., Preparation, Design, and Characterization of the Novel Long Persistent Phosphors: Na_2ZnGeO_4 and $Na_2ZnGeO_4:Mn^{2+}$. *J. Am. Ceram. Soc.*, **2015**, 98, 1555-1561.

[226] Zhuang Y. X.; Ueda J.; Tanabe S. Multi-color persistent luminescence in transparent glass ceramics containing spinel nano-crystals with Mn^{2+} ions. *Appl. Phys. Lett.*, **2014**, 105, 191904.

[227] Li C. Y.; Yu Y. N.; Wang S. B.; Su Q. Photo-stimulated long-lasting phosphorescence in Mn^{2+}-doped zinc borosilicate glasses. *J. Non-Cryst. Sol.*, **2003**, 321, 191-196.

[228] Katayama Y.; Kayumi T.; Ueda J.; Tanabe S. Enhanced persistent red luminescence in Mn^{2+}-doped (Mg,Zn)GeO_3 by electron trap and conduction band engineering. *Opt. Mater.*, **2018**, 79, 147-151.

[229] Chi F. F.; Wei X. T.; Jiang B.; Chen Y. H.; Duan C. K.; Yin M. Luminescence properties and the thermal quenching mechanism of Mn^{2+} doped Zn_2GeO_4 long persistent phosphors. *Dalton T.*, **2018**, 47, 1303-1311.

[230] Zheng Y. J.; Zhang H. M.; Zhang H. R.; Zhang X. J.; Liu Y. L.; Lei B. F. Enhanced persistent properties of Mn^{2+} activated CaZnOS. *RSC Adv.*, **2017**, 7, 38498-38505.

[231] Zhang Y.; Zhong R. X.; Zhang X.; Ren X. G.; Hao Z. D.; Zhang J. H. Synthesis and Luminescent Properties of Green Long-lasting Phosphorescent Materials $MgAl_2O_4:Mn^{2+}$. *Chin. J. Lumin.*, **2010**, 31, 489-492.

[232] Xu X. H.; Wang Y. H.; Yu X.; Li Y. Q.; Gong Y. Investigation of Ce–Mn Energy Transfer in $SrAl_2O_4:Ce^{3+},Mn^{2+}$. *J. Am. Ceram. Soc.*, **2011**, 94, 160-163.

[233] Ye Q. F.; Wang Y. H.; Guo H. J.; Zhou X. F.; Feng P.; Ding S. S. Designing a novel red to near-infrared persistent phosphor $CaMgGe_2O_6:Mn^{2+},Sm^{3+}$ based on a vacuum referred binding energy diagram. *Dalton T.*, **2019**, 48, 11052-11062.

[234] Zheng W. X.; Wu H. Y.; Ju G. F.; Mo Z.; Dong H. F.; Hu Y. H.; Jin Y. H. Crystal field modulation-control, bandgap engineering and shallow/deep traps tailoring-guided design of a color-tunable long-persistent phosphor (Ca,Sr)$Ga_4O_7:Mn^{2+},Bi^{3+}$. *Dalton T.*, **2019**, 48, 253-265.

[235] Katayama Y.; Ueda J.; Tanabe S. Effect of Bi_2O_3 doping on persistent luminescence of $MgGeO_3:Mn^{2+}$ phosphor. *Opt. Mater. Express*, **2014**, 4, 613-623.

[236] Su F. H.; Ma B. S.; Ding K.; Li G. H.; Wang S. P.; Chen W.; Joly A. G.; McCready D. E. Luminescence temperature and pressure studies of Zn_2SiO_4 phosphors doped with Mn^{2+} and Eu^{3+} ions. *J. Lumin.*, **2006**, 116, 117-126.

[237] Zhang S. A.; Li Y.; Lv Y.; Fan L. M.; Hu Y. H.; He M. A full-color emitting phosphor $Ca_9Ce(PO_4)_7:Mn^{2+},Tb^{3+}$: Efficient energy transfer, stable thermal stability and high quantum efficiency. *Chem. Eng. J.*, **2017**, 322, 314-327.

[238] Kück S.; Sokólska, I. Spectroscopic investigation of Mn^{2+}, Pr^{3+} codoped $KMgF_3$ under vacuum-ultraviolet excitation. *J. Phys.: Condens. Mat.*, **2006**, 18, 5447-5457.

[239] Xu W.; Zhang X. Y.; Xu X. R. Single- and multi-step energy transfer from Mn^{2+} to Sm^{3+} in ZnS:Mn,Sm. *J. Lumin.*, **1984**, 31-32, 808-810.

[240] Gong Y.; Wang Y.; Xu X.; Li Y.; Xin S.; Shi L. The persistent energy transfer of Eu^{2+} and Mn^{2+} and the thermoluminescence properties of long-lasting phosphor $Sr_3MgSi_2O_8:Eu^{2+}$, Mn^{2+}, Dy^{3+}. *Opt. Mater.*, **2011**, 33, 1781-1785.

[241] Song F.; Ming C. G.; An L. Q.; Wang Q. R.; Yu Y.; Yu H.; Sun T. Q.; Tian J. G. $Tm^{3+}/Tb^{3+}/Mn^{2+}$ tri-doped phosphate glass ceramic for enhanced white-light-emitting material. *Mater. Lett.*, **2011**, 65, 3140-3142.

[242] Guo N.; Huang Y. J.; You H. P.; Yang M.; Song Y. H.; Liu K.; Zheng Y. H. $Ca_9Lu(PO_4)_7:Eu^{2+},Mn^{2+}$: A Potential Single-Phased White-Light-Emitting Phosphor Suitable for White-Light-Emitting Diodes. *Inorg. Chem.*, **2010**, 49, 10907-10913.

[243] Li G. G.; Zhang Y.; Geng D. L.; Shang M. M.; Peng C.; Cheng Z. Y.; Lin J. Single-Composition Trichromatic White-Emitting $Ca_4Y_6(SiO_4)_6O:Ce^{3+}/Mn^{2+}/Tb^{3+}$ Phosphor: Luminescence and Energy Transfer. *ACS Appl. Mater. Interfaces*, **2012**, 4, 296-305.

[244] Chen X.; Dai P. P.; Zhang X. T.; Li C.; Lu S.; Wang X. L.; Jia Y.; Liu Y. C. A Highly Efficient White Light $(Sr_3,Ca,Ba)(PO4)_3Cl:Eu^{2+},Tb^{3+},Mn^{2+}$ Phosphor via Dual Energy Transfers for White Light-Emitting Diodes. *Inorg. Chem.*, **2014**, 53, 3441-3448.

[245] Zhang Z.; Tang W. J. Tunable luminescence and energy transfer of $Ce^{3+}/Eu^{2+}/Mn^{2+}$-tridoped $Sr_8MgLa(PO_4)_7$ phosphor for white light LEDs. *J. Alloy Compd.*, **2016**, 663, 731-737.

[246] Qu X. F.; Cao L. X.; Liu W.; Su G.; Wang P. P. Luminescence properties of $CdSiO_3:Mn^{2+}$, RE^{3+} (RE = Sm, Dy, Eu) phosphors. *J. Alloy Compd.*, **2009**, 487, 387-390.

[247] Zhao H. J.; Li L. H.; Wu L. M.; Chen L. Syntheses, Crystal and Electronic Structures, and Physical Properties of Quaternary Semiconductors: $Ln_2Mn_3Sb_4S_{12}$ (Ln = Pr, Nd, Sm, Gd). *Inorg. Chem.*, **2010**, 49, 5811-5817.

[248] Ming C. G.; Song F.; Qin Y. T.; Ren X. B.; An L. Q. M (Tm^{3+}, Tb^{3+}, Ho^{3+}, Dy^{3+}, Mn^{2+})-doped transparent fluorophosphate glasses for white light-emitting-diodes. *Opt. Commun.*, **2014**, 321, 195-197.

[249] Liu X. Y.; Guo H.; Liu Y.; Ye S.; Peng M. Y.; Zhang Q. Y. Thermal quenching and energy transfer in novel Bi^{3+}/Mn^{2+} co-doped white-emitting borosilicate glasses for UV LEDs. *J. Mater. Chem. C*, **2016**, 4, 2506-2512.

[250] Shao H.; Bai X.; Cui H. N.; Pan G. C.; Jing P. T.; Qu S. N.; Zhu J. Y.; Zhai Y.; Dong B. White light emission in Bi^{3+}/Mn^{2+} ion co-doped $CsPbCl_3$ perovskite nanocrystals. *Nanoscale*, **2018**, 10, 1023-1029.

[251] Zhou J.; Rong X. M.; Zhang P.; Molokeev M. S.; Wei P. J.; Liu Q. L.; Zhang X. W.; Xia Z. G. Manipulation of Bi^{3+}/In^{3+} Transmutation and Mn^{2+}-Doping Effect on the Structure and Optical Properties of Double Perovskite $Cs_2NaBi_{1-x}In_xCl_6$. *Adv. Opt. Mater.*, **2019**, 7, 1801435.

[252] Lee J.; Einaga Y.; Fujishima A.; Park S. M. Electrochemical Oxidation of Mn^{2+} on Boron-Doped Diamond Electrodes with Bi^{3+} Used as an Electron Transfer Mediator. *J. Electrochem. Soc.*, **2004**, 151, E265-E270.

[253] Holzapfel N. P.; Majher J. D.; Strom T. A.; Moore C. E.; Patrick P. W. $Cs_4Cd_{1-x}Mn_xBi_2Cl_{12}$ — A Vacancy-Ordered Halide Perovskite Phosphor with High-Efficiency Orange-Red Emission. *Chem. Mater.*, **2020**, 32, 3519-3516.

[254] Kim J. S.; Kim J. S.; Kim T. W.; Park H. L.; Kim Y. G.; Chang S. K.; Han S. D. Energy transfer among three luminescent centers in full-color emitting $ZnGa_2O_4:Mn^{2+},Cr^{3+}$ phosphors. *Solid State Commun.*, **2004**, 131, 493-497.

[255] Wakui Y.; Shan Y. J.; Tezuka K.; Imoto H.; Ando M. Crystal-site engineering approach for preparation of $MgB_2O_4:Mn^{2+},Mn^{4+}$ (B=Al, Ga) phosphors: Control of green/red luminescence properties. *Mater. Res. Bull.*, **2017**, 90, 51-58.

[256] Zhang H. H.; Chen Y. Y.; Zhu X. Y.; Zhou H. C.; Yao Y.; Li X. D. Mn^{2+}-doped Zn_2GeO_4 for photocatalysis hydrogen generation. *Int. J. Energy Res.*, **2019**, 43, 5013-5019.

[257] Zhang S. A.; Hu Y. H.; Chen R.; Wang X. J.; Wang Z. H. Photoluminescence and persistent luminescence in Bi^{3+}-doped Zn_2GeO_4 phosphors. *Opt. Mater.*, **2014**, 36, 1830-1835.
[258] Dou X. J.; Xiang H. W.; Wei P. L.; Zhang S. A.; Ju G. F.; Meng Z. M.; Chen L.; Hu Y. H.; Li Y. A novel phosphor $CaZnGe_2O_6:Bi^{3+}$ with persistent luminescence and photo-stimulated luminescence. *Mater. Res. Bull.*, **2018**, 105, 226-230.
[259] Jin Y. H.; Hu Y. H.; Chen L.; Wang X. J.; Ju G. F.; Mu Z. F. Persistent luminescence in Bi^{3+} doped $CaWO_4$ matrix. *Radiat. Meas.*, **2013**, 51-52, 18-24.
[260] Sun W. Z; Pang R.; Li H. M.; Li D.; Jiang L. H.; Zhang S.; Fu J. P.; Li C. Y. Investigation of a novel color tunable long afterglow phosphor $KGaGeO_4:Bi^{3+}$: luminescence properties and mechanism. *J. Mater. Chem. C*, **2017**, 5, 1346-1355.
[261] Wang X.; Boutinaud P.; Li L. Y.; Cao J. K.; Xiong P. X.; Li X. Y.; Luo H. Y.; Peng M. Y. Novel persistent and tribo-luminescence from bismuth ion pairs doped strontium gallate. *J. Mater. Chem. C*, **2018**, 6, 10367-10375.
[262] Zhuang Y. X.; Ueda J.; Tanabe S. Photochromism and white long-lasting persistent luminescence in Bi^{3+}-doped $ZnGa_2O_4$ ceramics. *Opt. Mater. Express*, **2012**, 2, 1378-1383.
[263] Jia D. D.; Zhu J.; Wu B. Q. Improvement of persistent phosphorescence of $Ca_{0.9}Sr_{0.1}S:Bi^{3+}$ by codoping Tm^{3+}. *J. Lumin.*, **2000**, 91, 59-65.
[264] Li J. Y.; Pang R.; Sun W. Z; Wu H. Y.; Li H. M.; Jiang L. H.; Zhang S.; Feng J.; Liu L. Y.; Li C. Y. A new blue long-lasting phosphorescence phosphor $Mg_2SnO_4:Bi^{3+}$: synthesis and luminescence properties. *J. Mater. Sci. - Mater. El.*, **2018**, 29, 4163-4170.
[265] Shi J. P.; Sun X.; Zheng S. H.; Fu X. Y.; Yang Y.; Wang J. N.; Zhang H. W. Super-Long Persistent Luminescence in the Ultraviolet A Region from a Bi^{3+}-Doped $LiYGeO_4$ Phosphor. *Adv. Opt. Mater.*, **2019**, 0, 1900526.
[266] Jia D. D.; Zhu J.; Wu B. Q. Trapping Centers in $CaS:Bi^{3+}$ and $CaS:Eu^{2+},Tm^{3+}$. *J. Electrochem. Soc.*, **2000**, 147, 386-389.
[267] Yang Z. W.; Liao J. Y.; Wang T. Y.; Wu H. J.; Qiu J. B.; Song Z. G.; Zhou D. C. Ultraviolet long afterglow emission in Bi^{3+} doped $CdSiO_3$ phosphors. *Mater. Express*, **2014**, 4, 172-176.
[268] Hu R.; Zhang Y.; Zhao Y.; Wang X. S.; Li G. R.; Wang C. Y. UV-Vis-NIR broadband photostimulated luminescence of $LiTaO_3:Bi^{3+}$ long-persistent phosphor and the optical storage properties. *Chem. Eng. J.*, **2020**, 392, 124807.
[269] Wang S. B.; Chen W. B.; Zhou D. C.; Qiu J. B.; Xu X. H; Yu X. Long persistent properties of $CaGa_2O_4:Bi^{3+}$ at different ambient temperature. *J. Am. Ceram. Soc.*, **2017**, 100, 3514-3521.
[270] Kuang J. Y.; Liu Y. L. Luminescence Properties of a Pb^{2+} Activated Long-Afterglow Phosphor. *J. Electrochem. Soc.*, **2006**, 153, G245-G247.
[271] Fu J. Orange- and Violet-Emitting Long-Lasting Phosphors. *J. Am. Ceram. Soc.*, **2002**, 85, 255-257.
[272] Yi S. J.; Liu Y. L.; Zhang J. X.; Yuan D. S. Long Phosphorescence Persistence Property of $Cd_2Ge_7O_{16}$:Pb. *Chem. J. Chin. Univ.*, **2004**, 25, 1400-1402.
[273] Liang Y. J.; Liu F.; Chen Y. F.; Sun K. N.; Pan Z. W. Long persistent luminescence in the ultraviolet in Pb^{2+}-doped $Sr_2MgGe_2O_7$ persistent phosphor. *Dalton Trans.*, **2016**, 45, 1322-1326.

[274] Kang F. W.; Zhang H. S.; Wondraczek L.; Yang X. B.; Zhang Y.; Lei D. Y.; Peng M. Y. Band-Gap Modulation in Single Bi^{3+}-Doped Yttrium-Scandium-Niobium Vanadates for Color Tuning over the Whole Visible Spectrum. *Chem. Mater.*, **2016**, 28, 2692-2703.

[275] Blasse G.; Bril A. Investigations on Bi^{3+}-Activated Phosphors. *J. Phys. Chem.*, **1968**, 48, 217-222.

[276] Chen L. M.; Long Y. M.; Qin Y. M.; Li W. F. Co-precipitation preparation, characterization and optical properties of blue $CaSb_2O_6$:Bi^{3+} nano-phosphor. *Mater. Lett.*, **2013**, 102-103, 59-61.

[277] Han J.; Pan F. J.; Molokeev M. S.; Dai J. F.; Peng M. Y.; Zhou W. J.; Wang J. Redefinition of Crystal Structure and Bi^{3+} Yellow Luminescence with Strong Near-Ultraviolet Excitation in La_3BWO_9:Bi^{3+} Phosphor for White Light-Emitting Diodes. *ACS Appl. Mater. Interfaces*, **2018**, 10, 13660-13668.

[278] Kang F. W.; Peng M. Y.; Zhang Q. Y.; Qiu J. R. Abnormal Anti-Quenching and Controllable Multi-Transitions of Bi^{3+} Luminescence by Temperature in a Yellow-Emitting $LuVO_4$:Bi^{3+} Phosphor for UV-Converted White LEDs. *Chem. - Eur. J.*, **2014**, 20, 11522-11530.

[279] Kang F. W.; Peng M. Y.; Lei D. Y.; Zhang Q. Y. Recoverable and Unrecoverable Bi^{3+}-Related Photoemissions Induced by Thermal Expansion and Contraction in $LuVO_4$:Bi^{3+} and $ScVO_4$:Bi^{3+} Compounds. *Chem. Mater.*, **2016**, 28, 7807-7815.

[280] Tang Z. B.; Wang D. Y.; Wang Y. H.; Khan W. U.; Du S. S. Photoluminescence of $BaZrSi_3O_9$:Bi^{3+} as a yellow-emitting phosphor for White LEDs. *Mater. Res. Bull.*, **2016**, 83, 336-339.

[281] Han J.; Li L. J.; Peng M. Y.; Huang B. L.; Pan F. J.; Kang F. W.; Li L. Y.; Wang J.; Lei B. F. Toward Bi^{3+} Red Luminescence with No Visible Reabsorption through Manageable Energy Interaction and Crystal Defect Modulation in Single Bi^{3+}-Doped $ZnWO_4$ Crystal. *Chem. Mater.*, **2017**, 29, 8412-8424.

[282] Kang F. W.; Yang X. B.; Peng M. Y.; Wondraczek L.; Ma Z. J.; Zhang Q. Y.; Qiu J. R. Red Photoluminescence from Bi^{3+} and the Influence of the Oxygen-Vacancy Perturbation in $ScVO_4$: A Combined Experimental and Theoretical Study. *J. Phys. Chem. C*, **2014**, 118, 7515-7522.

[283] Wei Y.; Xing G. C.; Liu K.; Li G.; Dang P. P,; Liang S. S.; Liu M.; Cheng Z. Y.; Jin D. Y.; Lin J. New strategy for designing orangish-red-emitting phosphor via oxygen-vacancy-induced electronic localization. *Light - Sci. Appl.*, **2019**, 8, 15.

[284] Kang F. W.; Peng M. Y.; Yang X. B.; Dong G. P.; Nie G. C.; Liang W. J.; Xu S. H.; Qiu J. R. Broadly tuning Bi^{3+} emission via crystal field modulation in solid solution compounds (Y,Lu,Sc)VO_4:Bi for ultraviolet converted white LEDs. *J. Mater. Chem. C*, **2014**, *2*, 6068-6076.

[285] Kang F. W.; Sun G. H.; Boutinaud P.; Gao F.; Wang Z. G.; Lu J.; Li, Y. Y.; Xiao, S. S. Tuning the Bi^{3+}-photoemission color over the entire visible region by manipulating secondary cations modulation in the $ScV_xP_{1-x}O_4$:Bi^{3+} ($0 \leq x \leq 1$) solid solution. *J. Mater. Chem. C*, **2019**, 7, 9865-9877.

[286] Yan S. X.; Zhang J. H.; Zhang X.; Lu S. Z.; Ren X. G.; Nie Z. G.; Wang X. J. Enhanced Red Emission in $CaMoO_4$:Bi^{3+},Eu^{3+}. *Phys. Chem. C*, 2007, 111, 13256-13260.

[287] Chen L.; Jiang Y.; Yang Y. G.; Huang J.; Shi Y.; Chen S. F. The energy transfer of $Bi^{3+} \rightarrow Eu^{3+}$ and $Bi^{3+} \rightarrow Tb^{3+}$ in YBO_3 host to produce light. *J. Phys. D: Appl. Phys.*, **2009**, 42, 215104.

[288] Yu X.; Zhang L.; Xu X. H.; Wang T.; Yu H. L.; Jiang T. M.; Jiao Q.; Yang Z. W.; Zhou D. C.; Qiu J. B. Development of a single-phased $Ca_3SnSi_2O_9:Bi^{3+},Dy^{3+},Eu^{3+}$ phosphor with tri-colors for white light-emitting diodes. *J. Lumin.*, **2014**, 145, 114-118.

[289] Lai S. F.; Yang Z. W.; Liao J. Y.; Qiu J. B.; Song Z. G.; Yang Y.; Zhou D. C. Investigation of persistent luminescence property of Bi^{3+}, Dy^{3+} co-doped $CdSiO_3$ phosphor. *Mater. Res. Bull.*, **2014**, 60, 714-718.

[290] Jia W. Y.; Pérez-Andújar A.; Rivera I. Energy Transfer Between Bi^{3+} and Pr^{3+} in Doped $CaTiO_3$. *J. Electrochem. Soc.*, **2003**, 150, H161-H164.

[291] Luitel H. N.; Watari T.; Chand R.; Torikai T.; Yada M. Photoluminescence properties of a novel orange red emitting $Sr_4Al_{14}O_{25}:Sm^{3+}$ phosphor and PL enhancement by Bi^{3+} co-doping. *Opt. Mater.*, **2012**, 34, 1375-1380.

[292] Cao R. P.; Ren Y.; Chen T.; Wang W. H.; Guo Q. D.; Hu Q. L.; Liao C. X.; Fan T. Emission improvement and tunable emission properties of $SrZrSi_2O_7$:R (R = Sm^{3+} and Sm^{3+}/Bi^{3+}) phosphors. *J. Lumin.*, **2020**, 225, 117350.

[293] Zhu Y. J.; Qiu Z. X.; Ai B. Y.; Lin Y. T.; Zhou W. L.; Zhang J. L.; Yu L. P.; Mi Q. H.; Lian S. X. Significant improved quantum yields of $CaAl_{12}O_{19}:Mn^{4+}$ red phosphor by co-doping Bi^{3+} and B^{3+} ions and dual applications for plant cultivations. *J. Lumin.*, **2018**, 201, 314-320.

[294] Qiu Z. X.; Luo T. T.; Zhang J. L.; Zhou W. L.; Yu L. P.; Lian S. X. Effectively enhancing blue excitation of red phosphor $Mg_2TiO_4:Mn^{4+}$ by Bi^{3+} sensitization. *J. Lumin.*, **2015**, 158, 130-135.

[295] Zhou Z.; Zhong Y.; Xia M.; Zhou N.; Lei B. F.; Wang J.; Wu F. F. Tunable dual emission of $Ca_3Al_4ZnO_{10}:Bi^{3+},Mn^{4+}$ via energy transfer for indoor plant growth lighting. *J. Mater. Chem. C*, **2018**, 6, 8914-8922.

[296] Xing G. C.; Feng Y. X.; Pan M.; Wei Y.; Li G. G.; Dang P. P.; Liang S. S.; Molokeev M. S.; Cheng Z. Y.; Lin J. Photoluminescence tuning in a novel Bi^{3+}/Mn^{4+} co-doped La_2ATiO_6:(A = Mg, Zn) double perovskite structure: phase transition and energy transfer. *J. Mater. Chem. C*, **2018**, 6, 13136-13147.

[297] Liu C. Y.; Xia Z. G.; Molokeev M. S.; Liu Q. L. Synthesis, Crystal Structure, and Enhanced Luminescence of Garnet-Type $Ca_3Ga_2Ge_3O_{12}:Cr^{3+}$ by Codoping Bi^{3+}. *J. Am. Ceram. Soc.*, **2015**, 98, 1870-1876.

[298] Chen L.; Chen K. J.; Hu S. F.; Liu R. S. Combinatorial chemistry approach to searching phosphors for white light-emitting diodes in (Gd-Y-Bi-Eu)VO_4 quaternary system. *J. Mater. Chem.*, **2011**, 21, 3677-3685.

[299] Xu Y.; Sheng Y.; Yuan B.; Guan X.; Ma C.; Song H.; Zou F.; Zheng Y. Luminescence properties, energy transfer and multisite luminescence of $Bi^{3+}/Sm^{3+}/Eu^{3+}$-coactivated $Ca_{20}Al_{26}Mg_3Si_3O_{68}$ as a potential phosphor for white-light LEDs. *RSC Adv.*, **2016**, **6**, 89984-89993.

[300] Cao R. P.; Liao C. L.; Xiao F.; Zheng G. T.; Hu W.; Guo Y. M.; Ye Y. X. Emission enhancement of $LiLaMo_2O_8:Eu^{3+}$ phosphor by co-doping with Bi^{3+} and Sm^{3+} ions. *Dyes Pigments*, **2018**, 149, 574-580.

[301] Fan B.; Liu J.; Zhao W. Y.; Qi S. M. Luminescence and energy transfer of a single-phased phosphor Y_2GeO_5:Bi^{3+},Tm^{3+},Tb^{3+},Eu^{3+} for white UV LEDs. *Opt. Mater.*, **2019**, 90, 33-39.

[302] Yu T.; Yu D. C.; Zhang Q. Y.; Meijerink A. Thermally deactivated energy transfer in Bi^{3+}-Yb^{3+} codoped Y_2O_3: Evidence for the exchange interaction mechanism. *Phys. Rev. B*, **2018**, 98, 134308.

[303] Xiao S. X.; Chen Z. S.; Huang H. Q.; Zheng J. G.; Xu J. P. Upconversion enhancement in $NaYF_4$:Yb^{3+},Er^{3+} crystal via Bi^{3+} doping. *IOP Conf. Series: Materials Science and Engineering*, **2018**, 359, 012043.

[304] Huang S. Q.; Lou Z. Y.; Qi Z. B.; Zhu N. W.; Yuan H. P. Enhancing upconversion emissions of Er^{3+}/Tm^{3+}/Yb^{3+} tridoped ($NaY(WO_4)_2$/YF_3) through TiO_2 coating and Bi^{3+} doping and its photocatalytic applications. *Appl. Catal. B - Environ.*, **2015**, 168-169, 313-321.

[305] Du M. H. Chemical trends of electronic and optical properties of ns^2 ions in halides. *J. Mater. Chem. C*, **2014**, 2, 4784-4791.

[306] Singh V.; Tiwari M. K. Pb^{2+} doped diopside $CaMgSi_2O_6$: New UV luminescent phosphor. *J. Lumin.*, **2020**, 202, 163542.

[307] Wang S. F., Lü M. K.; Gu F.; Song C. F.; Xu D.; Yuan D. R.; Zhou G. J.; Qi Y. X. Photoluminescence characteristics of Pb^{2+} ion in sol-gel derived $ZnTiO_3$ nanocrystals. *Inorg. Chem. Commun.*, **2003**, 6, 185-188.

[308] Motloung S. V.; Dejene F. B.; Swart H. C.; Ntwaeaborwa O. M. Effects of Pb^{2+} ions concentration on the structure and PL intensity of Pb-doped $ZnAl_2O_4$ nanocrystals synthesized using sol-gel process. *J. Sol-Gel. Sci. Techno.*, **2014**, 70, 422-727.

[309] Yılmaz, M.; Erdoğmuş E. Luminescence properties of ZnB_2O_4:Pb^{2+} phosphors: Suppression of concentration quenching. *J. Lumin.*, **2020**, 218, 116868.

[310] Zeng C. M.; Hu T.; Hou N. J.; Liu S. Y.; Gao W. L.; Cong R. H.; Yang T. Photocatalytic pure water splitting activities for $ZnGa_2O_4$ synthesized by various methods. *Mater. Res. Bull.*, **2015**, 61, 481-485.

[311] Ma X. L.; Zhang J. C.; Li H. H.; Duan B. C.; Guo L. N.; Que M. D.; Wang Y. H. Violet blue long-lasting phosphorescence properties of Mg-doped $BaZrO_3$ and its ability to assist photocatalysis. *J. Alloy Compd.*, **2013**, 580, 564-569.

[312] Mei Y. H.; Xu H.; Zhang J. C.; Ci Z. P.; Duan M. X.; Peng S. L.; Zhang Z. Y.; Tian T.; Lu Y.; Wang Y. H. Design and spectral control of a novel ultraviolet emitting long lasting phosphor for assisting TiO_2 photocatalysis: Zn_2SiO_4:Ga^{3+},Bi^{3+}. *J. Alloy Compd.*, **2015**, 622, 908-912.

[313] Feng P. F.; Zhang J. C.; Wu C. Q.; Liu X.; Wang Y. H. Self-activated afterglow luminescence of un-doped $Ca_2ZrSi_4O_{12}$ material and explorations of new afterglow phosphors in a rare earth element-doped $Ca_2ZrSi_4O_{12}$ system. *Mater. Chem. Phys.*, **2013**, 141, 495-501.

[314] Wang T.; Gou J.; Xu X. H.; Zhou D. C.; Qiu J. B.; Yu X. Self-activated long persistent luminescence from different trapping centers of calcium germanate. *Opt. Express*, **2015**, 23, 12595-12604.

[315] Guan Y.; Qin L.; Huang Y. L.; Qin C. X.; Wei D. L.; Seo H. J. A self-activated silicate phosphor of $Na_5YZrSi_6O_{18}$. *Mater. Res. Bull.*, **2014**, 54, 24-27.

[316] Ding J. Y.; Wu Q. S.; Li Y. Y.; Long Q.; Wang Y. C.; Ma X. L.; Wang Y. H. Self-Activated Yellow Light Emitting Phosphors of α, β-$Ca_3B_2N_4$ with Long Afterglow Properties. *Inorg. Chem.*, **2016**, 55, 10990-10998.

[317] Zhou X. Q.; Ju G. F.; Li Y.; Jin Y. H.; Wu H. Y.; Hu Y. H. Tunable whole visible region color emission, enhancing emission intensity and persistent performance of a self-activated phosphor: $Na_2CaSn_2Ge_3O_{12}$. *Ceram. Int.*, **2018**, 44, 18809-18816.

[318] Takahashi Y.; Masai H.; Fujiwara T.; Kitamura K.; Inoue S. Afterglow in synthetic bazirite, $BaZrSi_3O_9$. *J. Ceram. Soc. Jpn.*, **2008**, 116, 357-360.

[319] Z. L.; Zhang J. C.; Zheng G. S.; Peng X. J.; Dai H. X. Violet-blue afterglow luminescence properties of non-doped $SrZrO_3$ material. *J. Lumin.*, **2013**, 144, 30-33.

[320] Xue F. H.; Hu Y. H.; Fan L. M.; Ju G. F.; Lin X. H.; Lv Y.; Mu Z. F. Reversible white-brown photochromism in a self-activated long-persistent phosphor Mg_2SnO_4. *Opt. Mater. Express*, **2017**, 7, 1014-1021.

[321] Yu R. J.; Yuan M. S.; Xiong Y. H.; Li J. B.; Wang J. Y. Structure characteristics and afterglow of $BaZr_4(PO_4)_6$ phosphor. *Opt. Mater. Express*, **2016**, 6, 1049-1055.

[322] Jiang B.; Chi F. F.; Wei X. T.; Chen Y. H.; Yin M. A self-activated $MgGa_2O_4$ for persistent luminescence phosphor. *J. Appl. Phys.*, **2018**, 124, 063101.

[323] Behrh G. K.; Isobe M.; Massuyeau F.; Serier-Brault H.; Gordon E. E.; Koo H. J.; Whangbo M. H.; Gautier R.; Jobic S. Oxygen-Vacancy-Induced Midgap States Responsible for the Fluorescence and the Long-Lasting Phosphorescence of the Inverse Spinel $Mg(Mg,Sn)O_4$. *Chem. Mater.*, **2017**, 29, 1069-1075.

[324] Ju G. F.; Hu Y. H.; Chen L.; Jin Y. H.; Zhang S. A.; Xue F. H.; Chen H. Self-activated photoluminescence and persistent luminescence in $CaZr_4(PO_4)_6$. *Mater. Res. Bull.*, **2016**, 83, 211-216.

[325] Li D. R.; Wang Y. H.; Xu K.; Li L.; Hu Z. F. Persistently luminescent and photocatalytic properties of $ZnGa_2O_4$ phosphors. *Mater. Res. Express*, **2015**, 2, 046202.

[326] Wu Y. T.; Chakoumakos B. C.; Shi H. L.; Du M. H.; Greeley I.; Loyd M.; Rutstrom D. J.; Stand L.; Koschan M.; Melcher C. L. Crystal structure, electronic structure, optical and scintillation properties of self-activated Cs_4YbI_6. *J. Lumin.*, **2018**, 201, 460-465.

[327] Iwasaki K.; Takahashi Y.; Masai H.; Fujiwara T. Blue photoluminescence, greenish-blue afterglow and their Ti-concentration dependence in rare earth-free bazirite-type $BaZr_{1-x}Ti_xSi_3O_9$. *Opt. Express*, **2009**, 17, 18054-18062.

[328] Li X. C.; Zou Z. H.; Wang Z. L.; Wu C. Q.; Zhang J. C.; Wang Y. H. A novel un-doped long lasting phosphorescence phosphor: $SrZrSi_2O_7$. *J. Rare. Earth.*, **2015**, 33, 37-41.

[329] Wang T.; Bian W. J.; Zhou D. C.; Qiu J. B.; Yu X.; Xu X. H. Tunable LLP via Energy Transfer between $Na_{2-y}(Zn_{1-x}Ga_x)GeO_4$ Sosoloid Host and Emission Centers with the Assistance of Zn Vacancies. *J. Phys. Chem. C*, **2015**, 119, 14047-14055.

[330] Vokhmintsev A. S.; Weinstein I. A.; Spiridonov D. M. Afterglow in bulk AlN single crystals under β-irradiation. *J. Lumin.*, **2012**, 132, 2109-2113.

[331] Wang Z. L.; Zhang J. C.; Zheng G. S.; Liu Y. Q.; Zhao Y. L. The unusual variations of photoluminescence and afterglow properties in monoclinic ZrO_2 by annealing. *J. Lumin.*, **2012**, 132, 2817-2821.

[332] Ju G. F.; Hu Y. H.; Chen L.; Jin Y. H.; Li Y. Persistent luminescence in the self-activated $K_2Zr(BO_3)_2$. *RSC Adv.*, **2017**, 7, 4190-4195.

[333] Xu X. H.; He Q. L.; Yan L. T. White-light long persistent and photo-stimulated luminescence in $CaSnSiO_5:Dy^{3+}$. *J. Alloy Compd.*, **2013**, 574, 22-26.

[334] Xu J.; Chen D. Q.; Yu Y. L.; Zhu W. J.; Zhou J. C.; Wang Y. S. Cr^{3+}:$SrGa_{12}O_{19}$: A Broadband Near-Infrared Long-Persistent Phosphor. *Chem. Asian J.*, **2014**, 9, 1020-1025.

[335] Xiong P. X.; Peng M. Y. Visible to near-infrared persistent luminescence from Tm^{3+}-doped two-dimensional layered perovskite Sr_2SnO_4. *J. Mater. Chem. C*, **2019**, **7**, 8303-8309.

[336] Liu C. B.; Che G. B. Luminescent Properties of the Self-activated White-light Emitting Phosphor $Ba_2TiP_2O_9$. *Chin. J. Inorg. Chem.*, **2006**, 22, 503-506.

[337] Dierkes T.; Jüstel T. Novel red-emitting nitridoborates-$SrBa_8[BN_2]_6:Ln^{2+/3+}$ (Ln=Pr^{3+}, Eu^{2+}). *J. Lumin.*, **2017**, 187, 513-520.

[338] Long Z. W.; Zhou J. H.; Qiu J. B.; Wang Q.; Zhou D. C.; Xu X. H.; Yu X.; Wu H.; Li Z. C. Thermally stable photoluminescence and long persistent luminescence of $Ca_3Ga_4O_9:Tb^{3+}/Zn^{2+}$. *J. Rare Earth.*, **2018**, 36, 675-679.

[339] Yu X.; Wang S. B.; Zhu Y. C.; Liang J. J.; Qiu J. B.; Xu X. H.; Lu W. High-temperature long persistent and photo-stimulated luminescence in Tb^{3+} doped gallate phosphor. *J. Alloy Compd.*, **2017**, 701, 774-779.

[340] Wang T.; Bian W. J.; Zhou D. C.; Qiu J. B.; Yu X.; Xu X. H. Red long lasting phosphorescence in $Ca_2Ge_7O_{16}:Sm^{3+}$ via persistent energy transfer from the host to Sm^{3+}. *Mater. Res. Bull.*, **2016**, 74, 151-155.

[341] Jin Y. H.; Hu Y. H.; Chen L.; Wang X. J. Luminescence properties of long persistent phosphors $BaZrSi_3O_9:R^{3+}$ (R = Eu, Sm, Dy, Tb and Pr) based on host sensitization. *Opt. Mater.*, **2014**, 36, 1814-1818.

[342] Li D. R.; Wang Y. H.; Xu K.; Zhao H.; Hu Z. F. Persistent luminescent and photocatalytic properties of $Zn_xGa_2O_{3+x}$ ($0.8 \leq x \leq 1$) phosphors. *RSC Adv.*, **2015**, 5, 20972-20975.

[343] Li Z. J.; Huang L.; Zhang Y. W.; Zhao Y.; Yang H.; Han G. Near-infrared light activated persistent luminescence nanoparticles via upconversion. *Nano Res.*, **2017**, 10, 1840-1846.

[344] Wu Y. L.; Li Y.; Qin X. X.; Chen R. C.; Wu D. K.; Liu S. J.; Qiu J. R. Dual mode NIR long persistent phosphorescence and NIR-to-NIR Stokes luminescence in $La_3Ga_5GeO_{14}:Cr^{3+},Nd^{3+}$ phosphor. *J. Alloy Compd.*, **2015**, 649, 62-66.

[345] Wang Z. B.; Wang W. X.; Zhou H.; Zhang J. C.; Peng S. L.; Zhao Z. Y.; Wang Y. H. Superlong and Color-Tunable Red Persistent Luminescence and Photostimulated Luminescence Properties of $NaCa_2GeO_4F:Mn^{2+},Yb^{3+}$ Phosphor. *Inorg. Chem.*, **2016**, 55, 12822-12831.

[346] Ge P. H.; Sun K. N.; Cheng Y. Design and synthesis of up-converted persistent luminescence $Zn_3Ga_2SnO_8:Cr^{3+},Yb^{3+},Er^{3+}$ phosphor. *Optik*, **2019**, 188, 200-204.

[347] Xu J.; Tanabe S.; Sontakke A. D.; Ueda J. Near-infrared multi-wavelengths long persistent luminescence of Nd^{3+} ion through persistent energy transfer in Ce^{3+}, Cr^{3+} co-doped $Y_3Al_2Ga_3O_{12}$ for the first and second bio-imaging windows. *Appl. Phys. Lett.*, **2015**, 107, 081903.

[348] Liang Y. J.; Liu F.; Chen Y. F.; Wang X. J.; Sun K. N.; Pan Z. New function of the Yb^{3+} ion as an efficient emitter of persistent luminescence in the short-wave infrared. *Light: Sci. Appl.*, **2016**, 5, e16124.

[349] Yi X.; Chen Z. T.; Ye S.; Li Y.; Song E. H.; Zhang Q. Multifunctionalities of near-infrared upconversion luminescence, optical temperature sensing and long persistent luminescence in $La_3Ga_5GeO_{14}$:Cr^{3+},Yb^{3+},Er^{3+} and their potential coupling. *RSC Adv.*, **2015**, 5, 49680-49687.

[350] Chen D. Q.; Chen Y.; Lu H. W.; Ji Z. G. A Bifunctional Cr/Yb/Tm:$Ca_3Ga_2Ge_3O_{12}$ Phosphor with Near-Infrared Long-Lasting Phosphorescence and Upconversion Luminescence. *Inorg. Chem.*, **2014**, 53, 8638-8645.

[351] Ueda J.; Miyano S.; Tanabe S. Formation of Deep Electron Traps by Yb^{3+} Codoping Leads to Super-Long Persistent Luminescence in Ce^{3+}-Doped Yttrium Aluminum Gallium Garnet Phosphors. *ACS Appl. Mater. Interfaces*, **2018**, 10, 20652-20660.

[352] Martín-Rodríguez R.; Valiente R.; Bettinelli M. Room-temperature green upconversion luminescence in $LaMgAl_{11}O_{19}$:Mn^{2+},Yb^{3+} upon infrared excitation. *Appl. Phys. Lett.*, **2009**, 95, 091913.

[353] Zhou X. F.; Geng W. Y.; Guo H. J.; Ding J. Y.; Wang Y. H. $K_4CaGe_3O_9$:Mn^{2+},Yb^{3+}: a novel orange-emitting long persistent luminescent phosphor with a special nanostructure. *J. Mater. Chem. C*, **2018**, 6, 7353-7360.

[354] Zhu Q.; Song C. Y.; Li X. D.; Sun X. D.; Li J. G. Up-conversion monodispersed spheres of $NaYF_4$:Yb^{3+}/Er^{3+}: green and red emission tailoring mediated by heating temperature, and greatly enhanced luminescence by Mn^{2+} doping. *Dalton T.*, **2018**, 47, 8646-8655.

[355] Han X. X.; Song E. H.; Zhou B.; Zhang Q. Y. Color tunable upconversion luminescent perovskite fluoride with long-/short-lived emissions toward multiple anti-counterfeiting. *J. Mater. Chem. C*, **2019**, 7, 8226-8235.

[356] Xue Z. L.; Li X. L.; Li Y. B.; Jiang M. Y.; Ren G. Z.; Liu H. R.; Zeng S. J.; Hao J. H. A 980 nm laser-activated upconverted persistent probe for NIR-to-NIR rechargeable in vivo bioimaging. *Nanoscale*, **2017**, 9, 7276-7283.

[357] Zou Z. H.; Feng L.; Cao C.; Zhang J. C.; Wang Y. H. Near-Infrared Quantum Cutting Long Persistent Luminescence. *Sci. Rep.*, **2016**, 6, 24884.

[358] Li Y. J.; Yan X. P. Synthesis of functionalized triple-doped zinc gallogermanate nanoparticles with superlong near-infrared persistent luminescence for long-term orally administrated bioimaging. *Nanoscale*, **2016**, 8, 14965-14970.

[359] Zhang J.; Zhai Z. Y.; Hua Z. H. Investigations on luminescence of $Ca_8MgGd(PO_4)_7$:Eu^{2+}, Mn^{2+}, Yb^{3+}, Er^{3+}, Ho^{3+}, Tm^{3+} phosphors. *Mater. Res. Bull.*, **2016**, 74, 34-40.

[360] Hu L. D.; Fan Y.; Liu L.; Li X. M.; Zhao B. Z.; Wang R.; Wang P. Y.; El-Toni A. M.; Zhang F. Orthogonal Multiplexed Luminescence Encoding with Near-Infrared Rechargeable Upconverting Persistent Luminescence Composites. *Adv. Opt. Mater.*, **2017**, 5, 1700680.

[361] Qiu X. C.; Zhu X. J.; Xu M.; Yuan W.; Feng W.; Li F. Y. Hybrid Nanoclusters for Near-Infrared to Near-Infrared Upconverted Persistent Luminescence Bioimaging. *ACS Appl. Mater. Interfaces*, **2017**, 9, 32583-32590.

[362] Liu F.; Chen Y. F.; Liang Y. J.; Pan Z. W. Phonon-assisted upconversion charging in $Zn_3Ga_2GeO_8$:Cr^{3+} near-infrared persistent phosphor. *Opt. Lett.*, **2016**, 41, 954-957.

[363] Sharma S. K.; Gourier D.; Teston E.; Scherman D.; Richard C.; Viana B. Persistent luminescence induced by near infra-red photostimulation in chromium-doped zinc gallate for *in vivo* optical imaging. *Opt. Mater.*, **2017**, 63, 51-58.

[364] Li L.; Xu K.; Wang Y. H.; Hu Z. F.; Zhao H. Enhanced persistent luminescence and photocatalytic properties of Ga_2O_3:Cr^{3+} by In^{3+} doping. *Opt. Mater. Express*, **2016**, 6, 1122-1130.

[365] Wang Y. H.; Xu K.; Li D. R.; Zhao H.; Hu Z. F. Persistent luminescence and photocatalytic properties of Ga_2O_3:Cr^{3+},Zn^{2+} phosphors. *Opt. Mater.*, **2014**, 36, 1798-1801.

[366] Sun H. C.; Wu H. Y.; Jin Y. H.; Lv Y.; Ju G. F.; Chen L.; Feng Z. Y.; Hu Y. H. Photocatalytic titanium dioxide immobilized on an ultraviolet emitting ceramic substrate for water purification. *Mater. Lett.*, **2019**, 240, 100-102.

[367] Fujishima A.; Zhang X.; Tryk D. A. TiO_2 photocatalysis and related surface phenomena. *Surf. Sci. Rep.*, **2008**, 63, 515-582.

[368] Wu H. Y.; Wu X. L.; Wang Z. M.; Aoki H.; Kutsuna S.; Jimura K.; Hayashi S. Anchoring titanium dioxide on carbon spheres for high-performance visible light photocatalysis. *Appl. Catal. B - Environ.*, **2017**, 207, 255-266.

[369] Zhang X. M.; Chen Y. L.; Liu R. S.; Tsai D. P. Plasmonic photocatalysis. *Rep. Prog. Phys.*, **2013**, 76, 046401.

[370] Turchi C. S.; Ollis D. F. Photocatalytic degradation of organic water contaminants: Mechanisms involving hydroxyl radical attack. *J. Catal.*, **1990**, 122, 178-192.

[371] Tang J. W.; Durrant J. R.; Klug D. R. Mechanism of Photocatalytic Water Splitting in TiO_2. Reaction of Water with Photoholes, Importance of Charge Carrier Dynamics, and Evidence for Four-Hole Chemistry. *J. Am. Chem. Soc.*, **2008**, 130, 13885-13891.

[372] Habisreutinger S. N.; Schmidt-Mende L.; Stolarczyk J. K. Photocatalytic Reduction of CO_2 on TiO_2 and Other Semiconductors. *Angew. Chem. Int. Ed.*, **2013**, 52, 7372-7408.

[373] Smith A. M.; Nie S. M. Semiconductor Nanocrystals: Structure, Properties, and Band Gap Engineering. *Acc. Chem. Res.*, **2010**, 43, 190-200.

[374] Tan H. L.; Abdi F.F.; Ng Y. H. Heterogeneous photocatalysts: an overview of classic and modern approaches for optical, electronic, and charge dynamics evaluation. *Chem. Soc. Rev.*, **2019**, 48, 1255-1271.

[375] Zhang Z. B.; Wang C. C.; Zakaria R.; Ying J. Y. Role of Particle Size in Nanocrystalline TiO_2-Based Photocatalysts. *J. Phys. Chem. B*, **1998**, 102, 10871-10878.

[376] Li F. F.; Li Z. H.; Cai Y. F.; Zhang M. X.; Shen Y.; Wang W. Afterglow photocatalysis of Ag_3PO_4 through different afterglow coatings and photocatalysis mechanism. *Mater. Lett.*, **2017**, 208, 111-114.

[377] Wu H. Y.; Wang Z. M.; Koike K.; Negishi N.; Jin Y. H. Hybridization of silver orthophosphate with a melilite-type phosphor for enhanced energy-harvesting photocatalysis. *Catal. Sci. Technol.*, **2017**, 7, 3736-3746.

[378] Li H. H.; Yin S.; Wang Y. H.; Sato T. Persistent Fluorescence-Assisted $TiO_{2-x}N_y$-Based Photocatalyst for Gaseous Acetaldehyde Degradation. *Environ. Sci. Technol.*, **2012**, 46, 7741-7745.

[379] Zhou Q.; Peng F. P.; Ni Y. R.; Kou J. H.; Lu C. H.; Xu Z. Z. Long afterglow phosphor driven round-the-clock g-C_3N_4 photocatalyst. *J. Photoch. Photobio. A*, **2016**, 328, 182-188.

[380] Zhou J. X.; Wang R.; Jiao T. F.; Bai Z. H.; Wang X. X.; Guo Y.; Zhang Q.; Peng Q. M. $Mg_3Y_2Ge_3O_{12}$:Bi^{3+} UV fluorescent phosphor as the TiO_2 "sensitizer" for enhancing the heavy oil viscosity reduction. *Ceram. Int.*, **2019**, 45, 13112-13118.

[381] Yin H. B.; Chen X. F.; Hou R. J.; Zhu J.; Li S. Q.; Huo Y. N.; Li H. X. Ag/BiOBr Film in a Rotating-Disk Reactor Containing Long-Afterglow Phosphor for Round-the-Clock Photocatalysis. *ACS Appl. Mater. Inter.*, **2015**, 7, 20076-20082.

[382] Huang H. J.; Wang Y. H.; Li H.; Li J.; Hu Z. F.; Zhao H.; Yi S. P; Wei Z. G. Enhancing persistent luminescence and photocatalytic properties in Ti as a trap center in $ZnGa_2O_4$. *J. Mater. Sci. - Mater. El.*, **2017**, 28, 1294-1300.

[383] Locardi F.; Sanguineti E.; Fasoli M.; Martini M.; Costa G. A.; Ferretti M.; Caratto V. Photocatalytic activity of TiO_2 nanopowders supported on a new persistent luminescence phosphor. *Catal. Commun.*, **2016**, 74, 24-27.

[384] Sacco, O.; Vaiano, V.; Han, C.; Sannino, D.; Dionysiou, D. D.; Ciambelli, P. Long afterglow green phosphors functionalized with Fe-N doped TiO_2 for the photocatalytic removal of emerging contaminants. *Chem. Eng. T.*, 2015, 43, 2107-2112.

[385] Li H. H.; Yin S.; Wang Y. H.; Sekino T.; Lee S. W.; Sato T. Roles of Cr^{3+} doping and oxygen vacancies in $SrTiO_3$ photocatalysts with high visible light activity for NO removal. *J. Catal.*, **2013**, 297, 65-69.

[386] Hu K. H.; Liu Z.; Huang F.; Hu X. G.; Han C. L. Synthesis and photocatalytic properties of nano-MoS_2/kaolin composite. *Chem. Eng. J.*, **2010**, 162, 836-843.

[387] Lee J. C.; Kim M. S.; Kim B. W. Removal of paraquat dissolved in a photoreactor with TiO_2 immobilized on the glass-tubes of UV lamps. *Water Res.*, **2002**, 36, 1776-1782.

[388] Tian J.; Zhao Z. H.; Kumar A.; Boughton R. I.; Liu H. Recent progress in design, synthesis, and applications of one-dimensional TiO_2 nanostructured surface heterostructures: a review. *Chem. Soc. Rev.*, **2014**, 43, 6920-6937.

[389] Pachfule P.; Acharjya A.; Roeser J.; Langenhahn T.; Schwarze M.; Schomäcker R.; Thomas A.; Schmidt J. Diacetylene Functionalized Covalent Organic Framework (COF) for Photocatalytic Hydrogen Generation. *J. Am. Chem. Soc.*, **2018**, 140, 1423-1427.

[390] Li H.; Yin S.; Wang Y.; Sekino T.; Lee S. W.; Sato T. Green phosphorescence-assisted degradation of rhodamine B dyes by Ag_3PO_4. *J. Mater. Chem. A*, **2013**, 1, 1123-1126.

[391] Cao J.; Luo B. D.; Lin H. L.; Xu B. Y.; Chen S. F. Visible light photocatalytic activity enhancement and mechanism of AgBr/Ag_3PO_4 hybrids for degradation of methyl orange. *J. Hazard. Mater.*, **2012**, 217-218, 107-115.

[392] Ismael M.; Elhaddad E.; Taffa D. H.; Wark M. Synthesis of Phase Pure Hexagonal $YFeO_3$ Perovskite as Efficient Visible Light Active Photocatalyst. *Catalysts*, **2017**, 7, 326.

[393] Shi A. Y.; Li H. H.; Yin S.; Zhang J. C.; Wang Y. H. H_2 evolution over g-C_3N_4/Cs_xWO_3 under NIR light. *Appl. Catal. B - Environ.*, **2018**, 228, 75-86.

[394] Ge L.; Han C. C.; Liu J. Novel visible light-induced g-C_3N_4/Bi_2WO_6 composite photocatalysts for efficient degradation of methyl orange. *Appl. Catal. B - Environ.*, **2011**, 108-109, 100-107.

[395] Han C. C.; Ge L.; Chen C. F.; Li Y. J.; Xiao X. L.; Zhang Y. N.; Guo L. L. Novel visible light induced Co_3O_4-g-C_3N_4 heterojunction photocatalysts for efficient degradation of methyl orange. *Appl. Catal. B - Environ.*, **2014**, 147, 546-553.

[396] Wang C.; Wang X. M.; Xu B. Q.; Zhao J. C.; Mai B. X.; Peng P. A.; Sheng G. Y.; Fu J. M. Enhanced photocatalytic performance of nanosized coupled ZnO/SnO_2 photocatalysts for methyl orange degradation. *J. Photoch. Photobio. A*, **2004**, 168, 47-52.

[397] Zhang K. L.; Liu, C. M.; Huang F. Q.; Zheng C.; Wang W. D. Study of the electronic structure and photocatalytic activity of the BiOCl photocatalyst. *Appl. Catal. B - Environ.*, **2006**, 68, 125-129.

[398] Luo Y. J.; Zhou S. Y.; Sun Y. F.; Zhao D. Q.; Gu X. S.; Yan Q. T.; Ji F. Y.; Xu X. Study of the photocatalytic performance and carrier migration of reduced graphene oxide-modified infrared-responsive photocatalyst β-$NaYF_4$:Yb^{3+},Er^3@BiOCl-rGO. *Opt. Mater.*, **2019**, 96, 109312.

[399] Lin X. P.; Huang F. Q.; Wang W. D.; Wang Y. M.; Xia Y. J.; Shi J. L. Photocatalytic activities of $M_2Sb_2O_7$ (M = Ca, Sr) for degrading methyl orange. *Appl. Catal. A - Ge.*, **2006**, 313, 218-223.

[400] Wang S. H.; Zhou Q. Photodegradation of methyl orange by photocatalyst of CNTs/P-TiO_2 under UV and visible-light irradiation. *J. Hazard. Mater.*, **2011**, 185, 77-85.

[401] Cao F.; Chen X. Y.; Yin K. B.; Dong S.; Ren Z. F.; Yuan F.; Yu T.; Zou Z. G.; Liu J. M. Visible-Light Photocatalytic Properties of Weak Magnetic $BiFeO_3$ Nanoparticles. *Adv. Mater.*, **2007**, 19, 2889-2892.

[402] Cao J.; Luo B. D.; Lin H. L.; Chen S. F. Photocatalytic activity of novel AgBr/WO_3 composite photocatalyst under visible light irradiation for methyl orange degradation. *J. Hazard. Mater.*, **2011**, 190, 700-706.

[403] Siham Q.; Salman R. S. Photocatalytic degradation of methyl orange as a model compound. *J. Photoch. Photobio. A*, **2002**, 148, 161-168.

[404] Das M. C.; Xu H.; Wang Z. Y.; Srinivas G.; Zhou W.; Yue Y. F.; Nesterov V. N.; Qian G. D.; Chen B. L. A Zn_4O-containing doubly interpenetrated porous metal-organic framework for photocatalytic decomposition of methyl orange. *Chem. Commun.*, **2011**, 47, 11715-11717.

[405] Kang Y.; Wu X. M.; Gao Q. Plasmonic-Enhanced Near-Infrared Photocatalytic Activity of F-Doped $(NH_4)_{0.33}WO_3$ Nanorods. *ACS Sustainable Chem. Eng.*, **2019**, 7, 44210-4219.

[406] Molla A.; Sahu M.; Hussain S. Under dark and visible light: fast degradation of methylene blue in the presence of Ag–In–Ni–S nanocomposites. *J. Mater. Chem. A*, **2015**, 3, 15616-15625.

[407] Qu Y. Q.; Duan X. F. Progress, challenge and perspective of heterogeneous photocatalysts. *Chem. Soc. Rev.*, **2013**, 42, 2568-2580.

[408] Dalton J. S.; Janes P. A.; Jones N. G.; Nicholson J. A.; Hallam K. R.; Allen G. C. Photocatalytic oxidation of NO_x gases using TiO_2: a surface spectroscopic approach. *Environ. Pollut.*, **2002**, 120, 415-422.

[409] Xu M. X.; Wang Y. H.; Geng J. F.; Jing D. W. Photodecomposition of NO_x on Ag/TiO_2 composite catalysts in a gas phase reactor. *Chem. Eng. J.*, **2017**, 307, 181-188.

[410] Wu Q. P.; van de Keol R. Selective Photoreduction of Nitric Oxide to Nitrogen by Nanostructured TiO_2 Photocatalysts: Role of Oxygen Vacancies and Iron Dopant. *J. Am. Chem. Soc.*, **2012**, 134, 22, 9369-9375.

[411] Su C. Y.; Ran X.; Hu J. L.; Shao C. L. Photocatalytic Process of Simultaneous Desulfurization and Denitrification of Flue Gas by TiO_2-Polyacrylonitrile Nanofibers. *Environ. Sci. Technol.*, **2013**, 47, 20, 11562-11568.

[412] Takeuchi M.; Hidaka M.; Anpo M. Efficient removal of toluene and benzene in gas phase by the TiO_2/Y-zeolite hybrid photocatalyst. *J. Hazard. Mater.*, **2012**, 237-238, 133-139.

[413] Yuan Y.; Zhang J. Y.; Li H. L.; Li Y.; Zhao Y. C.; Zheng C. G. Simultaneous removal of SO_2, NO and mercury using TiO_2-aluminum silicate fiber by photocatalysis. *Chem. Eng. J.*, **2012**, 192, 21-28.

[414] Zou Z. G.; Ye J. H.; Sayama K.; Arakawa H. Direct splitting of water under visible light irradiation with an oxide semiconductor photocatalyst. *Nature*, **2001**, 414, 625-627.

[415] Tran P. D.; Wong L. H.; Barber J.; Loo J. S. C. Recent advances in hybrid photocatalysts for solar fuel production. *Energy Environ. Sci.*, **2012**, 5, 5902-5918.

[416] Moriya Y.; Takata T.; Domen K. Recent progress in the development of (oxy)nitride photocatalysts for water splitting under visible-light irradiation. *Coordin. Chem. Rev.*, **2013**, 257, 1957-1969.

[417] Wang H. L.; Zhang L. S.; Chen Z. G.; Hu J. Q.; Li S. J.; Wang Z. H.; Liu J. S.; Wang X. C. Semiconductor heterojunction photocatalysts: design, construction, and photocatalytic performances. *Chem. Soc. Rev.*, **2014**, 43, 5234-5244.

[418] Park Y.; McDonald K. J.; Choi K. S. Progress in bismuth vanadate photoanodes for use in solar water oxidation. *Chem. Soc. Rev.*, 2013, **42**, 2321-2337.

[419] Chen S. S.; Takata T.; Domen K. Particulate photocatalysts for overall water splitting. *Nat. Rev. Mater.*, **2017**, 2, 17050.

[420] Xie G. C.; Zhang K.; Guo B. D.; Liu Q.; Fang L.; Gong J. R. Graphene-Based Materials for Hydrogen Generation from Light-Driven Water Splitting. *Adv. Mater.*, **2013**, 25, 3820-3829.

[421] Wang X. C.; Maeda K.; Thomas K.; Thomas A.; Takanabe K.; Xin G.; Carlsson J. M.; Domen K.; Antonietti M. A metal-free polymeric photocatalyst for hydrogen production from water under visible light. *Nat. Mater.*, **2009**, 8, 76-80.

[422] Kudo A.; Miseki Y. Heterogeneous photocatalyst materials for water splitting. *Chem. Soc. Rev.*, **2009**, 38, 253-278.

[423] Maeda K.; Teramura K.; Lu D. L.; Takata T.; Saito N.; Inoue Y.; Domen K. Photocatalyst releasing hydrogen from water. *Nature*, **2006**, 440, 295.

[424] Takeda H.; Ohashi K.; Sekine A.; Ishitani O. Photocatalytic CO_2 Reduction Using Cu(I) Photosensitizers with a Fe(II) Catalyst. *J. Am. Chem. Soc.*, **2016**, 138, 4354-4357.

[425] Guo J. J.; Hu A. H.; Chen Y. L.; Sun J. F.; Tang H. M.; Zuo Z. W. Photocatalytic C−C Bond Cleavage and Amination of Cycloalkanols by Cerium(III) Chloride Complex. *Angew. Chem. Int. Ed.*, **2016**, 49, 15319-15322.

[426] Litter M. I.; San Román E.; Grela M. A.; Meichtry J. M.; Rodríguez H. B. Sensitization of TiO_2 by Dyes: A Way to Extend the Range of Photocatalytic Activity of TiO_2 to the Visible Region. Chapter 10 in "Visible light-active photocatalysis. Nanostructured catalyst design, mechanisms, and applications". Edited by Srabanti Ghosh. Wiley-VCH Verlag GmbH & Co. KGaA, 2018. DOI: 10.1002/9783527808175.ch10

[427] Sonl P. K.; Navas. P. ZnO/Polyethylene-Glycol and ZnO/Au Nanocomposites for Enhanced Photocatalytic Degradation of Organic Dye. *J. Nanoeng. Nanomanuf.*, **2013**, 3, 1-7.

[428] Emeline A. V.; Ryabchuk V. K.; Kuznetsov V. N.; Serpone N. Interplay between Physical and Chemical Events in Photoprocesses in Heterogeneous Systems. Chapter 9 in "Photocatalysis: Fundamentals and Perspectives". Edited by Jenny Schneider, Detlef Bahnemann, Jinhua Ye, Gianluca Li Puma, and Dionysios D Dionysiou. Royal Society of Chemisty, 2016. DOI: 10.1039/9781782622338-00218.

[429] Liu J.; Liu Y.; Liu N. Y.; Han Y. Z.; Zhang X.; Huang H.; Lifshitz Y.; Lee S. T.; Kai Z. H. Metal-free efficient photocatalyst for stable visible water splitting via a two-electron pathway. *Science*, **2015**, 347, 970-974.

[430] Wang Q.; Hisatomi T.; Jia Q. X.; Tokudome H.; Zhong M.; Wang C. Z.; Pan Z. H.; Takata T.; Nakabayashi M.; Shibata N.; Li Y. B.; Sharp I. D.; Kudo A.; Yamada T.; Domen K. Scalable water splitting on particulate photocatalyst sheets with a solar-to-hydrogen energy conversion efficiency exceeding 1%. *Nat. Mater.*, **2016**, 15, 611-615.

[431] Liao L.; Zhang Q. H.; Su Z. H.; Zhao Z. Z.; Wang Y. N.; Li Y.; Lu X. X.; Wei D. G.; Feng G. Y.; Yu Q. K.; Cai X. J.; Zhao J. M.; Ren Z. F.; Fang H.; Francisco R. H.; Baldelli S.; Bao J. M. Efficient solar water-splitting using a nanocrystalline CoO photocatalyst. *Nat. Nanotechnol.*, **2016**, 9, 69-73.

Figure captions

Figure 1 Schematic organization of this review work along with each section heading and its subdivision headings. Meanwhile, seven pictures are also selected to illustrate the core point and the logical thinking of this review, including the persistent luminescence of MPLs whose colors broadly span from blue to green (**top**), photocatalytic degradation of Rhodamine B (RhB) and its mechanism (**left**), TiO_2/$BiVO_4$/ZnO catalysts (**bottom**), $CaAl_2O_4$:(Eu,Nd)@$TiO_{2-x}N_y$ composite and its mechanism (**right**), and the photocatalytic mechanism of Ag-BiOBr PCM coupled blue NL-PA MPL composite with the external irradiation source on and off (**center**). These pictures can reflect that a suitable combination of MPLs and PCMs enables us to sustain the photocatalytic activity in the absence of the external irradiation source.

Figure 2 (**a**) (**i**) Normalized emission spectra of $Y_{2.96}Sc_2Ga_{3-x}Al_xO_{12}$:$0.04Ce^{3+}$ [78], (**ii**) emission spectra of $(Ca_{1.998}Eu_{0.002})BO_3Cl$ and $(Ca_{1.996}Eu_{0.002}Dy_{0.002})BO_3Cl$ and phosphorescence *(*persistent) spectra of $(Ca_{1.996}Eu_{0.002}Dy_{0.002})BO_3Cl$ [81], (**iii**) emission spectra of $Ba_4(Si_3O_8)_2$:Eu^{2+} and $Ba_4(Si_3O_8)_2$:Eu^{2+},Dy^{3+} [88], and (**iv**) persistent spectra of $Ca_4(PO_4)_2O$:Eu^{2+},Y^{3+} measured at 10 min, 30 min, and 2 h after removal of the excitation source [93]; (**b**) (**i**) Digital emission images of $Y_3Al_2Ga_3O_{12}$:Ce^{3+}-Cr^{3+} and $SrAl_2O_4$:Eu^{2+}-Dy^{3+} under a white LED irradiation (**upper**), and 5 min after ceased the white LED light (**middle**), as well as Ce-Cr-doped $Lu_3Al_2Ga_3O_{12}$, $Y_3Al_2Ga_3O_{12}$, and $Gd_3Al_2Ga_3O_{12}$ after ceased the white LED (**bottom**) [84], (**ii**) digital emission images of $Sr_{2-x-y}Al_2SiO_7$:xCe^{3+},yDy^{3+} (x = 0.005, y = 0, **A**; x = 0.005, y = 0.03, **B**; x = 0, y = 0.03, **C**) [89], and (**iii**) digital images of body, and emission of $BaCaSiO_4$:Eu^{2+},Mn^{2+} under 254 nm UV lamp *via* different YF_3 addition, together with the persistent colors measured at 30 s and 60 s after removing the 254 nm UV source [90]. In the figure, the irradiation or pre-irradiation sources are given.

Figure 3 (**a**) Persistent spectra of (**i**) $Ca_{2-x}SnO_4$:xPr^{3+} (x=0.3%) [111], (**ii**) $Sr_3Al_2O_5Cl_2$:$0.02\%Tb^{3+}$ [117], (**iii**) Sr_2SiO_4:Dy^{3+} [124], and (**iv**) Sr_2SnO_4:Sm^{3+} [131]; (**b**) (**i**) CIE chromaticity diagram under UV light excitation (**A**-**C**) and persistent luminescent chromaticity coordinates (**D**-**F**) of Lu_2O_3:R^{3+},M (R, M =Pr, Hf^{IV}; Eu; and Tb, Ca^{2+}) [121], (**ii**) persistent spectra of $CdSiO_3$:R^{3+} (R = Pr^{3+}, Sm^{3+}, Gd^{3+}, Tb^{3+}, and Dy^{3+}) and their corresponding CIE chromaticity coordinates [133]; (**c**) Photographs of 4*f* RE emissions, from the left to right are Dy^{3+} in Gd_2O_3 [144], Tm^{3+} and Dy^{3+} in $Ca_2La_8(GeO_4)_6O_2$ [145], Dy^{3+} in $LiLaP_4O_{12}$ [146], Tb^{3+} in $KNaCa_2(PO_4)_2$:Na^+ [147] and $Ca_2La_8(GeO_4)_6O_2$ [145], Sm^{3+} in $KNaCa_2(PO_4)_2$:Na^+ [147], Eu^{3+} in $Ca_2La_8(GeO_4)_6O_2$ [145], Pr^{3+} in (Ca,Zn)TiO_3 [128], Eu^{3+} in X2-type Y_2SiO_5:Bi^{3+} [149].

Figure 4 (**a**) (**i**) Emission and excitation spectra of $LaAlO_3$:Mn^{4+},Ge^{4+} [151], (**ii**) persistent spectra of Mg_2GeO_4:Mn^{4+} co-doped with and without Re^{3+} (Re = Pr, Er, Nd, Yb) ions [155], and emission spectra of $LaAl_{1-x}Ga_xO_3$ (**iii**) and $La_{1-x}Gd_xAlO_3$ solid solutions (**iv**) [156]; (**b**) (**i**) Persistent imaging patterns of $GdAlO_3$:Mn^{4+},Ge^{4+} and $LaAlO_3$:Mn^{4+},Ge^{4+} under 325 nm pre-irradiation for 10 min (**A**) and recorded at the post-irradiation time of 1 min (**B**), 10 min (**C**), 30 min (**D**), 2 h (**E**), and 20 h min (**F**) [151], and (**ii**) $GdAlO_3$:Mn^{4+},Ge^{4+}@Au (**A**), $GdAlO_3$:Mn^{4+},Ge^{4+}@SiO_2 (**B**), and $GdAlO_3$:Mn^{4+},Ge^{4+} (**C**) from 0 min to 24 h [154].

Figure 5 (**a**) (**i**) Normalized photoluminescence and (**ii**) long-persistence phosphorescence spectra (λ_{ex} = 320 nm) as a function of Al concentration in the $Zn_{2-x}Al_{2x}Sn_{1-x}O_4$ (x = 0.001, 0.005, 0.01, 0.05, 0.1, 0.2, and 0.4, corresponding to **ZS4**-**ZS10**) [164], (**iii**) excitation and emission spectra of $Zn_3Al_2Ge_2O_{10}$:$0.01Cr^{3+}$ [177], and (**iv**) excitation and emission spectra of $ZnGa_2O_4$:Cr^{3+},Bi^{3+} and $ZnGa_2O_4$:Cr^{3+} pellets [196]; (**b**) (**i**) Digital photos and NIR images of $Zn_3Ga_2GeO_8$:Cr^{3+} (**left**) and

$Zn_3Ga_2SnO_8:Cr^{3+}$ (**right**) powders after being acquired at different time intervals (from 5 min to 300 h) [160], (**ii**) persistent imaging of $SrAl_{12}O_{19}:Cr^{3+},Ti^{4+}$ (**right**), $SrAl_2O_4:Cr^{3+}$ (**middle**), and $SrAl_{12}O_{19}:Cr^{3+}$ powders (**left**) recorded from 3 min to 5 h [182], and (**iii**) NIR persistent images of $Zn_3Ga_2Ge_2O_{10}:Cr^{3+}$ ceramic disks (**right row**) and LumiNova-G pills (**left row**) taken from 2 min to 50 h after irradiated by a 365 nm UV lamp (**left column**) and direct sunlight (**right column**) for 5 min [39].

Figure 6 Persistent spectra of (**a**) $CaZnGe_2O_6:Mn^{2+}$ recorded from 1 min to 8 min [199], (**b**) γ-$Zn_3(PO_4)_2:Mn^{2+},Ga^{3+}$ [203], (**c**) $LiGaSiO_4:xMn^{2+}$ [206], (**d-f**) $(89-x)GeO_2$-$11Al_2O_3$-xCaO-1MnO (x = 10) from 30 s to 24 h [208]; (**g**) Li_2ZnGeO_4 (LZGO) and $Li_2ZnGeO_4:xMn^{2+}$ (LZGO:Mn) after removal of 254 nm excitation and the corresponding photos (**inset**) taken under sunlight and 254 nm irradiation, and after removal of 254 nm excitation [215]; (**h**) Photoluminescence spectra of $(Mg,Zn)GeO_3:Mn^{2+},yYb^{3+}$ [228]; (**i**) photoluminescence (PL) and persistent luminescence (PersL) spectra of $CaMgGe_2O_6:Mn^{2+}$ [233].

Figure 7 (**a**) (**i**) Fluorescent (**upper**) and afterglow (**bottom**) images of $Ca_2Sn_2Al_2O_9:Mn^{2+}$ [210], (**ii**) persistent images (0-180 s) of the $8Na_2O$-$12Ga_2O_3$-$80GeO_2 \cdot Mn^{2+}$ glass prepared upon different crystallization times (0-5 h) a after removal of 254 nm UV light [222], and (**iii**) photographs of $(89-x)GeO_2$-$11Al_2O_3$-xCaO-1MnO (x = 10) placed on different patterns of mesh paper and taken at the persistent time of 40 s after removal of 254 nm illumination [208]; (**b**) (**i**) CIE chromaticity coordinates of γ-$Zn_3(PO_4)_2:1\%Mn^{2+},y\%Ga^{3+}$ (y = 1-8) [203], and (**ii**) $LiGaSiO_4:xMn^{2+}$ and their relevant photographs (**inset**) [206].

Figure 8 (**a**) (**i**) Persistent spectra of $KGaGeO_4:xBi^{3+}$ and the relationship between the persistent intensity and the Bi^{3+} content (**inset**) [260], (**ii**) intensity-normalized photoluminescence (PL), long-lasting (LPL), and photostimulated (PSL) spectra of $CaGa_2O_4:Bi^{3+}$ and a photo (**inset**) [269], and (**iii-iv**) persistent spectra of $Sr_{2.997}Bi_{0.003}Ga_4O_9$ from 30 s to 246 min [261]; (**b**) Photographs of (**i**) $Sr_{2.985}Bi_{3x}Ga_4O_9$ taken within the range of 0-600s after removal of 254 nm UV lamp [261], and (**ii**) $LiYGeO_4:Bi^{3+}$ in the range of 24-300 h and its relevant PSL luminescent images under 980 nm, 808 nm, and a red LED irradiation and taken after 300 h (bottom row) [265]; (**c**) (**i**) Persistent spectrum of $CdSiO_3:Pb^{2+}$ [270], (**ii**) florescence spectra of $CaO:Pb^{2+}$ (**A**) and $SrO:Pb^{2+}$ (**B**) and persistent spectrum of $SrO:Pb^{2+}$ (**C**) [271], (**iii**) persistent spectra of $Sr_2MgGe_2O_7:Pb^{2+}$ [273].

Figure 9 (**a**) (**i**) Excitation, photoluminescence (PL) and persistent spectra of $SrZrO_3$ [319], (**ii**) PL (**1**) and the persistent (PerL) spectra of $SrZrSi_2O_7$ sintered in reducing atmosphere (**2**) and air (**3**), the insets are persistent (**left**) and PL images (**right**) of the sample [328], (**iii**) persistent spectra of $Na_2(Zn_{1-x}Ga_x)GeO_4$ and the image of $Na_2(Zn_{0.8}Ga_{0.2})GeO_4$ after removal of femtosecond laser (**inset**) [329], (**iv**) normalized PL and persistent spectra of ZrO_2 [331]; (**b**) Persistent images of (**i**) Mg_2SnO_4 [320], and (**ii**) $MgGa_2O_4$ [322], (**iii**) PL colors of bazirite-type $BaZr_{1-x}Ti_xSi_3O_9$ under 254 nm and 312 nm light and persistent images of a pabstite-type $BaSn_{1-y}TiySi_3O_9$ [327].

Figure 10 (**a**) Upconverting persistent spectrum of $Zn_3Ga_2GeO_8:Cr^{3+},Yb^{3+},Er^{3+}$ phosphor and its decay curve monitored at 700 nm peak (**inset, upper right**) and NIR images (**inset, upper left**) [40]; (**b**) Upconversion fluorescent spectra of the β-$NaYF_4$:Yb,Er/$NaYF_4$ membrane achieved with different 980 laser powers [343]; (**c**) Emission spectra of $NaCa_2GeO_4F:0.2\%Mn^{2+},xYb^{3+}$ [345]; (**d**) Phonon-assisted upconversion persistent spectra of $Zn_3Ga_2GeO_8:Cr^{3+}$ recorded at 20 ^oC and 70 ^oC and the corresponding decay curves acquired within 60 min [362].

Figure 11 (**a**) Photographs of the $KCdF_3:Yb^{3+},Mn^{2+}$, $KCdF_3:Yb^{3+},Mn,Er^{3+}$, $KCdF_3:Yb^{3+},Mn,Ho^{3+}$, and $KCdF_3:Yb^{3+},Mn^{2+},Tm^{3+}$ (from bottom to upper) with the dynamic radiation of a 980 nm laser and luminescence images of a printed plantlet (the bottom left, inset) [355]; (**b**) Persistent images of $Y_3Al_{5-x}Ga_xO_{12}:Ce^{3+},Cr^{3+}$ (YAGG:Ce-Cr) and $Y_3Al_{5-x}Ga_xO_{12}:Nd^{3+},Ce^{3+},Cr^{3+}$ (YAGG:Nd-Ce-Cr) [347]; (**c**) Upconversion persistent decay images of $Zn_3Ga_2GeO_8:Yb^{3+},Er^{3+},xCr^{3+}$ (x = 0.2%, 0.5%, 0.8%) recorded from 5 min, 10 min, 30 min, and 120 min [356].

Figure 12 Energy positions of some mainstream semiconductors and noble metal photocatalysts [369].

Figure 13 (**a**) UV-vis diffuse reflectance spectra of $Sr_2MgSi_2O_7:Eu^{2+},Dy^{3+}$ (M, orange curve) phosphor coupled with different Ag_3PO_4 (A, black curve) contents (M:A = 20:1 (blue curve), 15:1 (green curve), 10:1 (violet curve), and 5:1 (red curve) [377], where the inset is the persistent images of $Sr_2MgSi_2O_7:Eu^{2+},Dy^{3+}$ before and after dispersed in CH_3OH [66]; (**b**) Persistent spectra of (**a**) samples of recorded at 10 s after removal of 360 nm UV light [377], where the curve colors are related that of (**a**); (**c**) Excitation (λ_{em} = 320 nm) and emission spectra (λ_{ex} = 380 nm) of $Ca_{1.995}MgSi_2O_7:0.005Ce^{3+}$ powder (**solid**), mixture of $Ca_{1.995}MgSi_2O_7:0.005Ce^{3+}$ and kaolin with 5:1 after compression (**dash**), and after 900 ^oC sintering (**dot**), and after depositing with TiO_2 in 6.3 mg/cm^2 [366]; (**d**) Transmission spectrum of TiO_2-deposited glass (■), and absorption spectrum of TiO_2-deposited $Ca_2MgSi_2O_7:Ce^{3+}$ ceramic (■), where the photographs (**inset**) of the light penetration (**i**), the ceramic substrate made from the $Ca_{1.995}MgSi_2O_7:Ce^{3+}{}_{0.005}$-kaolin with 6.3 mg/cm^2 of TiO_2 deposition (**ii**), and the ceramic substrate under UV irradiation (**iii**) [366].

Figure 14 Mechanism for the improved photocatalysis of Ag_3PO_4 by better photon utilization and charge separation with $Sr_2MgSi_2O_7:Eu^{2+},Dy^{3+}$ [377].

Figure 15 Schematic model of persistent $Sr_2MgSi_2O_7:Eu^{2+},Dy^{3+}$ phosphor-assisted photocatalytic reaction with light on and off [377].

Figure 16 (**a**) SEM image of $Ca_2MgSi_2O_7:Ce^{3+}$ substrate (**i**), and $Ca_2MgSi_2O_7:Ce^{3+}@TiO_2$ composite (**ii**) [366]; (**b**) Field emission SEM images of $Ca_2MgSi_2O_7:Eu^{2+},Ce^{3+}$ (**i**), g-C_3N_4 (**ii**), $Ca_2MgSi_2O_7:Eu^{2+},Ce^{3+}@$g-$C_3N_4$ (**iii**), and (**iv**) high-magnification FESEM image of (**iii**) [379]; (**c**) SEM image of $ZnGa_2O_4$ [310]; (**d**) SEM image of $(3ZnO:Ga_2O_3:2GeO_2):Cr@TiO_2$ [383]; (**e**) SEM images of $ZnGa_2O_4$ (**i**) and $ZnGa_2O_4:Cr^{3+}$ (**ii**) [197]; (**f-g**) TEM (**i**) and HRTEM (**ii**) images of $Sr_2MgSi_2O_7:Eu^{2+},Ce^{3+}@$g-$C_3N_4$ [379] and $BaZrO_3:Mg^{2+}@TiO_2$ composites [311]; and (**h**) SEM images of Ag_3PO_4 (**i**), $Sr_2MgSi_2O_7:Eu^{2+},Ce^{3+}$ (**ii**), and $Sr_2MgSi_2O_7$: $Eu^{2+},Ce^{3+}@Ag_3PO_4$ (**iii**) [377].

Figure 17 (**a**) Field emission SEM (**i**) and TEM (**ii**) images as well as EDX spectrum (**inset**) of $Ca_2Al_2SiO_7:Ce^{3+}$@Ag-AgCl (10:1) composite [63]; (**b**) SEM images of $MgAl_2O_4:Pr^{3+},Dy^{3+}$ (**i**), and $MgAl_2O_4:Pr^{3+},Dy^{3+}@$Cr-$TiO_2$ (**ii**) [107]; (**c**) TEM images of g-C_3N_4 (**i**) and $Sr_4Al_{14}O_{25}$:(Eu,Dy) MPL coupled with 60%wt of g-C_3N_4 (**ii**), and SEM images of $Sr_4Al_{14}O_{25}$:(Eu,Dy) (**iii**) and $Sr_4Al_{14}O_{25}$:(Eu,Dy) MPL coupled with 60%wt of g-C_3N_4 (**iv**) [65]; (**d**) SEM images of GP MPL (**i-ii**) and GP@Fe-N-TiO_2 prepared with PEG 200 (**iii**) and 400 (**iv**) [384]. Noted that GP MPL is denoted as a aluminate-based persistent phosphor ((provided by DB-Chemic).

Figure 18 (**a**) UV-Vis absorption spectra of MO degraded using UTSA-38 photocatalyst [404]; (**b**) C/C_i of MO degradation placed in $xSr_2MgSi_2O_7:Eu^{2+},Dy^{3+}@yAg_3PO_4$ (curves 1-5 are x:y = 5:1, 10:1, 15:1, 10:1, 1:0, respectively) and recored in the persistent step as a function of time [377]; (**c**) Time-dependent MO degradation process placed in the $Ca_2Al_2SiO_7:Ce^{3+}$ (**curve 1**), Ag-AgCl

(**curve 2**), and $Ca_2Al_2SiO_7:Ce^{3+}$@Ag-AgCl (**curve 3**), and recored in dark, under light irradiation and in the absence of light [63]; (**d**) Expanded persistent MO degradation step (*i.e.*, after-light-off) of (**c**) with the ordinate expressed by C/C_{A0} [63].

Figure 19 (**a-b**) Persistent photocatalysis degradation of RhB in the Ag_3PO_4@$Sr_2MgSi_2O_7$:Eu,Dy, Ag_3PO_4@$Sr_4Al_{14}O_{25}$:Eu,Dy,Er, Ag_3PO_4@$SrAl_2O_4$:Eu,Dy, and Ag_3PO_4@silicone-acrylic-emulsion coating systems in dark condition [376], where the $Sr_2MgSi_2O_7$:Eu,Dy is denoted as "SMSOED"; (**c**) Photocatalytic degradation of RhB in bulk $ZnGa_2O_4$ (S_1), $Zn_{0.95}Ga_2O_{3.95}$ (S_2), $Zn_{0.9}Ga_2O_{3.9}$ (S_3), $Zn_{0.85}Ga_2O_{3.85}$ (S_4), and $Zn_{0.8}Ga_2O_{3.8}$ (S_5) [342]; (**d**) Photocatalytic degradation of the RhB dye on different BiOBr films with and without long-afterglow phosphor [381], where the photocatalytic process is divided into two steps, *i.e.*, the light on (0- 60 min) and light off (60-120 min).

Figure 20 (**a**) Photocatalytic decomposition of MB dye in the $Sr_4Al_{14}O_{25}$:(Eu,Dy), g-C_3N_4, and various $Sr_4Al_{14}O_{25}$:(Eu,Dy)@g-C_3N_4 composites in dark condition (-0.5-0 h) and in the presence of visible-light irradiation (0-5 h) ; (**b**) Persistent luminescence assisted MB decomposition in dark with the the same reaction conditions of (**a**) [65]; (**c**) Decomposition curves of MB dye placed in $CdSiO_3:Gd^{3+},Bi^{3+}$@TiO_2 composite (**curve 1**), pure TiO_2 (**curve 2**) and $CdSiO_3:Gd^{3+},Bi^{3+}$ (**curve 3**) in dark (**iv**) [141], (**d**) Photocatalytic decomposition of MB dye placed in $BaZrO_3:Mg^{2+}$@TiO_2 composite, pure TiO_2 and $BaZrO_3:Mg^{2+}$ in dark without the UV light irradiation [311].

Figure 21 (**a**) Photocatalytic activity of NO destruction placed in Cr-doped $SrTiO_3$ (**curve 1**) and nonstoichiometric $SrTiO_3$ (**curve 2**) under UV, blue, green and LED irradiation [385]; (**b**) $DeNO_x$ process placed in $CaAl_2O_4$:(Eu,Nd)@Cr-doped $SrTiO_3$ and $CaAl_2O_4$:(Eu,Nd)@nonstoichiometric $SrTiO_3$ with and without the UV LED irradiation ($\lambda > 290$ nm) [385]; (**c-d**) Photocatalytic deNOx activity placed in $CaAl_2O_4$:(Eu,Nd)@$TiO_{2-x}N_y$ (**curve 1**), brookite-phase $TiO_{2-x}N_y$ (**curve 2**), and $CaAl_2O_4$:(Eu,Nd)@undoped TiO_2 (**curve 3**) under and without the UV LED irradiation [61].

Figure 22 (**a**) UV-vis diffuse reflectance spectra of pristine g-C_3N_4, g-C_3N_4@xwt%Au composites, and g-C_3N_4-Au@$SrAl_2O_4$:Eu,Dy composite, along with the absorption spectra of Au nanoparticle stock solution and persistent spectra of the $SrAl_2O_4$:Eu,Dy and g-C_3N_4@Au@$SrAl_2O_4$:Eu,Dy; (**b**) Time course for H_2 evolution of the g-C_3N_4, $SrAl_2O_4$:Eu,Dy, $SrAl_2O_4$:Eu,Dy@Au, g-C_3N_4@Au, g-C_3N_4@ $SrAl_2O_4$:Eu,Dy, and g-C_3N_4@Au@$SrAl_2O_4$:Eu,Dy composite with and without visible light irradiation; (**c**) Time course for H_2 evolution of the g-C_3N_4, g-C_3N_4@xwt%Au composites, the inset shows the photocatalytic activities as as a function of the embedded Au content; (**d**) Time course for H_2 evolution of g-C_3N_4@Au@x$SrAl_2O_4$:Eu,Dy composites with different mass ratios of g-C_3N_4@Au and $SrAl_2O_4$:Eu,Dy with and without visible light irradiation [57].

Figure 23 Dependence of pH reactive mediums (**a**), time course (**b**), irradiation duration (**c**), and temperature (**d**) on photocatalytic performance of $Sr_2MgSi_2O_7:Eu^{2+},Dy^{3+}$ in dark [66].

Figure 24 A distribution pattern of the persistent intensity maxima of the RE- and non-RE-doped MPLs, and bulk MPLs we exhibited in this review. Noted that there are 300 points but some of them are overlapped with each other.

Recent advances and prospects of persistent luminescent materials as inner secondary self-luminous light source for photocatalytic applications

Fengwen Kang, Guohuan Sun, Philippe Boutinaud, Haoyi Wu, Fei-Xiang Ma, Jian Lu, Jiulin Gan, Haidong Bian, Fei Gao, and Sanshui Xiao

Key words: persistent luminescence; inner light source; self-luminous; rare-earth (RE); non-RE; photocatalysis.

.

TOC figure

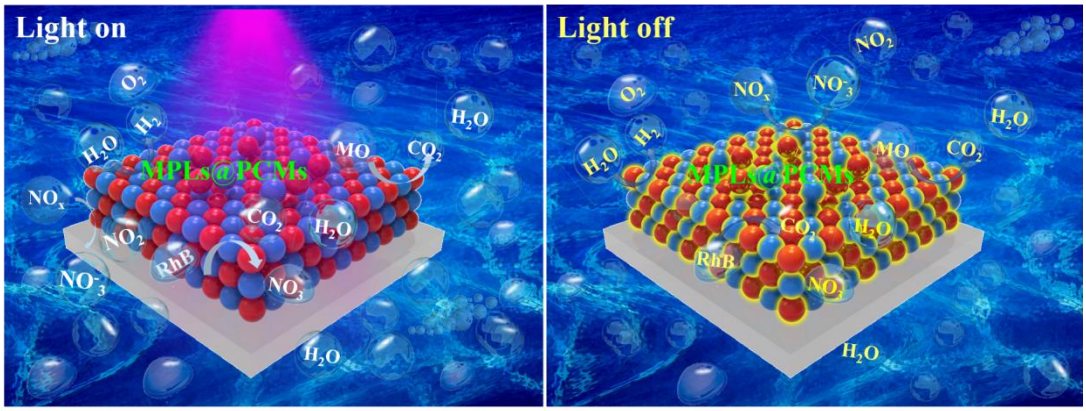

A suitable combination of MPLs and PCMs enables sustaining the photocatalytic activities when there is no external light irradiation source.

AUTHORS' CV

AUTHORS' RESEARCH INTRODUCTION AND BACKGROUND

1. *Dr.* Fengwen Kang

Fengwen Kang is now a Marie Skłodowska Curie postdoctoral fellow at DTU Fotonik, Department of Photonics Engineering at Technical University of Denmark. He received his *BSc* degree in 2009, *Master* degree in 2012, and *PhD* degree in 2015 from the Qiqihar University, Guangdong University of Technology and South China University of Technology, respectively. After that, he worked as a research associate at The Hong Kong Polytechnic University and a senior research associate at City University of Hong Kong (CityU), from Oct-2015 to Dec-2018. His research interests include, but not limited to, rare earth (RE) and non-RE doped afterglow, downconversion and upconversion fluorescent materials, and relevant applications such as white LEDs, and photocatalytic materials. So far, he has authored more than 50 articles.

E-mail: kangfengwen0597@126.com.

2. *Dr.* Guohuan Sun

Guohuan Sun is now a PhD student in the State Key Laboratory of Experimental Hematology (SKLEH) at Chinese Academy of Medical Sciences. She received her *BSc* degree in 2015 from Sun Yat-sen University. Her major interests include fluorescent materials for photocatalytic and electrochemical applications, and stem cell and hematology-related researches.

E-mail: sungh0228@126.com.

3. *Prof.* Philippe Boutinaud

Philippe Boutinaud is now working at Institute of Chemistry of Clermont-Ferrand at Clermont Auvergne University. He has received his PhD degree in materials science in 1991 at the University of Bordeaux, France, in the laboratory funded by Prof. Paul Hagenmuller. Then he moved for three years as a post-doc fellow at the department chemical physics of the University of sciences of Geneva, Switzerland before getting a permanent position as an associate professor in 1994 in the Laboratory of Inorganic Materials of the University of Clermont-Ferrand, France. He has received his habilitation in 1997 and was promoted as full professor two years later. His research activity focuses on optical materials with specific interest on modelling luminescence-structure relationships and long-term behaviors upon thermal and photonic stresses.

E-mail: philippe.boutinaud@sigma-clermont.fr.

4. *Assoc. Prof.* Haoyi Wu

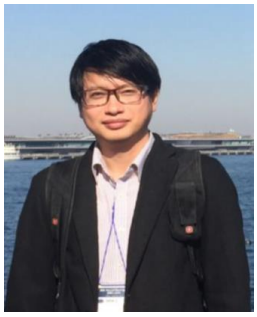

Haoyi Wu received his Ph.D. degree in Applied Chemistry from Guangdong University of Technology in 2011. Then, he worked as a postdoctoral fellow in Tsinghua University (2012-2014), Japan Society for the Promotion of Science (JSPS) fellow (2014-2016) and researcher scientist (2016-2017) in National Institute of Advanced Industrial Science and Technology, respectively. Now, he is an associated professor in School of Physics and Optoelectronic Engineering at Guangdong University of Technology. His research interests span from versatile fabrication techniques and fundamental mechanisms for rare earth (RE) and non-RE afterglow, fluorescent and photochromic materials, multifunctional composites and to their applications in the fields such as white LEDs,

sensor, a photocatalysis for water purification *etc*. So far, he has published more than 60 peer-reviewed journal articles.

E-mail: manofchina1@outlook.com.

5. *Dr.* Feixiang Ma

Fei-Xiang Ma received his Ph.D. degree in Materials Science from Harbin Institute of Technology, in 2017. He was a visiting student at Nanyang Technological University from 2014 to 2015. Now, he is a postdoctoral researcher at City University of Hong Kong. So far, he has published 25 peer-reviewed journal articles since 2013, including Angew. Chem. Int. Ed., Adv. Mater, Energ. Environ. Sci.. His research interests focus on the catalytic, photocatalytic and electrochemical fields, including the design strategy of novel electrode materials for supercapacitors and electrocatalysis, the catalytic mechanism for hydrogen production for addressing the environmental problems, and the synthetic methods for photocatalytic activity, *etc*.

E-mail: mfx89@gmail.com.

6. *Prof.* Jian Lu

Jian Lu is now chair professor in the Department of Mechanical Engineering at City University of Hong Kong. He is also the winner of Habilitation (Sorbonne University (Pierre et Marie Curie)) (UPMC Paris 6), Fellow SEM, Fellow HKAES, Fellow HKIS, Academician: National Academy of Technologies of France and Academician of Hong Kong Academy of Engineering. He got the *BSc* degree and *Habilitation* from Peking University in 1978 and Sorbonne University (Université Pierre et Marie CURIE) in 1993,

respectively, and a *PhD* degree from University of Technology of Compiegne (UTC) in 1986. He was a Senior Research Engineer and Head of the Residual Stress and Coating Adhesion Laboratory in the French Technical Center for Mechanical Industries (CETIM, 1987-1994), Professor (Part time) in University of Technology of Compiegne (1993-1994), Co-leader of the UTC (Compiegne)-UTT (Troyes) Doctor Program in Science of Mechanics for Engineer (1995-1999), Professor and Head of the Mechanical Systems Engineering Department (1994-2005) as well as Director of the Mechanical Systems and Concurrent Engineering Laboratory in University of Technology of Troyes (1994-2005), Chair Professor of Mechanical Engineering and Head of Department of Mechanical Engineering as well as Associate Dean of Faculty of Engineering ((Feb 2008 - Aug 2010) in The Hong Kong Polytechnic University (2005-2010). From Sep 2010 to now, he is the Chair Professor of Mechanical Engineering, Vice-President (Research and Technology) and Dean of Graduate Studies, Director of Centre for Advanced Structural Materials and Hong Kong Branch of National Precious Metals Material Engineering Research Centre, and Dean of College of Science and Engineering. He has published more than 330 articles, including *Nature, Science, Nature Materials, etc*, with the total citations of over 20000 and the *h*-index of 66 (Source: google scholar)..

E-mail: jianlu@cityu.edu.hk

7. *Assoc. Prof.* Jiulin Gan

Jiulin Gan is now working in School of Materials Science and Engineering at South China University of Technology (SCUT), Guangdong, China. He received the BSc degree from Huazhong University of Science and Technology in 2006, and the PhD degree from Shanghai Institute of Optics and Fine Mechanics, Chinese Academy of Sciences in 2011. Then he went to SCUT as a postdoctor. Since 2013 he has been working as an associate professor in SCUT, with the major research interests on fluorescence probe materials, composite optical fiber, fiber sensor and fiber laser, along with their applications in measurement and sensing.

E-mail: msgan@scut.edu.cn.

8. Dr. Haidong Bian

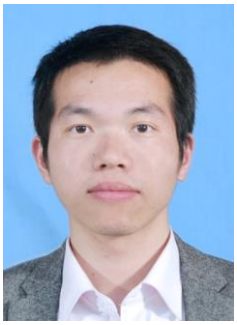

Haidong Bian received his Ph.D. degree in material science from City University of Hong Kong in 2017. His research interests focus on the design and synthesis of porous nanomaterials for photocatalytic water splitting and electrochemical energy conversion.

E-mail: Hbian2@cityu.edu.hk

9. *Dr.* Fei Gao

Dr. Fei Gao received her Ph. D. degree in Physics from Institute of Physics, Chinese Academy of Sciences in 2015 and is currently a postdoc in DTU Physics at Technical University of Denmark. Her research activities focus on computational physics, with the major interests on modeling spin manipulation, photocatalytic activity, and luminescence-structure relationships by use of density functional theory (DFT) calculations.

E-mail: fega@dtu.dk.

10. *Assoc. Prof.* Sanshui Xiao

Sanshui Xiao received his Ph.D. degree (2004) at Zhejiang University. He joined Technical University of Denmark (DTU) in 2006 and now is an Associate Professor at DTU. His current research interests focus on light-matter interactions in nanoplasmonics and their applications in optoelectronic devices.

E-mail: saxi@fotonik.dtu.dk.